

THE INVESTIGATION OF BIAXIAL STRESS EFFECTS AND THE
TRANSVERSE PIEZOELECTRIC (d_{31}) CHARACTERIZATION OF LEAD
ZIRCONATE TITANATE THIN FILMS

1998

JOSEPH F. SHEPARD JR.

The Pennsylvania State University
The Graduate School
Department of Materials Science and Engineering

THE INVESTIGATION OF BIAXIAL STRESS EFFECTS AND THE TRANSVERSE
PIEZOELECTRIC (d_{31}) CHARACTERIZATION OF LEAD ZIRCONATE TITANATE
THIN FILMS

A Thesis in
Materials Science and Engineering

by
Joseph F. Shepard Jr.

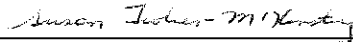
Submitted in Partial Fulfillment
of the Requirements
for the Degree of

Doctor of Philosophy

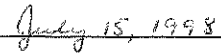
August 1998

We approve the thesis of Joseph F. Shepard Jr.

Date of Signature

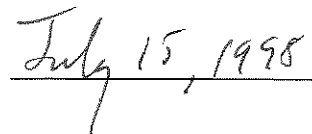


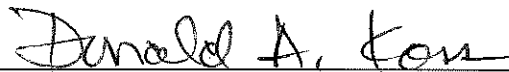
Susan Trolier-McKinstry
Associate Professor of Ceramic Science and Engineering
Thesis Advisor





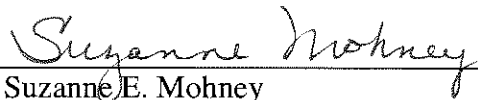
Clive A. Randall
Associate Professor of Materials Science and Engineering





Donald A. Koss
Professor of Materials Science and Engineering





Suzanne E. Mohney
Assistant Professor of Materials Science and Engineering
Chair of Committee





Kwadwo Osseo-Asare
Professor of Metallurgy
In Charge of Metals Science and Engineering Option



Abstract

The recent advances in silicon micromachining technology have led to a considerable interest in the design and construction of microelectromechanical systems (MEMS). MEMS devices are most often actuated by electrostatic means, however piezoelectric materials present an opportunity to conduct sensing and actuation functions with the same material on a single chip. There are a number of candidate piezoelectric films, including zinc oxide, aluminum nitride, and several ferroelectric compositions. Of these, the large piezoelectric coefficients and high energy densities of lead zirconate titanate (PZT) make it particularly attractive.

There are a number of outstanding issues which must be addressed for the efficient implementation of PZT films into MEMS devices. Two of considerable importance are the limited number of techniques by which the piezoelectric coefficients can be measured and the lack of information regarding the factors which influence the electromechanical characteristics. The work described herein was designed to investigate these questions.

The effect of biaxial mechanical stress on the low and high-field electrical characteristics of lead zirconate titanate (PZT) thin films was investigated. Films with 52/48, 48/52, 56/44, 40/60 and 60/40 zirconium to titanium ratios were prepared using a sol-gel procedure. Controlled stress states (compressive or tensile) were then imposed upon the films with a uniform pressure rig designed to apply a constant gas pressure to either the surface of a PZT coated silicon wafer or a PZT chip bonded to a predeformed steel substrate. The remanent polarization, coercive field strength, dielectric constant, and

$\tan \delta$ were measured as a function of stress for levels on the order of ± 100 MPa. It was found that the dielectric constant, as well as the saturation and remanent polarizations decrease with applied tensile stress and increase with applied compressive stress. Changes in the magnitude of the remanent polarization were typically between 15 to 25% while changes in the dielectric constant were less than 5%. The dielectric loss and coercive field strengths were also monitored and results showed that $\tan \delta$ increased less than 20% regardless of the sign of the stress and the coercive field strength increased less than 10% with applied compression. Comparison of the results with earlier studies on bulk PZT ceramics suggests that, for applied stresses on the order of ± 100 MPa, non- 180° domain wall motion contributes little to the stress response of PZT thin films. This implies that ferroelastic wall motion is strongly constrained in these films, which will in turn limit both the dielectric and piezoelectric properties to values characteristic of hard PZT ceramics.

The wafer flexure technique was developed as a simple and inexpensive characterization tool for the transverse piezoelectric coefficient (d_{31}) of piezoelectric thin films. The technique relies upon the cyclical flexure of a coated substrate to impart an AC two-dimensional stress to the piezoelectric film. The surface charge generated via the mechanical loading is converted to a voltage by an active integrator. Plate theory and elastic stress analyses are used to calculate the principal stresses applied to the film. The d_{31} coefficient can then be determined from knowledge of the electric charge produced and the calculated mechanical stress.

The wafer flexure method is capable of characterizing 3" or 4" wafers or millimeter sized test chips. Results collected from a number of different sol-gel and RF-

sputtered PZT films show the values of the transverse coefficients to depend upon film thickness and poling conditions. Typical d_{31} values for well poled 52/48 sol-gel films were found to be between -50 and -60 pC/N. The RF sputtered films possessed large as-deposited polarizations which produced d_{31} coefficients on the order of -70 pC/N in some unpoled films. The subsequent poling of the material, in a direction parallel to the preferred direction increased the d_{31} coefficient to values of about -85 pC/N.

The wafer flexure rig was used to investigate the aging of the d_{31} coefficient of PZT thin films. Experiments were conducted on 52/48 sol-gel films as a function of thickness with poling times of either 1 or 2 minutes (room temperature). The aging rate was found to be independent of poling direction and range from 4% per decade for the thickest $2.5 \mu\text{m}$ film to 8% per decade for a $0.6 \mu\text{m}$ film. In contrast, the aging rate of sputtered films was strongly dependent on poling direction. When the sputtered films were poled parallel to the preferred polarization direction, small gains of the d_{31} coefficient were produced and modest aging rates of 2 to 4% per decade were observed. However, when they were poled anti-parallel to the preferred direction, large changes of the d_{31} coefficient were produced and the aging rates accelerated to values between 20 and 26% per decade. These aging rates are very high in light of the limited twin wall motion in PZT films. The reasons for the accelerated aging rates in PZT films are believed to result from the depolarizing effects of internal electric fields in the RF sputtered films and interfacial defects in the sol-gel films.

Table of Contents

Abstract	III
Table of Contents	VI
List of Figures	XI
List of Tables.....	XVIII
Acknowledgments	XIX
1. Introduction	1
2. Literature Review	4
2.1. Introduction.....	4
2.2. Microelectromechanical Systems (MEMS).....	4
2.2.1. Piezoelectric Thin Films in MEMS Devices	5
2.3. Ferroelectric Materials	7
2.4. Piezoelectric Materials.....	10
2.4.1. The Direct and Converse Piezoelectric Effects	11
2.4.2. Intrinsic and Extrinsic Contributions to the Piezoelectric Response.....	12
2.5. Lead Zirconate Titanate (PZT)	14
2.5.1. Hard and Soft PZT Ceramics	16
2.6. Mechanical Plate Theory	17
2.7. Stresses in Thin Films.....	19
2.7.1. Sources of Film Stress	19
2.7.2. The Measurement of Residual Film Stress.....	20
2.7.3. Residual Film Stress in Lead Zirconate Titanate Thin Films.....	21
2.7.4. The Transformation Stress Model	22
2.8. The Effects of Applied Mechanical Stress on PZT Ceramics	23
2.8.1. The Effects of Uniaxial Stress on the Dielectric and Piezoelectric Characteristics of PZT Ceramics.....	24
2.8.2. The Effects of Biaxial (Two-Dimensional) Stress on the Dielectric and Piezoelectric Characteristics of PZT Ceramics	27
2.9. Characterization of the Piezoelectric Coefficients of Thin Films.....	30

2.9.1. Converse Techniques for the Piezoelectric Characterization of Thin Films	31
2.9.2. Direct Techniques for the Piezoelectric Characterization of Thin Films	34
2.9.3. Measurements of the Transverse Piezoelectric Coefficients of PZT Thin Films	37
3. Experimental Procedure	41
3.1 Introduction	41
3.2. Deposition of PZT Thin Films	41
3.2.1. Rapid Thermal Annealed Films	42
3.2.2. Conventional Furnace Annealed Samples	43
3.2.3. RF Magnetron Sputtered 50/50 PZT Films	43
3.3. Residual Stress Measurements	44
3.4. Characterization of the Effects of Biaxial Stress on the Dielectric Properties of PZT Thin Films	45
3.4.1. The Uniform Pressure Rig	45
3.4.2. Characterization of the Magnitude of Applied Stress	47
3.4.3. Chip-on-Steel Design	48
3.4.4. High and Low-Field Electrical Characterization	50
3.5. The Wafer Flexure Technique for the Characterization of the d_{31} Piezoelectric Coefficient	51
3.5.1. Principle of Operation	51
3.5.1.1. Uniform Pressure Rig	53
3.5.1.2. Charge Integrator	54
3.5.1.3. Peripheral Electronics	56
3.5.1.4. Mercury Drop Electrode	56
3.5.2. Stress Analysis and the Calculation of d_{31}	57
3.5.3. Numerical Considerations	60
3.5.3.1. Elastic Modulus of the PZT Film	60
3.5.3.2. Anisotropy of the Silicon Substrate	61
3.6. Validation of the Wafer Flexure Technique for the Transverse Piezoelectric Characterization of Thin Films	62

3.6.1. Resistance Strain Gauge Measurements.....	62
3.6.2. The Variation of the d_{31} Coefficient with Radial Location on a Wafer	62
3.7. Experiments with the Wafer Flexure Method for the Transverse Piezoelectric Characterization (d_{31}) of Thin Films	63
3.7.1. The Influence of Excitation Stress on the d_{31} Coefficient.....	63
3.7.2. The Effects of Poling Time and Poling Direction on the d_{31} Coefficient	64
3.7.3. The Effects of Film Thickness on the Magnitude of the d_{31} Coefficient	64
3.7.4. The Aging Rate of the d_{31} Coefficient of PZT Thin Films.....	65
3.8. The Characterization of the d_{31} Coefficient of Test Chips Coated with Piezoelectric Thin Films	66
4. The Effects of Biaxial Stress on the Low and High-Field Properties of PZT Thin Films	68
4.1. Introduction.....	68
4.2. Residual Film Stresses in PZT Thin Films on Platinized Silicon Substrates	69
4.3. Strain on the 3" PZT Films as a Function of Applied Pressure.....	69
4.4. Strain on PZT Chips Bonded to Predeformed Steel Substrates.....	72
4.5. Low-Field Characteristics of PZT Films as a Function of Applied Biaxial Stress	74
4.5.1. The Low-Field Stress Response of 3" 52/48 Films in the Wafer and O- ring Configuration	74
4.5.2. Low-Field Tensile Stress Response of 3" 40/60 and 60/40 Films	77
4.5.3. The Effects of Film Thickness on the Low-Field Biaxial Stress Response.....	79
4.5.3.1. The Low-Field Biaxial Stress Response of (111) Oriented RTA'd Samples	81
4.6. Low-Field Data Taken with the Chip-on-Steel Design	85
4.6.1. The Effects of Biaxial Stress on Dielectric Loss.....	88
4.6.2. The Effects of Crystallographic Orientation on the Low-Field Compressive Stress Response	89
4.7. The Effects of Biaxial Stress on the High-Field Characteristics of PZT Thin Films	90

4.7.1. The Effects of Applied Tension on the High-Field Characteristics of PZT Thin Films	91
4.7.2. The Effects of Applied Compression on the High-Field Characteristics of PZT Thin Films	93
4.8. Discussion of The Biaxial Stress Response of PZT Thin Films	97
4.8.1. Low-Field Biaxial Stress Response of PZT Thin Films	97
4.8.2. High-Field Biaxial Stress Response of PZT Thin Films	100
4.9. Consideration of the Mechanisms of the Thin Film Biaxial Stress Response	100
4.10. Possible Reasons for the Limited Extrinsic Response of PZT Thin Films	102
5. The Wafer Flexure Method for the Determination of the Transverse Piezoelectric Coefficient (d_{31}) of PZT Thin Films	105
5.1. Introduction	105
5.2. Validation of the Mechanical Plate Theory	106
5.2.1. Strains Measurements Made on 3" Substrates	107
5.2.2. Strain Measurements Made on 4" Substrates	111
5.2.3. Analysis of the Mechanical Anisotropy of the Silicon Wafer	112
5.3. Transverse Piezoelectric Characterization with the Prototype Configuration	114
5.3.1. Variation of d_{31} over the Surface of a 3" Wafer	115
5.3.2. d_{31} Measured as a Function of the Excitation Stress in the Uniform Pressure Rig	116
5.3.3. Resolution of the Wafer Flexure Technique	117
5.4. Measurements Made with the Modified Wafer Flexure Technique	118
5.4.1. Statistical Evaluation of the Modified Wafer Flexure Rig	119
5.4.2. The Variation of the Transverse Piezoelectric Response as a Function of Radial Location	121
5.4.3. The Influence of Film Thickness on the Magnitude of the d_{31} Coefficient of 52/48 Sol-Gel PZT Thin Films	123
5.4.4. Characterization of the d_{31} Coefficients of 50/50 RF Magnetron Sputtered PZT Thin Films	127
5.5. Aging Behavior of the Transverse (d_{31}) Piezoelectric Coefficient	131
5.5.1. Aging Work with the Prototype Wafer Flexure Rig	131

5.5.2. Aging Work with the Modified Wafer Flexure Rig	133
6. Conclusions and Recommendations for Future Work	141
6.1. The Effects of Biaxial Stress on the Low and High-Field Characteristics of PZT Thin Films.....	141
6.2. The Wafer Flexure Technique for the Characterization of the Transverse (d_{31}) Piezoelectric Coefficient of Thin Films.....	142
6.3. Recommendations for Future Work.....	145
6.3.1. Experiments with Sub-Micron Ceramic Samples	145
6.3.2. Investigations into the Mechanisms Responsible for the Accelerated Aging Rates of the Transverse Piezoelectric Coefficients of PZT Thin Films	146
6.3.3. The Investigation of the Influence of Stress at the Curie Point on the Microstructural Texture of PZT Thin Films.....	147
References	149

List of Figures

- Figure 2.1. A micro-steam engine constructed on a silicon wafer by researchers at Sandia National Laboratory. The three pistons contain water that is heated electrically. Steam then pushes the pistons forward and capillary forces draw the pistons back. 5
- Figure 2.2. The perovskite unit cell. In PZT ceramics the central atom can be either Zr^{4+} or Ti^{4+} . The corner atoms are Pb^{2+} and the face centered atoms are O^{2-} . The dipole moment in the crystal is often described as a consequence of a shift of the zirconium or titanium atoms relative to the oxygen atoms..... 8
- Figure 2.3. An illustration of the polarization hysteresis (P-E) loop of a ferroelectric material. The loop defines the saturation polarization P_s , the remanent polarization P_r , and the coercive field E_c 9
- Figure 2.4. The ferroelectric distortion of a tetragonal perovskite. The polarization direction is along the (100) direction of the prototype unit cell. 10
- Figure 2.5. The ferroelectric distortion of a rhombohedral perovskite. The polarization direction is along the (111) direction of the prototype unit cell. 10
- Figure 2.6. The lead zirconate titanate phase diagram. In the figure, P_C refers to the paraelectric cubic phase, F_T is ferroelectric tetragonal, $F_{R(HT)}$ is high temperature rhombohedral, $F_{R(LT)}$ is low temperature rhombohedral, A_O is antiferroelectric orthorhombic, and A_T is antiferroelectric tetragonal. 15
- Figure 2.7. The effects of applied uniaxial compressive stress on the dielectric constant of PZT-4 (left side) and PZT 5A (right side). Stress was applied parallel to the polar axis. 25
- Figure 2.8. The experimental biaxial stress configuration of Brown. The ceramic cylinder was poled radially and the setup placed in a hydrostatic water tank. An increase of the pressure in the tank increased the biaxial stress in the walls of the ceramic. 28

Figure 2.9. The effects of biaxial compressive stress on the low-field characteristics of PZT ceramics. Data on the left are for PZT-4 while data on the right were taken from PZT-5 (note that $1 \text{ kg/cm}^2 \sim 0.1 \text{ MPa}$).	29
Figure 2.10. An example of a configuration used for the identification of piezoelectricity in piezoelectric thin films.	31
Figure 2.11. A schematic of a double beam Mach-Zehnder interferometer. In the plot BS and PBS stand for beam splitter and polarized beam splitter, respectively.	33
Figure 2.12. The normal load method for the piezoelectric characterization of thin films. The motor driven ram was used to drive a metal bellows which applied a hydraulic pulse to the piezoelectric film. The stress on the film created an electrical voltage which was registered on the screen of an oscilloscope.	35
Figure 2.13. The piezoelectric characterization device designed by Surowiak and Czekaj. The piezoelectric sample (#1) is held between the two hemispherical electrodes (#2) while the shaft is oscillated. The bottom electrode (#2) is connected to ground and the top electrode (#4) is fed to the charge detection equipment (#6).	37
Figure 3.1. The uniform pressure rig for the controlled bending of 3" PZT coated silicon substrates.	47
Figure 3.2. The chip on steel design for the application of large compressive stresses to PZT thin films.	49
Figure 3.3. The wafer flexure d_{31} measurement setup.	52
Figure 3.4. An illustration of the modified pressure rig. The rig is capable of handling either 3" or 4" PZT coated substrates.	54
Figure 3.5. Schematic of the electric charge integrator.	55
Figure 3.6. The modified wafer flexure apparatus for the characterization of millimeter sized test chips.	67
Figure 4.1. The tensile strain at the center of a PZT coated test wafer when clamped between two O-rings in the uniform pressure rig. Maximum	

strains achieved were about 800 μ strain, which translates to about 115 MPa of stress in the PZT.....	70
Figure 4.2. The compressive strain at the center of a PZT coated test wafer when clamped between two O-rings in the uniform pressure rig. Maximum strains achieved were about 300 μ strain, which translates to about -40 MPa of stress in the PZT.....	71
Figure 4.3. The strain applied to a 6.5 mm PZT coated test chip bonded to a predeformed steel substrate. The data were taken from the first pressure cycle, i.e. as the steel dome was folded inside out.....	73
Figure 4.4. The strain applied to a 6.5 mm PZT coated test chip bonded to a steel substrate. The data shown were taken from three tests conducted on a PZT chip rebonded to the substrate after the dome had been forced inside out on the first pressure cycle.....	73
Figure 4.5. The X-ray diffraction pattern for a 0.4 μ m thick 52/48 sol-gel film.....	75
Figure 4.6. The change in capacitance of an unpoled 0.4 μ m thick 52/48 sample with applied biaxial stress. The pressure range given corresponds to an applied film stress ranging from approximately -40 to 115 MPa.....	76
Figure 4.7. The change in capacitance of a poled 0.4 μ m thick 52/48 samples with compressive stress. The pressure range given corresponds to an applied film stress ranging from approximately -40 to 115 MPa.....	77
Figure 4.8. The low-field biaxial stress response of a 0.45 μ m thick 40/60 film deposited on a 3" platinized silicon substrate.....	78
Figure 4.9. The low-field biaxial stress response of a 0.55 μ m thick 60/40 film deposited on a 3" platinized silicon substrate.....	79
Figure 4.10. The variation of dielectric constant with film thickness. Data from both the RTA'd and furnace annealed samples are presented.....	80
Figure 4.11. The stress response of a 0.6 μ m thick 52/48 PZT thin film. The film was prepared on a 3" platinized silicon substrate and had a (111) orientation.....	81

- Figure 4.12. The stress response of a 0.8 μm thick 52/48 PZT thin film. The film was prepared on a 3" platinized silicon substrate and had a (111) orientation..... 82
- Figure 4.13. The stress response of a 1.8 μm thick 52/48 PZT thin film. The film was prepared on a 3" platinized silicon substrate and had a (111) orientation..... 82
- Figure 4.14. The stress response of a 2.5 μm thick 52/48 PZT thin film. The film was prepared on a 3" platinized silicon substrate and had a (111) orientation..... 83
- Figure 4.15. The stress response of a 3.0 μm thick furnace annealed sample. The film was prepared on a 3" platinized substrate and had a (100) orientation. 84
- Figure 4.16. The stress response of a 5.0 μm thick furnace annealed sample. The film was prepared on a 3" platinized substrate and had a (100) orientation. 84
- Figure 4.17. The change of capacitance for a 1 μm thick 52/48 PZT chip as a function of applied compressive strain and poling condition. 86
- Figure 4.18. The change of capacitance for 1.2 μm (111) oriented 56/44 (rhombohedral) PZT as a function of the magnitude of the compressive strain and poling condition..... 87
- Figure 4.19. The change of capacitance for a 1.2 μm thick (111) oriented 48/52 (tetragonal) PZT as a function of the magnitude of the compressive strain and poling condition..... 88
- Figure 4.20. The change of capacitance for a 1.2 μm thick (100) 52/48 PZT as a function of the magnitude of the compressive strain and poling condition. 90
- Figure 4.21. Comparison of the stressed and as-deposited polarization hysteresis loops of a 0.6 μm thick 52/48 PZT film. The average remanent polarization of the as-deposited film was 21 $\mu\text{C}/\text{cm}^2$ and the average coercive field was 55 kV/cm. 92
- Figure 4.22. Comparison of the stressed and as-deposited polarization hysteresis loops of a 5.0 μm thick 52/48 PZT film prepared with a (100) orientation using a conventional furnace annealing procedure (sec. 3.2.2). The

average remanent polarization of the as-deposited film was $23 \mu\text{C}/\text{cm}^2$ and the average coercive field was $26 \text{ kV}/\text{cm}$	92
Figure 4.23. A comparison of the compressively stressed and as-deposited polarization hysteresis loops for a $1.0 \mu\text{m}$ thick (111) oriented 52/48 sol-gel PZT film. The average remanent polarization for the unstressed film was $23 \mu\text{C}/\text{cm}^2$ and the average coercive field was $34 \text{ kV}/\text{cm}$	93
Figure 4.24. The variation of the average coercive field and average remanent polarization with the application of compressive strain. Data were taken from the first pressure cycle in the chip-on-steel experiments.....	94
Figure 4.25. A comparison of the compressively stressed and as-deposited polarization hysteresis loops for a (100) oriented $1.2 \mu\text{m}$ thick 52/48 sol-gel PZT film. The average remanent polarization for the unstressed film was $18 \mu\text{C}/\text{cm}^2$ and the average coercive field was $31 \text{ kV}/\text{cm}$	95
Figure 4.26. A comparison of the compressively stressed and as-deposited polarization hysteresis loops for a $1.2 \mu\text{m}$ thick 56/44 (rhombohedral) sol-gel PZT film. The average remanent polarization for the unstressed film was $23 \mu\text{C}/\text{cm}^2$ and the average coercive field was $31 \text{ kV}/\text{cm}$	96
Figure 4.27. A comparison of the compressively stressed and as-deposited polarization hysteresis loops for a $1.2 \mu\text{m}$ thick 48/52 (tetragonal) sol-gel PZT film. The average remanent polarization for the unstressed film was $24 \mu\text{C}/\text{cm}^2$ and the average coercive field was $34 \text{ kV}/\text{cm}$	97
Figure 4.28. Comparison of bulk ceramic and thin film low-field stress response.....	99
Figure 5.1. The comparison of experimental and theoretical strains at the center of a 3" silicon wafer. Data were collected from the prototype rig.	108
Figure 5.2. The comparison of experimental and theoretical strains at the center of a 3" silicon wafer. Data were collected from the modified rig.	108
Figure 5.3. The comparison of experimental and theoretical strains (for a clamped plate) at the center of a $0.8 \mu\text{m}$ thick sol-gel PZT coated silicon wafer in the modified rig.	110

- Figure 5.13. A comparison of the polarization hysteresis loops produced by 0.6 μm and 2.5 μm thick 52/48 sol-gel films. 126
- Figure 5.14. The change of the d_{31} coefficient of a 3.3 μm thick 50/50 sputtered film with poling time. The data show a strong sensitivity to poling direction. As-deposited values of d_{31} were measured at about -70 pC/N. 128
- Figure 5.15. The polarization hysteresis loop for a ~ 3 μm thick 50/50 RF sputtered PZT film. The plot shows the average remanent polarization of the film is 41 $\mu\text{C}/\text{cm}^2$ and the average coercive field is 70 kV/cm. The internal bias field is calculated from the offset on the field axis to be 15 kV/cm. 130
- Figure 5.16. The normalized d_{31} coefficients as a function of poling time. Data for both a 3 μm sol-gel film and a 3.3 μm sputtered film. 130
- Figure 5.17. The aging behavior of the d_{31} coefficient for a 0.3 μm thick sol-gel 52/48 PZT thin film. 132
- Figure 5.18. The normalized aging behavior of the data shown in Figure 5.17. 133
- Figure 5.19. The aging of the d_{31} coefficient for four sol-gel films ranging in thickness from 0.6 to 2.5 μm . Samples were all poled with three times the coercive field for 1 minute with the top electrode positive. 134
- Figure 5.20. The aging of the d_{31} coefficient for four sol-gel films ranging in thickness from 0.6 to 2.5 μm . Samples were all poled with three times the coercive field for 1 minute with the top electrode negative. 134
- Figure 5.21. The aging rate of the d_{31} coefficient of a 3.0 μm thick 50/50 RF sputtered PZT film. The film had been poled for 1 minute with a field of ± 150 kV/cm. 136
- Figure 5.22. The aging rate of the d_{31} coefficient of a 3.0 μm thick 50/50 RF sputtered PZT film. The film had been poled for 15 minutes with a field of ± 150 kV/cm. 136

List of Tables

TABLE 2.1. The Electromechanical Characteristics of Bulk c-Axis Oriented Zinc Oxide and Lead Zirconate Titanate.....	6
TABLE 2.2. Assumptions Made for the Small Deflection Analysis of a Thin Clamped Plate	19
TABLE 2.3. Transverse Piezoelectric Coefficients (d_{31}) of PZT Thin Films.....	39
TABLE 3.1. Sputtering Conditions for the Deposition of 4" PZT Thin Films.....	44
TABLE 3.2. The Elastic Properties of the Silicon Substrate and PZT Thin Films.....	61
TABLE 5.1. The d_{31} Coefficients of a 0.3 μm Thick 52/48 Sol-Gel Film Measured as a Function of Radial Location on a 3" Substrate	115
TABLE 5.2. The Variation of the d_{31} Coefficient for a 3 μm Thick 52/48 Sol-Gel Film in the Modified 3" Configuration	121
TABLE 5.3. The Variation of the d_{31} Coefficient for a 3.3 μm Thick 50/50 RF Sputtered Film in the Modified 4" Configuration.....	121
TABLE 5.4. Aging Rates (percent per decade) of the d_{31} Coefficient of 52/48 Sol-Gel PZT Thin Films	135

Acknowledgments

I would like to thank Dr. Susan Trolier-McKinstry for her assistance over the past three years. Her office door was always open, and although I was a complete novice in the field, I was never meant to feel like anything less than a colleague. Jon-Paul Maria and Brady Gibbons answered a lot of the more general questions early on and later provided a forum for ideas and a pressure release for dissertation stress. Clive Randall and Tom Shrout were always ready to fill in the gaps but more importantly impressed upon me the work hard, play hard attitude that characterizes the MRL. Don Koss was the only connection to my Metallurgical course work and over the years became a good friend, foil, and advisor. I have often said that the most valuable portion of my graduate education was the friends I've made. The British, Latin, Indian, and African contingencies, as they came to be called, made my tenure at Penn State truly special and will make leaving the most difficult part of my education. Lastly, I would like to acknowledge my parents, Joe and Mary Ann, and my sister Allison. Their confidence and support has driven me and without them little of this would have been possible.

This work was funded under DARPA contract DABT63-95-C-0053.

1. Introduction

The continued development of silicon micromachining technology has led to rapid advances in the design and construction of novel microelectromechanical systems (MEMS). Strongly piezoelectric materials such as lead zirconate titanate (PZT) are attractive for thin film sensors and actuators in numerous MEMS designs as a result of their large piezoelectric coefficients and high energy densities [1, 2]. Electromechanical characterization of PZT films has indicated however, that the piezoelectric response, both longitudinal [3] and transverse [4], is often smaller than that of bulk ceramics of the same composition. The reason for that reduction is often attributed to the residual stress on the film, but experimental confirmation of this hypothesis is lacking.

In addition to the limited understanding of the effects of film stress, there is relatively little data on the piezoelectric coefficients of thin films. As a result, many device designers are using bulk values for the piezoelectric coefficients in their calculations. Due to the tremendous differences in the grain size, the defect chemistry, and the mechanical boundary conditions between bulk ceramics and thin films however, it is not clear that this is appropriate. What is needed is a rapid, accurate tool for the measurement of the piezoelectric constants. Given these observations, the objectives of this thesis are to evaluate the role of biaxial stress on the properties of PZT thin films and to develop a measurement technique for the characterization of thin film piezoelectric coefficients.

The residual stresses on PZT thin films are considerable (magnitudes of +100 MPa for sol-gel films deposited on silicon) and have been identified as a potential cause of their reduced electromechanical coefficients [3]. Experiments were designed therefore, in which PZT films were subjected to a controlled biaxial stress and their ferroelectric characteristics measured *in situ*. The changes produced in the film's high and low-field properties could then be correlated to the applied load and used to evaluate the effects of mechanical stress on the film's characteristics.

The design and development of novel microelectromechanical systems (MEMS) which utilize piezoelectric thin films requires explicit knowledge of the material's longitudinal (d_{33}) and transverse (d_{31} or d_{32}) piezoelectric coefficients. When prepared in bulk ceramic form, piezoelectric coefficients are characterized by numerous methods, the most common of which are the resonance and dynamic load techniques (e.g. the Berlincourt meter). Those techniques however, are inadequate for the piezoelectric characterization of thin film materials and for that reason a number of alternative techniques have been proposed [5, 6].

Laser interferometers are the most well established method for the characterization of both the longitudinal and transverse piezoelectric coefficients of thin films. Interferometric methods however, require careful optical alignment, meticulous operation, and in the case of a d_{31} measurement, appropriate sample preparation (cantilever beam construction). In contrast, the wafer flexure technique was conceived as an alternative method for the characterization of the transverse piezoelectric coefficient (d_{31}) of thin films [7]. The measurement is a direct technique (i.e. it utilizes the direct effect) and as such it eliminates a number of the complexities associated with other

designs. Experiments conducted have produced d_{31} values comparable to those measured with more established methods (e.g. interferometric) and it was the intention of the second portion of the investigation to validate the technique, expand its capabilities, and characterize its limitations.

2. Literature Review

2.1. Introduction

The investigations conducted here have been directed at the development of lead zirconate titanate (PZT) thin films for microelectromechanical applications. Interpretation of the empirical data required knowledge of the previous work conducted and a familiarity with both ferroelectric and piezoelectric phenomena. Therefore, this review will treat the general subjects of both ferroelectricity and piezoelectricity (sec. 2.3 and 2.4) and will define a number of the terms which recur throughout chapters 4 and 5. The effects of mechanical stress on the ferroelectric characteristics of PZT ceramics will then be presented (sec. 2.8) with techniques for the piezoelectric characterization of thin films reviewed last (sec. 2.9).

2.2. Microelectromechanical Systems (MEMS)

In recent years the field of microelectromechanical systems, or MEMS, has experienced rapid development. MEMS can generally be described as miniature mechanical devices (often micro-sensors or micro-actuators) which are typically fabricated on silicon substrates using technologies based on the VLSI processes of the semiconductor industry. MEMS devices have taken a number of forms to date, with considerable success achieved for the fabrication of pressure transducers [8, 9],

condenser microphones [10, 11], and accelerometers [12]. In addition, aggressive programs have been initiated in which micromotors [13], steam engines (see Figure 2.1), and fuel atomizers have been constructed [14]. Market forecasts for the MEMS industry are impressive, with a number of publications listing the value of the industry in multi-billion dollar quantities by the turn of the century [15, 16].

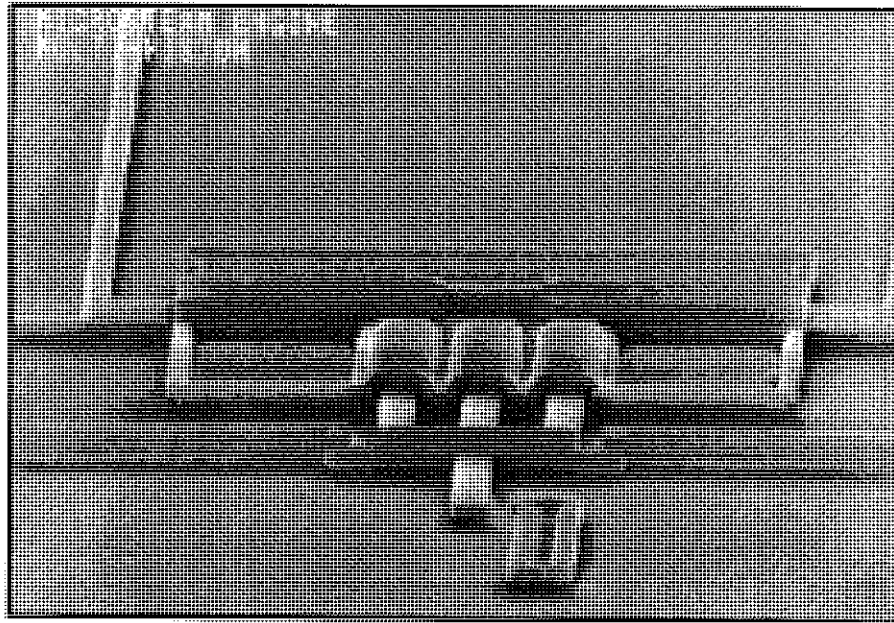


Figure 2.1. A micro-steam engine constructed on a silicon wafer by researchers at Sandia National Laboratory. The three pistons contain water that is heated electrically. Steam then pushes the pistons forward and capillary forces draw the pistons back [17].

2.2.1. Piezoelectric Thin Films in MEMS Devices

The overwhelming majority of the sensing or actuating functions in MEMS designs are based on either electrostatic or piezoresistive effects. Examples are the polysilicon comb drives in the micromirror scanners reported by Kiang et al. [18] and the

piezoresistive air bag accelerometer marketed by Analog Devices [14]. In contrast, the piezoelectric effect offers the potential for the sensing and actuation functions to be performed by the same material and housed in a single device.

The review of Foster [19] dates the first reports of thin piezoelectric films at 1964 by researchers at both Bell Laboratories and Westinghouse. The applications which drove these efforts were related to high frequency (> 100 MHz) ultrasonic transducers and in both cases the material used was c-axis oriented cadmium sulphide (CdS). Later efforts developed the techniques used to deposit other materials and at present, most of the piezoelectric films in MEMS devices are c-axis oriented zinc oxide [11, 20]. In contrast, the larger piezoelectric constants and electromechanical coupling coefficients of lead zirconate titanate (see Table 2.1) makes it an attractive alternative and work is underway in a number of laboratories to exploit its potential.

TABLE 2.1. The Electromechanical Characteristics of Bulk c-Axis Oriented Zinc Oxide and Lead Zirconate Titanate [21]

Material	Longitudinal Piezoelectric Coefficient, d_{33} (pC/N)	Transverse Piezoelectric Coefficient, d_{31} (pC/N)	Electromechanical Coupling Factor, k_{33}	Electromechanical Coupling Factor, k_{31}
c-axis Oriented Zinc Oxide	12.3	-5.12	0.46	0.18
52/48 PZT	223	-93.5	0.670	0.313

There have been a number of successful attempts at the utilization of PZT thin films in MEMS devices. Prototypes of acoustic and thermal sensors have been demonstrated at the University of Minnesota, with more recent work devoted to biomedical devices and surgical tools [1, 22]. Efforts at other laboratories have focused

on the development and construction of micromotors [23, 24], novel accelerometers [25], scanning force microscopy tips [26], and micro-sonar arrays [27].

2.3. Ferroelectric Materials

Following the identification of ferroelectricity in Rochelle salt by Valasek in 1921, a number of review articles and text books have been devoted to the topic [28]. Subjects covered have ranged from the physics of ferroelectrics [29] to their engineering applications [30]. The review here is not intended to examine the mechanisms that govern ferroelectricity, however the general characteristics of ferroelectric materials will be treated.

Ferroelectric behavior is limited to temperature ranges within which the materials display a spontaneous polarization. For temperatures below the paraelectric to ferroelectric phase transition, T_c (designated the Curie point), ferroelectric materials develop a dipole moment which results in the creation of a spontaneous polarization. In perovskite ferroelectrics such as barium titanate and lead zirconate titanate (the perovskite structure is illustrated in Figure 2.2) the spontaneous polarization results from a shift of the relative positions of the oxygen octahedra and the central atom as the material is cooled through T_c .

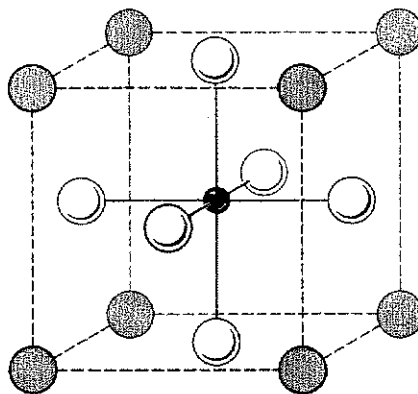


Figure 2.2. The perovskite unit cell [31]. In PZT ceramics the central atom can be either Zr^{4+} or Ti^{4+} . The corner atoms are Pb^{2+} and the face centered atoms are O^{2-} . The dipole moment in the crystal is often described as a consequence of a shift of the zirconium or titanium atoms relative to the oxygen atoms.

For temperatures above the Curie point, the reversible spontaneous polarization of the material goes to zero and a normal ferroelectric's dielectric behavior can be described according to the Curie-Weiss law i.e.

$$\epsilon_r = \frac{C}{T - T_0} \quad (2.1)$$

where ϵ_r is the relative dielectric constant, C is a constant for a given material (typically on the order of 10^3 to 10^5 degrees), T is temperature, and T_0 is the Curie-Weiss temperature. Ferroelectric materials display a maximum of their dielectric constant at T_c and the value decreases on either side of that temperature.

The most recognizable feature of a ferroelectric is the polarization-electric field hysteresis loop (i.e. the P-E loop), an example of which is shown in Figure 2.3 [31]. The P-E loop describes the change in the net polarization of the material as a strong AC

electric field is applied across the ferroelectric test capacitor. The dielectric displacement (charge per unit area), when plotted as a function of the electric field, displays the characteristic hysteresis and illustrates a number of the distinctive features of ferroelectric materials.

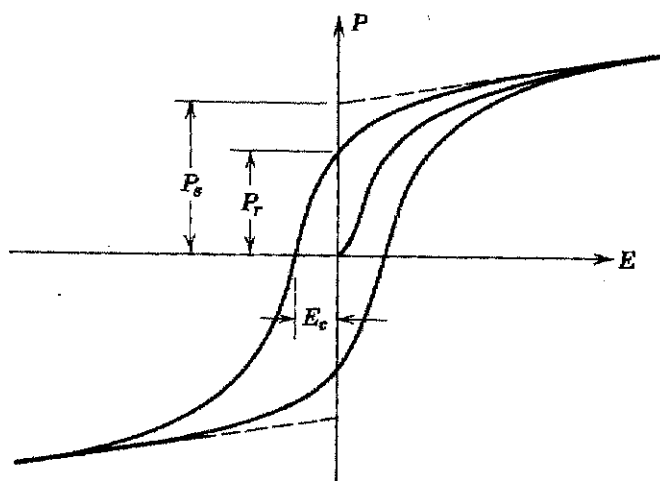


Figure 2.3. An illustration of the polarization hysteresis (P-E) loop of a ferroelectric material [31]. The loop defines the saturation polarization P_s , the remanent polarization P_r , and the coercive field E_c .

The saturation polarization, P_s , is defined as the linear extrapolation of the high field polarization back to the zero field point. This is a measure of the maximum degree of alignment of the spontaneous dipoles which is possible for a given material. The remanent polarization, P_r , is the polarization that remains in the material after the electric field is reduced to zero. The coercive field, E_c is the electric field required to eliminate (i.e. reduce to zero) the net polarization of the material via the reorientation of ferroelectric domains. The P-E loop is an important illustration of ferroelectric behavior

with the reorientable nature of the material's polarization taken as a fundamental criterion for the identification of ferroelectricity.

Ferroelectric materials develop a reorientable spontaneous polarization in each unit cell when cooled through the Curie point, T_c . The polarization vectors of the material are arranged in random directions throughout the ceramic, though within each crystallite only certain polarization directions are allowed. Regions with the same polarization direction are referred to as domains and the relative orientation of the domains is dictated by the prototype symmetry of the unit cell. The ferroelectric distortions of tetragonal and rhombohedral crystals are illustrated in Figures 2.4 and 2.5. Tetragonally distorted perovskites may have 90° and 180° domain walls while rhombohedral perovskites can have 71° , 109° , and 180° domain walls [32].

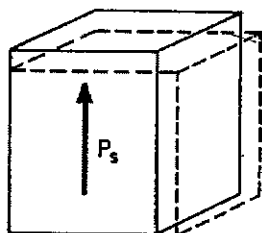


Figure 2.4. The ferroelectric distortion of a tetragonal perovskite. The polarization direction is along the (100) direction of the prototype unit cell.

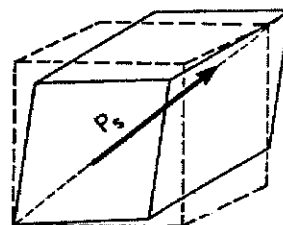


Figure 2.5. The ferroelectric distortion of a rhombohedral perovskite. The polarization direction is along the (111) direction of the prototype unit cell.

2.4. Piezoelectric Materials

Piezoelectric materials are materials which, when exposed to an applied stress, develop an electric polarization. Piezoelectric phenomena have been treated extensively

in the literature [33, 34] with work on piezoelectric ceramics covered most thoroughly by Jaffe, Cook and Jaffe [35]. From a fundamental viewpoint, piezoelectricity can be discussed in terms of its crystallographic origins [32]. The piezoelectric effect is based upon the creation or alteration of an electric dipole in the material due to an applied stress. Such a dipole can only be produced in crystals that lack a center of symmetry. A consideration of the 32 classes (i.e. point groups) of single crystal materials shows that 11 are centrosymmetric and thus non-polar. The remaining 21 crystal classes are non-centrosymmetric and of those, 20 exhibit the piezoelectric effect. The remaining exception is in the cubic system (point group 432), which possesses symmetry elements that combine to eliminate the piezoelectric effect.

Ferroelectric ceramics consist of a random array of polarization vectors after cooling through T_c . The net polarization of the material is therefore zero and it is not piezoelectric. The material may be made piezoelectric however, by "poling" it with a large DC electric field (typically at an elevated temperature). The application of the electric bias reorients the polarization vectors of the individual crystal grains to directions parallel (or close to parallel) with the applied electric field. The subsequent removal of the bias field leaves the material with a net polarization. Thus, when strained, the poled ceramic generates a piezoelectric charge.

2.4.1. The Direct and Converse Piezoelectric Effects

The direct piezoelectric effect is defined as the generation of an electric charge in response to an applied mechanical stress. The equation that describes the direct effect is written as:

$$D_i = d_{ij}\sigma_j \quad (2.2)$$

where σ_j is the applied stress (N/m^2), D_i is the dielectric displacement (C/m^2), and d_{ij} is the piezoelectric coefficient (C/N). The convention used for assignment of the subscripts in a ceramic is to define the poling direction as the 3-axis with the two orthogonal directions denoted as the 1 and 2-axes. The shear terms are denoted by the subscripts 4, 5 and 6. For example, the longitudinal piezoelectric coefficient d_{33} is the proportionality constant which describes the change of the dielectric displacement in the poling direction (i.e. D_3) in response to a stress applied parallel to that direction (i.e. σ_3).

There is also a converse piezoelectric effect that is defined as the strain produced in response to an applied electric field:

$$x_i = d_{ij}E_j \quad (2.3)$$

where x_i is the strain produced, E_j is the applied field (V/m), and d_{ij} is the piezoelectric coefficient (m/V). It should be noted that the coefficients derived from either the direct or converse relations (eqs. 2.2 or 2.3) are identical.

2.4.2. Intrinsic and Extrinsic Contributions to the Piezoelectric Response

The dielectric and piezoelectric properties of ferroelectric ceramics, when measured at room temperature, have been found to originate from both intrinsic and extrinsic sources. Intrinsic contributions are those characteristics that would arise from the properties of a single domain material. In contrast, extrinsic contributions result from

the motion of domain walls as well as from defects in the material. The relative contribution of each component to the characteristics of ferroelectric materials has been the subject of considerable research [36-38].

Zhang et al. [36] measured the dielectric and piezoelectric properties of four kinds of doped lead zirconate titanate ceramics as a function of temperature from 4.2 to 300 K. They showed that although the dielectric constants and $\tan \delta$ of acceptor-doped (hard) and donor-doped (soft) PZT ceramics were different at room temperature, they converged to comparable values at 4.2 K. The differences at higher temperatures were the result of the extrinsic contributions, since domain wall and defect motion are thermally activated. The data indicated that at room temperature, about 60% of the piezoelectric response in hard PZT's is from thermally activated extrinsic effects while in soft PZT's the number is close to 80%.

The investigation by Zhang et al. [37] attempted to quantify the relative contributions of the intrinsic and extrinsic effects in PZT ceramics with compositions near the morphotropic phase boundary. They reasoned that for an intrinsic response, any polarization change must be accompanied by a change in the unit cell volume while the polarization change brought about from domain wall motion results in no volume changes. The result of that difference is that the hydrostatic piezoelectric coefficient d_h (i.e. the charge produced in response to the application of a hydrostatic stress) will be comprised solely of intrinsic effects with no domain wall contributions.

Experiments were conducted in which the d_{33} and d_{31} coefficients of an undoped and a soft PZT ceramic were measured via resonance techniques at temperatures from 10 to 300 K. It was found that d_h was almost constant over the temperature range

investigated even though the longitudinal and transverse coefficients increased substantially with temperature. That result indicated that in the PZT ceramics tested the large change in the piezoelectric activity with temperature was caused by the reduction of extrinsic contributions. Zhang et al. assumed the extrinsic contributions to be the result of non-180° domain wall motion and quantified their effect at more than 50% of the room temperature response.

The recent investigations of Damjanovic et al. have also addressed the problem of extrinsic contributions to the piezoelectric response of PZT ceramics [38-40]. Experiments were constructed in which samples were driven with AC stresses of different amplitudes under different bias loads. The piezoelectric charge produced was then measured and plotted as a function of the amplitude of the applied stress. The contributions from the irreversible displacement of non-180° domain walls (to the direct longitudinal coefficient) was then measured quantitatively using the Rayleigh law. It was found that irreversible domain wall contributions could comprise between 20 and 40% of the piezoelectric response under the experimental conditions used.

2.5. Lead Zirconate Titanate (PZT)

PZT materials were developed in the 1950's and are the most widely used of the piezoelectric ceramics [35]. Lead zirconate titanate, $\text{Pb}(\text{Zr}_{1-x}\text{Ti}_x)\text{O}_3$, is a perovskite type solid solution between PbTiO_3 and PbZrO_3 . Variations in the zirconium to titanium ratio in the ceramic change both the ferroelectric and piezoelectric characteristics. The phase diagram is shown in Figure 2.6 and illustrates the existence of a morphotropic phase boundary (MPB). Moulson and Herbert [32] have described the MPB as an abrupt

compositions to be effectively poled. Tetragonal perovskites have six allowed polarization directions (along the $\langle 100 \rangle$ directions of the cubic prototype cell, see Figure 2.4, sec. 2.3) while the rhombohedral phase has eight (along the $\langle 111 \rangle$ directions of the cubic prototype cell, see Figure 2.5, sec. 2.3). When present in a polycrystalline ceramic the number of directions available is the sum of those present in the discrete phases which increases the number in a MPB composition to fourteen.

2.5.1. Hard and Soft PZT Ceramics

The dielectric and piezoelectric properties of PZT ceramics can be significantly changed via the introduction of different ionic species into the perovskite lattice [35]. There are a large range of properties which can be achieved, with the characteristics of the materials produced classified as either hard or soft. PZT ceramics which are donor doped, that is, doped with an atom of higher valence than the one it is replacing, are said to be soft. Typical dopants used are Nb^{5+} on the octahedral site and La^{3+} on the Pb site. The general characteristics of soft materials include low coercive fields, large remanent polarizations, large dielectric constants, high $\tan \delta$, and low aging rates. In contrast, hard materials are acceptor doped, i.e. doped with elements of lower valence than the one they are replacing. Common dopants used in PZT are Sc^{3+} , Fe^{3+} , and Cr^{3+} which substitute for Zr^{4+} or Ti^{4+} . Hard materials have larger coercive fields, relatively small dielectric and piezoelectric constants, low dielectric losses, and large aging rates. The difference between the two types of materials is largely attributed to the ease of domain wall motion, with the soft material having more mobile domain walls, and thus larger extrinsic contributions to the properties.

2.6. Mechanical Plate Theory

The determination of the transverse piezoelectric coefficient (d_{31}) of PZT thin films is the subject of chapter 5. The wafer flexure technique, which was developed to characterize the d_{31} coefficient, relies upon mechanical plate theory to calculate the magnitude of the biaxial stresses applied to the films. There has been extensive work devoted to plate mechanics, with perhaps the most well-known summary provided by Timoshenko and Woinowsky-Krieger [41]. Plate problems are defined by a number of criteria such as the loading conditions, the geometry of the plate, the boundary conditions, and the amount of deflection the plate experiences.

For a simply supported plate the boundary conditions for the position $r = a$ (where r is distance from the center of the plate and a is the support radius) are the deflection (w) and the radial bending moment (M_r) are zero, i.e.

$$\text{at } r = a: w, M_r = 0 \quad (2.4)$$

while for a clamped condition at $r = a$ the deflection is zero and the slope of the deflection with radius is zero, i.e.

$$\text{at } r = a: w, \frac{dw}{dr} = 0. \quad (2.5)$$

The wafer flexure technique utilizes uniformly loaded, clamped circular wafers for which the deflection at the center of the substrate is described as:

$$w = \frac{pa^4}{64D} \quad (2.6)$$

where w is deflection at the center of the plate (m), p is the applied pressure (N/m^2), a is the support radius (m), and D is the flexural rigidity of the plate ($\text{N}\cdot\text{m}$). The flexural rigidity is expressed as:

$$D = \frac{Et^3}{12(1-\nu^2)} \quad (2.7)$$

where E is the Young's modulus of the plate (N/m^2), t is the thickness of the plate (m), and ν is Poisson's ratio.

If the deflection predicted by eq. (2.6) is less than 20% of the plate's thickness, the radial (σ_r) and tangential stresses (σ_t) on the plate are described with small deflection plate theory and are written as

$$\sigma_r = \frac{3pz}{4t^3} [(1+\nu)a^2 - (3+\nu)r^2] \quad (2.8)$$

$$\sigma_t = \frac{3pz}{4t^3} [(1+\nu)a^2 - (1+3\nu)r^2] \quad (2.9)$$

where σ_r and σ_t are the radial and tangential stresses on the plate (N/m^2), p is the pressure applied to the plate (N/m^2), z is the distance from the neutral axis (m), and r is the distance from the center of the plate (m).

The derivation of eqs. 2.8 and 2.9 is well reported elsewhere (see e.g. ref. [41, 42]). However, the major assumptions inherent in the development are not immediately apparent and for that reason they are listed in Table 2.2.

TABLE 2.2. Assumptions Made for the Small Deflection Analysis of a Thin Clamped Plate [41]

(1)	There is no deformation in the middle plane of the plate. The plane remains neutral during bending.
(2)	Points of the plate lying initially on a normal-to-the-middle plane of the plate remain on the normal-to-the-middle surface of the plate after bending (i.e. no shear).
(3)	The normal stresses in the direction transverse to the plate can be disregarded.

2.7. Stresses in Thin Films

The observation has been made by a number of researchers that the limited electromechanical behavior of PZT thin films could be related to the mechanical clamping of ferroelectric domains (i.e. a reduction of the extrinsic contribution) brought about by the residual stress on the film [3]. The investigation described in chapter 4 was designed therefore to alter the state of residual stress and measure the changes brought about in the film's piezoelectric and ferroelectric characteristics.

2.7.1. Sources of Film Stress

The deposition of thin film materials onto thick substrates usually results in a state of biaxial stress being imposed on the film. The total stress (σ_{tot}) produced is comprised of both thermal (σ_{th}) and intrinsic components (σ_i) and can be expressed as [43]:

$$\sigma_{tot} = \sigma_{th} + \sigma_i \quad (2.10)$$

where the thermal stress can be quantified as [44]:

$$\sigma_{th} = \frac{E_f}{(1-\nu_f)} (\alpha_f - \alpha_s)(T_1 - T_2) \quad (2.11)$$

where E_f and ν_f are the Young's modulus and Poisson's ratio of the film, T_1 and T_2 are the annealing and ambient temperatures, and α_f and α_s are the thermal expansion coefficients of the film and substrate.

The intrinsic stress is that component of the measured in-plane stress that cannot be attributed to thermal expansion mismatch. The source of the intrinsic stress is commonly attributed to the effect of microstructural and/or crystallographic flaws that are built into the film during deposition when deposition temperatures are less than $1/3^{\text{rd}}$ the melting point. Muraka [43] has reviewed a number of sources for intrinsic stress components and among them are lattice mismatch between the film and substrate (epitaxial films), film microstructure and purity, defects in the film, and volume changes associated with chemical or metallurgical interactions. Intrinsic stresses primarily result from high temperature physical vapor deposition processes (e.g. sputtering) and investigations with sol-gel PZT films have indicated that the residual stresses in that system are primarily thermal in nature (see sec. 2.7.3).

2.7.2. The Measurement of Residual Film Stress

The experimental techniques used for measuring residual film stress consist of either direct X-ray methods for the measurement of elastic strains in the films, or wafer curvature measurements for the calculation of residual stress [43]. X-ray techniques permit the measurement of all components of stress in the film, i.e. in and out of plane components. The films however, must be crystalline, which precludes the characterization of amorphous films. Even for crystalline films, the characterization of

residual film stress is most often carried out via the measurement of either substrate curvature or deflection, which is often preferred as a result of its relative convenience and applicability to special conditions (e.g. high temperature measurements).

The characterization of residual film stress is made with wafer curvature measurements by determining the change in the radius of curvature of the substrate, R , before and after deposition (or conversely before and after removal) of a film. The radius of curvature is then input to the Stoney formula (derived by Stoney in 1909, modified for the biaxial condition of a plate by Hoffman in 1966) to determine the residual in-plane stress on the film. The expression for residual film stress is [45]:

$$\sigma_f = \frac{1}{6R} \cdot \frac{E_s t_s^2}{(1-\nu_s)t_f} \quad (2.12)$$

where σ_f is the film stress, E_s is the Young's modulus of the substrate, ν_s is the Poisson's ratio of the substrate, t_s is the substrate thickness, and t_f is the film thickness. It is important to note the elastic properties of the film need not be known in order to calculate the residual stress in the film.

2.7.3. Residual Film Stress in Lead Zirconate Titanate Thin Films

There have been relatively few experimental investigations of the magnitude of the residual film stress in PZT films. Investigations have been conducted by Tuttle et al. [46] and Spierings et al. [47] on submicron sol-gel films with compositions near the morphotropic phase boundary. Results from those studies showed that when deposited on platinized silicon substrates the residual stress is tensile with a magnitude of about 100

MPa.

Spierings et al. [47] investigated the origins of the residual film stress, i.e. whether the stress was thermal or intrinsic in nature. Empirical data were collected as a function of temperature and compared to predictions made with eq. 2.12. Calculations were made to account for the anisotropy of the thermal expansion coefficient of the PZT and the different crystallographic orientations of material in the film (i.e. random, (100) oriented, and (001) oriented). Reasonable agreement was obtained when the polarization vector was assumed to lie parallel to the plane of the substrate. The thermal stresses were calculated with the elastic properties of a bulk, unpoled PZT ceramic and although the authors accounted for the anisotropy of the thermal expansion coefficients, they did not account for the anisotropy of the mechanical constants. If it is assumed, based on the empirical results of Tuchiya et al. [48] and Kanno et al. [49], that the Young's modulus of the film is larger than that of a PZT ceramic, then the relative agreement between the calculated thermal stresses and the empirical data is improved, which yields even stronger evidence for the thermal nature of the film stress.

2.7.4. The Transformation Stress Model

The role of film stress has been proposed to play an important role in the domain structure of PZT thin films. Tuttle et al. [46, 50] proposed that the observed electrical properties of PZT films are directly related to the sign of the film stress at the transition temperature. Experiments were conducted with 0.3 μm thick 40/60 sol-gel films in which the films were deposited on magnesium oxide or silicon substrates. The differences in the thermal expansion coefficients of the two materials relative to the PZT film resulted in a

different sign of stress at the paraelectric to ferroelectric transition. The films which were in a state of compression (i.e. those on magnesium oxide substrates) transformed with the c-axes of their crystallites configured normal to the substrate surface and displayed large values of remanent polarization (from 50 to 60 $\mu\text{C}/\text{cm}^2$). In contrast, films subjected to a tensile stress (i.e. those on silicon substrates) at T_c transformed with their c-axes more parallel to the substrate surface and yielded smaller values of remanent polarization (less than 40 $\mu\text{C}/\text{cm}^2$). The film's textures were confirmed with X-ray diffraction and the differences in their electrical properties were reasoned to result from the relative orientation of their domains.

2.8. The Effects of Applied Mechanical Stress on PZT Ceramics

Because PZT ceramics are improper ferroelastics (and so are ferroelastic as well as ferroelectric) it is necessary to consider the effects of mechanical stress of their properties. Early investigations into the effects of mechanical stress on PZT were brought about in response to the aggressive design criteria outlined for deep-sea underwater transducers. As the depths at which the transducers were to operate increased, the hydrostatic pressures of the surrounding ocean rose commensurately. Depending upon the design of the transducer employed, the working material, typically PZT-4 (doped with Sr^{2+} or Cr^{3+}) or PZT-5A (donor doped with Nb^{5+}), can be subjected to either uniaxial or biaxial loads applied perpendicular or parallel to the poling direction of the material. To investigate the effects of such extreme working environments, a great deal of work was conducted throughout the 1960's on the effects of mechanical stress on the dielectric and piezoelectric characteristics of a number of ferroelectric ceramics [51, 52].

2.8.1. The Effects of Uniaxial Stress on the Dielectric and Piezoelectric Characteristics of PZT Ceramics

The seminal work on uniaxial stress effects was conducted by Krueger in a three part series published in 1967 [52-54]. The author conducted extensive studies on the stress dependence of the dielectric and piezoelectric properties of a number of hard and soft PZT ceramics. Loads were applied both parallel [52] and perpendicular [54] to the poling direction of $\frac{1}{2}$ " ceramic cubes while clamped in a uniaxial testing machine. The dielectric constant and $\tan \delta$, together with the d_{33} coefficient were then measured as a function of the magnitude of the applied stress and the number of stress cycles.

Figure 2.7 shows the stress response for PZT-4 and PZT-5A specimens loaded parallel to the poling direction over the first four stress cycles. Note that the scale on the PZT-5A data is changed from 20 kpsi (138 MPa) on the top graph to 10 kpsi (69 MPa) on the bottom three. The change was made because of the drastic degradation of polarization observed in the d_{33} coefficient beyond the 10 kpsi peak.

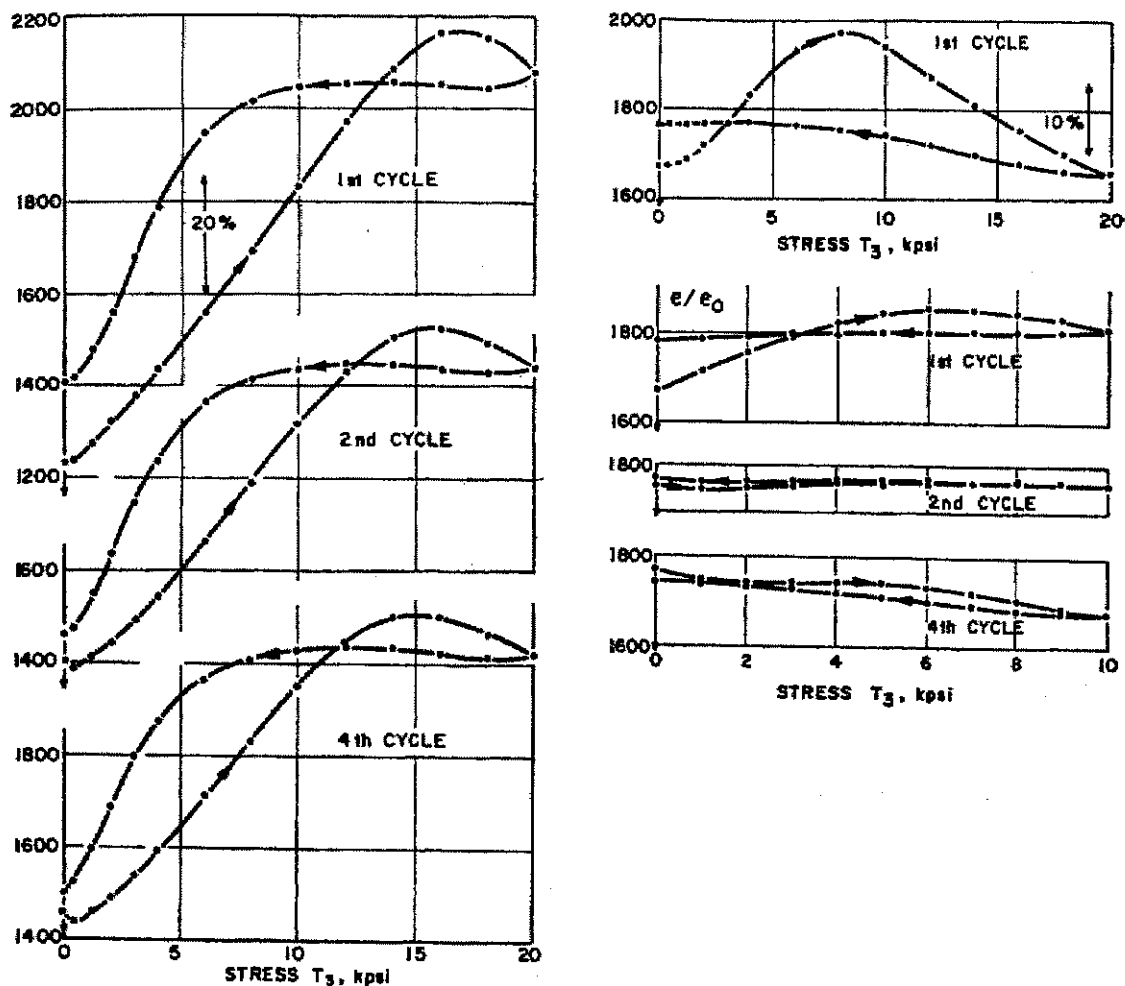


Figure 2.7. The effects of applied uniaxial compressive stress on the dielectric constant of PZT-4 (left side) and PZT 5A (right side). Stress was applied parallel to the polar axis. Data taken from Krueger [52].

The data from the 1st compressive load cycle shows that the dielectric constant increased by almost 80% for the PZT-4 and 15% for the PZT-5A with peaks of ϵ_r located at about 16.5 kpsi (114 MPa) and 8 kpsi (55 MPa), respectively. The later loading cycles showed a decrease in the magnitudes of the changes produced for both materials (maximum increase of 45% for PZT-4 and a 6% decrease for PZT-5A) with a superior stability and less hysteresis displayed by the PZT-5A. The flatter response for the PZT-

5A was a result of the permanent reorientation of dipoles under the first application of stress (so there was little driving force for domain reorientation on subsequent cycles).

The uniaxial stress response of the PZT-5A is composed of both intrinsic and extrinsic contributions to the dielectric characteristics. With the initial application of compressive stress, ferroelectric domain walls are depinned from their well-aged, low energy configurations, which increases both the domain wall mobility and the dielectric constant. Concurrent with the depinning effect is the depoling and reorientation of the ferroelectric domains, as was indicated by the rapid decrease of the d_{33} coefficient (not shown). With an additional increase of applied stress the ceramic is completely depoled, the extrinsic and intrinsic contributions become mechanically clamped, and as a result both the ϵ_r and $\tan \delta$ are reduced.

The effects of uniaxial stress on the ferroelectric characteristics of hard PZT's differs from that of soft PZT's due to the modulating influence of defect dipoles in the material. Recall from Figure 2.7 that the dielectric constant of PZT-4 increased by almost 80% as compared to the 15% increase for PZT-5A for a compressive stress of 17 kpsi (120 MPa). Nishi [55] showed a similar effect in hard PZT ceramics, with ϵ_r increasing by about 50% for 10 kpsi (69 MPa) of compression while Zhang et al. [56] reported a 60% increase for a stress range of 150 MPa.

The stability of the domain structure brought about by the presence of reorientable defect dipoles in PZT-4 is the fundamental source of the large increase of the dielectric constant. Zhang et al. [56] reasoned that when a stress is applied parallel to the polarization vector, the ferroelectric domains attempt to reorient to positions more perpendicular to the load. The defect dipoles however, oppose the reorientation, which

results in a metastable domain configuration. The domain structure has thus been destabilized and reset to a condition analogous to an early stage of the aging cycle, i.e. the material has been "de-aged". As such, the dielectric constant and $\tan \delta$ increase as additional stresses shift the polarization vectors to less energetically favorable configurations. Hard PZT ceramics can be depoled if the applied stress is high enough however, on unloading the defect dipoles tend to restore the original domain configuration.

2.8.2. The Effects of Biaxial (Two-Dimensional) Stress on the Dielectric and Piezoelectric Characteristics of PZT Ceramics

Investigations into the effects of planar (i.e. two-dimensional) stress on the characteristics of PZT ceramics were made in the 1960's [51, 57] with even earlier work conducted on barium titanate in the late 50's [58]. The data are critical to an understanding of ferroelectric films since virtually all films are under appreciable in-plane stress.

The most comprehensive treatments on the effects of biaxial stress have been presented in a series of papers by Brown [51] and Brown and McMahon [57]. The authors studied the effects of two-dimensional stress on the dielectric characteristics of a number of poled barium titanate and lead zirconate titanate ceramics. To investigate the effects, two different experimental configurations were used: either a ceramic cylinder (see Figure 2.8) or a ceramic sphere submerged in an hydrostatic water bath. Stresses applied to the material were calculated from the dimensions of the ceramic sample (sphere or cylinder) and the applied hydrostatic pressure.

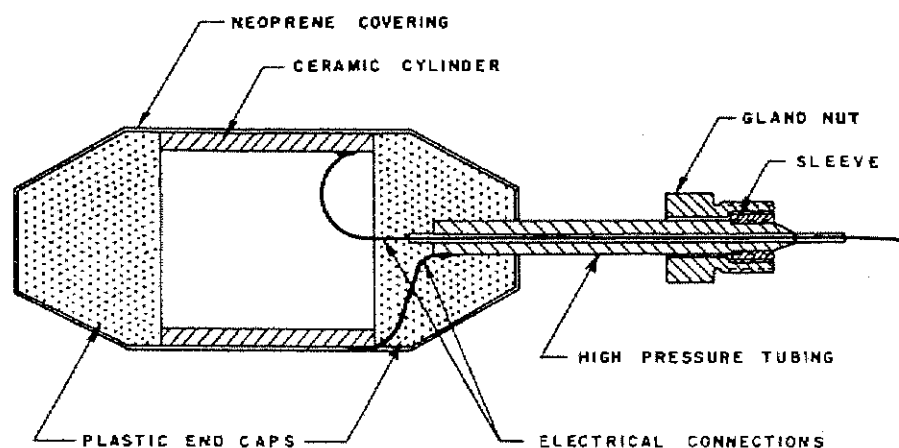


Figure 2.8. The experimental biaxial stress configuration of Brown [51]. The ceramic cylinder was poled radially and the setup placed in a hydrostatic water tank. An increase of the pressure in the tank increased the biaxial stress in the walls of the ceramic.

The results of the biaxial compression experiments showed that with an increase of stress, the dielectric constant decreased and $\tan \delta$ increased. Figure 2.9 shows the results for PZT-4 and PZT-5 ceramics. The data in the plots are normalized and presented as the *sum* of the principal stresses on the material. The data show that on the 1st stress cycle the dielectric constant decreased by about 50% for the PZT-4 and about 70% for the PZT-5 for an applied stress of 4000 kg/cm^2 (400 MPa). The changes produced in the PZT-4 were largely reversible while the PZT-5 experienced a permanent 40% reduction.

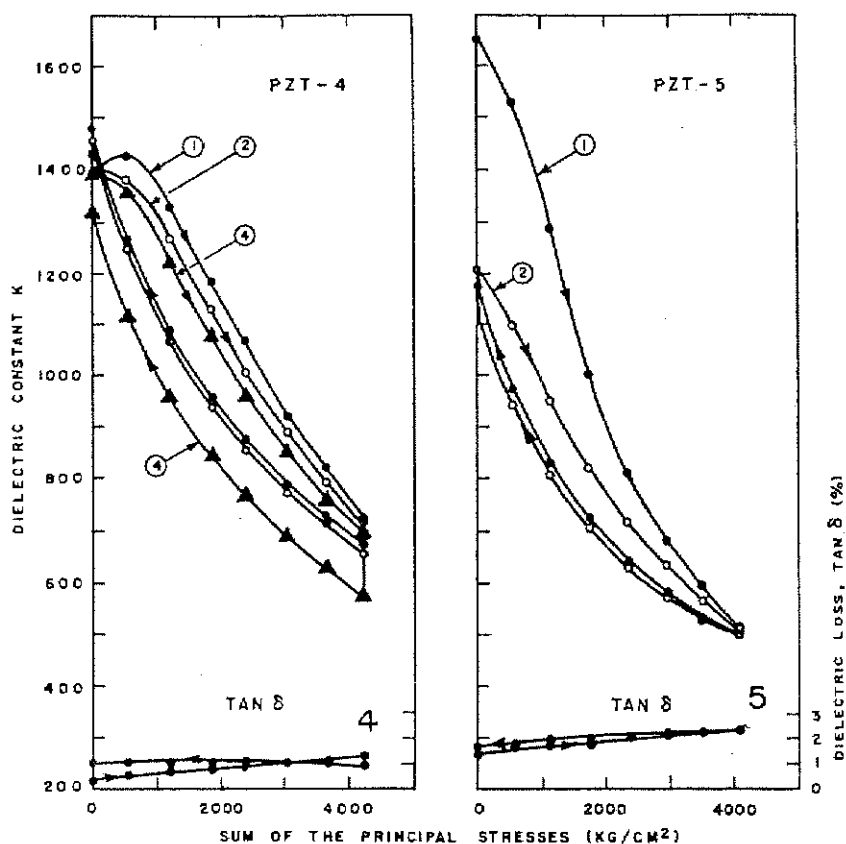


Figure 2.9. The effects of biaxial compressive stress on the low-field characteristics of PZT ceramics. Data on the left are for PZT-4 while data on the right were taken from PZT-5 (note that $1 \text{ kg/cm}^2 \sim 0.1 \text{ MPa}$).

The changes of the dielectric constant shown in Figure 2.9 are attributed by Brown to be the result of domain reorientation in the ceramics. Upon application of the compressive stress, the domains reorient into configurations normal to the applied load (the compressive stress is in the plane of the ceramic). The reorientation of the domains results in the decrease of the dielectric constant, which was assumed to result from the anisotropy of the dielectric constant ($\epsilon_3 < \epsilon_1$). Closer inspection of the data collected on the 1st pressure cycle showed that the dielectric constant of the PZT-4 underwent an initial increase with compressive stress. That increase was caused by the depinning of

domains, which increased the domain wall mobility and raised the dielectric constant. For stresses beyond the initial peak (PZT-4 only) the change of the dielectric constant was dominated by domain reorientation and ϵ_r decreased as is shown in Figure 2.9.

Piezoelectric measurements were also made as a function of applied planar compression [57]. The measurements were made on thin walled spheres fabricated from PZT-4 and PZT-5 ceramics. The samples were poled in the radial direction and measurements made of the transverse piezoelectric coefficients. Results were collected to maximum stresses of 240 MPa and indicated that the d_{31} coefficients decreased in a fashion similar to that of the dielectric constant.

This decrease in the piezoelectric coefficients was again attributed to reorientation of ferroelastic domains. As described by Rotenberg [59], when subjected to planar loads the domains which lie normal to the direction of polarization would be reoriented to a direction normal to the load (as is expected). The polarization vector of the reoriented domain would however, be configured antiparallel (and not parallel to) the poling direction. The antiparallel reorientation is more energetically favorable and would reduce both the net polarization of the material and its piezoelectric coefficients.

2.9. Characterization of the Piezoelectric Coefficients of Thin Films

The research in this dissertation was conducted with two separate objectives as was described in chapter 1. The first was concerned with the investigation of biaxial stress effects, while the second was devoted to the design and development of the wafer flexure technique for the characterization of the transverse piezoelectric coefficient (d_{31}) of thin films. The review given here is intended to provide a historical record of earlier

efforts at the piezoelectric characterization of films.

In many of the early reports on piezoelectric films, the films were integrated with prototype transducer designs (as illustrated in Figure 2.10) which did not require knowledge of the film's piezoelectric coefficients. Rather, the performance of the films was measured in terms of the relative coupling factor (compared to the single crystal material) and their insertion loss at operating frequencies. As a result, the database on thin piezoelectric films is limited, with few piezoelectric constants reported.

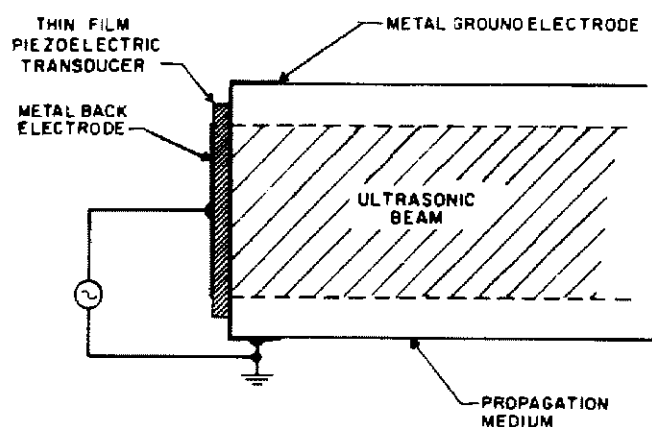


Figure 2.10. An example of a configuration used for the identification of piezoelectricity in piezoelectric thin films [19].

2.9.1. Converse Techniques for the Piezoelectric Characterization of Thin Films

There have been a number of converse techniques (i.e. those which are based on the converse piezoelectric effect) developed from which the piezoelectric coefficients of thin films have been determined [60, 61]. Perhaps the most well developed method for the piezoelectric characterization of thin films is laser beam interferometry. Early work

on interferometric characterization of ferroelectric materials was described by Allensworth [62], who utilized a variation of the Michelson interferometer to measure the mechanical strains produced by ferroelectric domain switching in a 65/35 PZT ceramic. Later interferometers were constructed to investigate the piezoelectric (or electrostrictive) response of both ceramics and thin films with the designs described in the papers from Zhang et al. [63], Pan and Cross [64], Li et al. [65], and Kholkin et al. [3].

Interferometers can be set up in either single beam (Michelson-Morley) or double beam (Mach-Zehnder) configurations depending upon the intended application. The schematic in Figure 2.11 is an illustration of a double beam setup [64]. The resolutions for interferometric techniques have been reported at between 10^{-4} to 10^{-5} Å [3]. For the investigation of bulk ceramic specimens a single beam configuration is sufficient provided the sample has been fabricated with a cubic geometry [65]. For thin films however, single beam setups are only applicable to transverse piezoelectric characterization (i.e. d_{31}). The reason for that restriction is related to production of additional displacements associated with substrate flexure due to the composite motions of the film-substrate system when a small area of the film is excited. With measurements made from only one face of the sample, the flexural motions cannot be distinguished from the piezoelectric dilation of the film. The result is anomalously large apparent strains and inflated d_{33} coefficients. The same error source can be important in any converse measurement conducted using a single surface measurement. As a result, the characterization of the d_{33} coefficients in thin films must be conducted with a double beam setup which is designed to account for the displacements of both the film and its substrate.

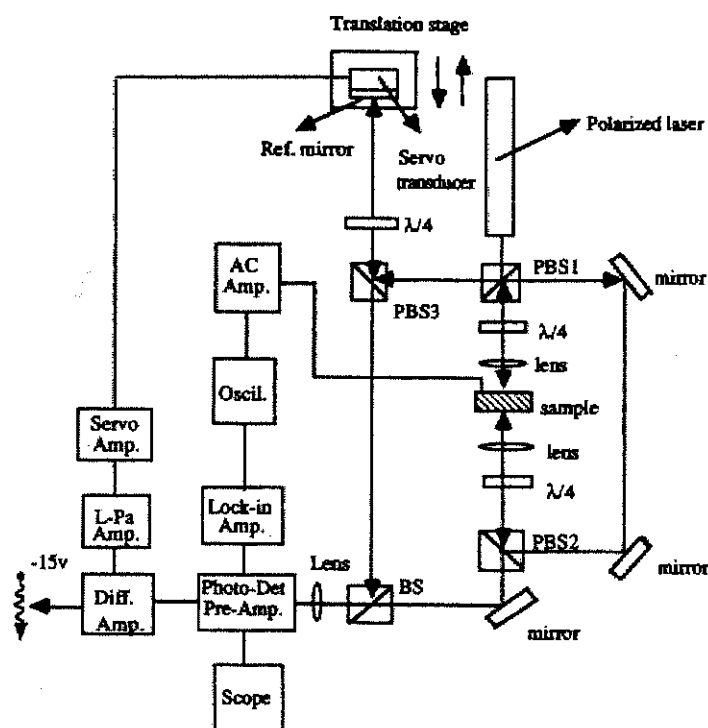


Figure 2.11. A schematic of a double beam Mach-Zehnder interferometer. From Pan et al. [64]. In the plot BS and PBS stand for beam splitter and polarized beam splitter, respectively.

The laser beam interferometer is based on the change of detected light intensity produced as a reference beam is recombined with a probe reflected off the surface of an oscillating piezoelectric sample. Interference between the two beams results in a variation of the light intensity at the photodetector which is expressed as [3]:

$$I = \frac{1}{2}(I_{\max} + I_{\min}) + \frac{1}{2}(I_{\max} - I_{\min}) \sin\left(\frac{4\pi\Delta L}{\lambda}\right) \quad (2.13)$$

where I_{\max} and I_{\min} are the maximum and minimum intensities of the interference fringes, ΔL is the optical path-length difference induced by the oscillation of the sample, and λ is

the wavelength of the laser light. When the displacement ΔL is much less than the full fringe range, the sine function in eq. 2.13 can be replaced with its argument. The light intensity at the photodetector is converted to a voltage which is expressed as:

$$V_{\text{out}}(t) = V_{\text{dc}} + \left(\frac{2\pi}{\lambda}\right)V_{\text{pp}}\Delta L(t) \quad (2.14)$$

where V_{pp} is the peak-to-peak voltage corresponding to the full fringe displacement (i.e. $I_{\text{max}} - I_{\text{min}}$) and V_{dc} is the dc offset. From knowledge of the peak-to-peak voltage, which is obtained by moving the reference mirror over a distance of greater than $\lambda/2$, and the wavelength of the laser, the change in the optical path length (ΔL) is measured. This gives the surface displacement of the piezoelectric sample, from which the piezoelectric coefficients can be characterized.

Interferometric techniques have been used with considerable success for the piezoelectric characterization of thin films. Their resolution and high-frequency capabilities make them attractive tools for piezoelectric thin film research however, there are drawbacks, with cost and complexity perhaps the most notable. In light of that fact, there has been a considerable effort over the years to develop a quick and simple technique to characterize the electromechanical behavior of thin films.

2.9.2. Direct Techniques for the Piezoelectric Characterization of Thin Films

There have been a number of attempts in the past to utilize the direct piezoelectric effect to characterize piezoelectric films. Perhaps the earliest technique was designed by Dybwad in 1971 [66]. The device is illustrated in Figure 2.12 and is analogous to the

Berlincourt meter. Pressure fluctuations were delivered to sample films by a hydraulic pulse and electrical contact was made with a gold plated bellows. Piezoelectric characterization was accomplished via the detection of a voltage pulse on the screen of an oscilloscope and the relative piezoelectric activity of different films was quantified by a direct comparison of the signals generated.

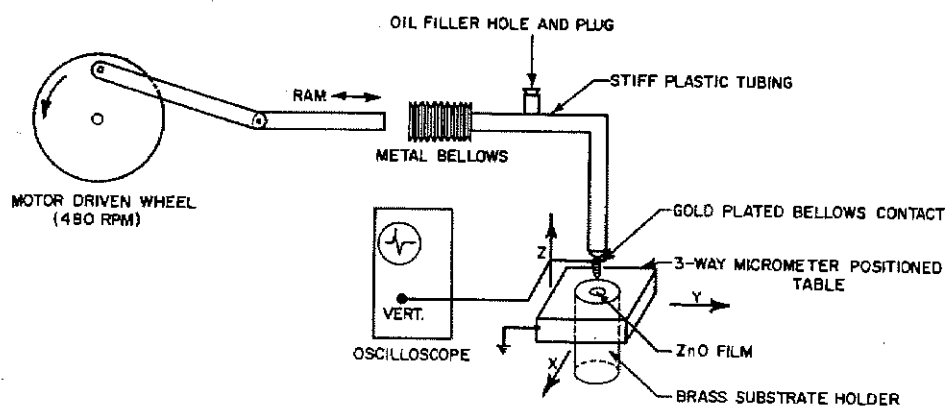


Figure 2.12. The normal load method for the piezoelectric characterization of thin films [66]. The motor driven ram was used to drive a metal bellows which applied a hydraulic pulse to the piezoelectric film. The stress on the film created an electrical voltage which was registered on the screen of an oscilloscope.

The device illustrated in Figure 2.12 could identify piezoelectricity in thin films, but could not quantify the longitudinal piezoelectric coefficient. That limitation was the result of the rig's unknown boundary conditions. The effects of lateral stress could not be controlled, which meant that transverse contributions (i.e. d_{31} components) to the electric charge could not be quantified. In addition, the electrode's contact area was flexible and the applied hydraulic load was an unknown. The resulting difficulties in the calculation of the normal stress leads to significant errors in the calculation of d_{33} .

There have been several authors that used similar probe type designs [5, 67] but the devices constructed were limited to simple charge generation and voltage measurements. Quantification of the d_{33} coefficient was not possible as a result of the numerous unknowns in those systems. In contrast, Surowiak and Czekaj [68] designed the rig shown in Figure 2.13 and directly measured the d_{33} coefficients of PZT thin films. The principle of operation is based upon the oscillation of solid hemispherical probe tips. The change of tip displacement stresses the film and results in the production of an electric charge. The charge is then converted to a voltage, amplified, and used to calculate the film's d_{33} coefficient. Data were reported for sputtered PZT films (0.6 and 4 μm thick) are between 70 and 120 pC/N and are in reasonable agreement with more recent d_{33} investigations.

Additional devices which use the direct effect have been reported by Lefki and Dormans [69] and Ren et al. [70]. The first was designed around the application of a mechanical force to the surface of a PZT film with a rectangular metallic tip. Charge was collected on a large shunt capacitor and the voltage across the capacitor measured with a high impedance voltmeter. Data collected from the rig were reported to be between 200 and 400 pC/N for CVD and sol-gel films, respectively. Those numbers are questionable in light of the limited extrinsic contributions to the ferroelectric characteristics of PZT thin films (discussed in chapter 4). Possible sources for the over approximation are contributions from lateral stresses (i.e. a mixed mode condition) or an uneven distribution of the applied stress (the films tested were between 0.2 and 0.6 μm thick, dust between the probe and PZT could affect the distribution of stress). Problems with Lefki's design were rectified by Ren et al. [70] who designed a similar rig with a conductive rubber tip.

The elastic nature of the tip insures intimate contact with the film's surface and thus a uniform stress distribution. The electronics and charge measurements were analogous to Lefki's setup. Data were collected from 0.8 μm thick 50/50 PZT films prepared by a metallo-organic deposition procedure. The d_{33} coefficients of the poled films were reported to be about 100 pC/N and are in acceptable agreement with the coefficients reported from other researchers [68, 71].

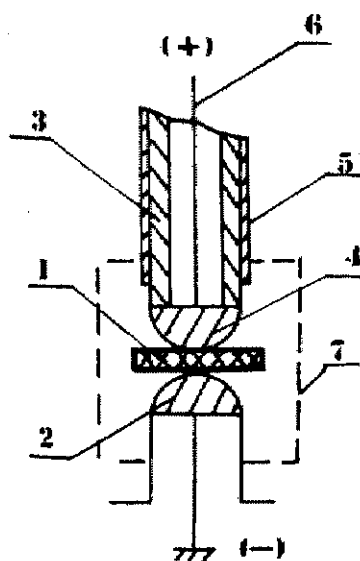


Figure 2.13. The piezoelectric characterization device designed by Surowiak and Czepak [68]. The piezoelectric sample (#1) is held between the two hemispherical electrodes (#2) while the shaft is oscillated. The bottom electrode (#2) is connected to ground and the top electrode (#4) is fed to the charge detection equipment (#6).

2.9.3. Measurements of the Transverse Piezoelectric Coefficients of PZT Thin Films

The characterization of the d_{31} coefficient of piezoelectric thin films has been accomplished with both direct [49] and converse methods [4, 72]. Interferometric and

other optical techniques have been used to derive the electrically-induced displacement of small PZT coated cantilevers (or diaphragms) from which the d_{31} coefficient (which is responsible for the displacement) can be calculated. The cantilever technique is an indirect method however, and requires that the d_{31} coefficient be calculated from the equations which describe the bending displacement of a piezoelectric bimorph [30, 73]. Because the models require knowledge of the film's in-plane elastic constants and those values are often unknown, the d_{31} coefficients derived can be incorrect.

Kanno et al. [49] developed an alternative technique which also requires the microfabrication of PZT-coated cantilever beams. The beams are constructed by wet etching the magnesium oxide substrate back from the platinum bottom electrode, thus leaving a composite beam consisting of Pt/PZT/Pt. The lateral expansion of the beam is then measured directly using a laser microscope. The change in length is used to calculate the strain produced in response to the applied field, from which the film's d_{31} coefficient can be directly calculated.

There has to this point been little work conducted on the d_{31} characterization of PZT thin films. The techniques used to collect most d_{31} data (direct or converse) all suffer from the same problem, that is the elastic properties of the PZT film must be known. The majority of authors utilize bulk ceramic moduli in their calculations. However, there could be a significant deviation between the Young's modulus of PZT films and their bulk ceramic counterparts. That discrepancy could be the source of the considerable scatter among the d_{31} data in the literature.

Table 2.3 is a compilation of d_{31} coefficients reported for a number of different PZT films measured by several different techniques. The magnitude of the coefficients

are given together with the film's specifications (i.e. thickness, composition, etc.). The data presented are taken only from films with large remanent polarizations, dielectric constants and low dielectric losses. Variations in the d_{31} data are expected to be the result of the different mechanical characteristics assigned to the PZT films, their different microstructures, and the different characterization techniques used to make the measurements.

TABLE 2.3. Transverse Piezoelectric Coefficients (d_{31}) of PZT Thin Films

Reference	d_{31}	Measurement Technique	Deposition (Zr/Ti Ratio)	Thickness (μm)	Elastic Modulus (GPa)	Poling Conditions
Toyama et al. 1994 [6]	-33	Oscillating beam	ECR sputtering (MPB)	0.40	63	As-deposited
Udayakumar et al. 1994 [23]	-88	Interferometer, cantilever beam	Sol-gel (MPB)	0.38	25	200 kV/cm AC field
Watanabe et al. 1995 [60]	-96	Interferometer	RF magnetron sputtering (MPB)	1.0	37	50 kV/cm for 10 min. ($E_c=100$ kV/cm)
Tuchiya et al. 1996 [48]	-30	Interferometer, diaphragm	Sol-gel (MPB)	3.1	101	Film was poled, conditions not given
Muralt et al. 1996 [72]	-35	Interferometer, diaphragm	Sputtered (45/55)	0.6	92	70 kV/cm DC bias
Luginbuhl et al. 1996 [4]	-32	Interferometer, cantilever beam	Sol-gel NA	0.44	72	270 kV/cm DC bias
Sakata et al. 1996 [74]	-100	Bending beam	Magnetron sputtering (45/55)	None given	75	100 kV/cm at 200°C
Kanno et al. 1997 [49]	-100	Optical lateral displacement	RF magnetron sputtering (Epitaxial 50/50)	3.6	NA	As-deposited

The elastic moduli reported in Table 2.3 show a significant amount of scatter and it is unclear how a number of the values were derived. The elastic modulus of polycrystalline PZT ceramic is reported to be about 70 to 90 GPa [32, 35]. Because the crystal structure of thin films is the same as the bulk materials, it is expected that Young's modulus would be comparable (the crystallographic texture of films, the submicron grain sizes, and the clamping of ferroelastic walls could lead to some deviation). However, magnitudes as small as 25 GPa [23] and as large as 400 GPa [22] have been reported. Because the d_{31} coefficient is inversely proportional to the applied stress, low values of the elastic modulus will yield high d_{31} coefficients and high values of the elastic modulus will yield low d_{31} coefficients.

3. Experimental Procedure

3.1 Introduction

The objectives of this investigation were divided along two fronts, with research devoted to (1) the investigation of the effects of biaxial stress on the dielectric characteristics of PZT thin films, and (2) the development of the wafer flexure method for the characterization of the d_{31} piezoelectric coefficient. This chapter describes the experimental procedures used for both of those investigations, as well as a description of the thin film fabrication.

3.2. Deposition of PZT Thin Films

Lead zirconate titanate thin films have been used throughout this investigation. Films were synthesized at Penn State using two sol-gel methods, a methoxyethanol solvent chemistry technique and an acetate-based approach. The former were relatively thin (less than 2.5 μm) while the latter were up to 5 μm in thickness. In general, the former were crystallized by rapid thermal annealing, while the latter were heat treated for longer times in a conventional furnace. Additional films were provided by Matsushita corporation and were fabricated by RF magnetron sputtering. This section details the processing of each type of film.

3.2.1. Rapid Thermal Annealed Films

PZT thin films were synthesized with compositions across the morphotropic phase boundary (zirconium to titanium ratios of 60/40, 56/44, 52/48, 48/52, 40/60) using a variation of the procedure described earlier by Budd, Dey, and Payne [75]. Lead acetate trihydrate was dissolved in 2-methoxyethanol, distilled and refluxed at 110°C, and combined with titanium-IV isopropoxide and zirconium-IV propoxide (Aldrich Chemical, Milwaukee, WI). Solutions were made in 0.5 molar concentrations and spin coated at 3000 rpm on platinized (100) silicon substrates (Nova Electronics, Richardson, TX). Each substrate had 1 μm of thermal oxide sputter coated with a 200 Å titanium adhesion layer and 1500 Å of (111) platinum. Following pyrolysis at 300 to 360°C, additional layers were spin-coated to build up the desired thickness. Lead volatilization was discouraged (during the subsequent annealing step) with either 12% excess lead in the solution or via the utilization of a lead oxide overlayer [76, 77]. Films were crystallized in an AG Associates, Heatpulse 210 rapid thermal annealer at 700°C for 60 sec. Individual crystallization steps were conducted for thicker films after every fourth coating to minimize cracking of the resulting film. Final film thicknesses ranged from 0.4 to 2.5 μm thick. Additional details on the processing are given elsewhere [78]. Pt top electrodes were sputtered through a 1.5 mm diameter shadow mask and post-annealed at 400°C for 60 sec.

3.2.2. Conventional Furnace Annealed Samples

Thicker films crystallized in a conventional furnace were also investigated in the study of biaxial stress effects. The films were synthesized using the sol-gel procedure described by Chen [79] with 52/48 compositions, thicknesses of 3 and 5 μm , and strong (100) textures. Precursor solutions were made with 20 mol% excess lead via the dissolution of lead acetate trihydrate in acetic acid. The solutions are taken through a distillation step at 105°C and mixed with zirconium *n*-propoxide and titanium isopropoxide after cooling to room temperature. Ethylene glycol and deionized water are then added to the solution to control the viscosity and concentration. The final solution was then spin cast at 7500 rpm onto platinized silicon substrates. Each layer was dried at 150°C to evaporate the solvent, rapidly heated to 400°C to remove residual organics, and preannealed at 600°C to densify the film. Multilayer films were then crystallized at 700°C for 1 hour in a conventional box furnace. Pt top electrodes were sputtered through a shadow mask with 1.5 mm diameter holes and post-annealed at 400°C for 60 sec.

3.2.3. RF Magnetron Sputtered 50/50 PZT Films

Several 4" diameter 50/50 RF magnetron sputtered films were used in the development of the wafer flexure technique (Matsushita Electric Industrial, Kyoto, Japan). The two films studied were approximately 3.0 and 3.3 μm thick and both displayed strong (111) textures. Details of the deposition procedure are given in Table 3.1 [49]. Pt top electrodes were sputtered through a 1.5 mm diameter shadow mask.

TABLE 3.1 Sputtering Conditions for the Deposition of 4" PZT Thin Films

Target	[Pb(Zr _{0.53} ,Ti _{0.47})O ₃]0.8+[PbO]0.2 (Hot pressed)
Substrate	Pt/Ti/(SiO ₂)/Si [Pt/Ti = 1000A/500A]
Stage Temperature	600°C
Target to Substrate Distance	10 cm
RF Power	500 W
Gas Flow	Ar/O ₂ = 9.5/0.5 sccm
Pressure	1.0 Pa
Deposition Rate	0.7 – 1.0 μm/hr

3.3. Residual Stress Measurements

The residual stresses of a number of Pt-Ti bottom electrodes and sol-gel PZT films were characterized using an Ionic Systems 30120 Stress Gauge (Salinas, CA). The PZT films measured had 52/48 compositions and thicknesses of about 0.4 μm (as measured via ellipsometry). The change of the radius of curvature of the substrate was determined from the change in reflected light intensity off the back of the silicon substrate. From knowledge of the radius of curvature, the residual film stress was calculated using the Stoney formula [45]:

$$\sigma_f = \frac{1}{6R} \cdot \frac{E_s t_s^2}{(1-\nu_s) t_f} \quad (3.1)$$

where σ_f is the film stress, E_s is the Young's modulus of the silicon (150 GPa), ν_s is the Poisson's ratio of the silicon (0.172), t_s is the substrate thickness (500 μm), and t_f is the film thickness.

Curvature measurements were made for the crystallized PZT films before and after chemically removing the film from the substrate using a mixture of 10% hydrofluoric acid in deionized water. The etch removed the PZT without damaging the underlying layers.

3.4. Characterization of the Effects of Biaxial Stress on the Dielectric Properties of PZT Thin Films

The effect of biaxial mechanical stress on the low and high-field characteristics of PZT thin films was investigated to evaluate the potential role of film stress on their electromechanical properties. Films with 60/40, 56/44, 52/48, 48/52, and 40/60 zirconium to titanium ratios were prepared with the sol-gel procedures described in secs. 3.2.1 and 3.2.2. The films tested ranged from 0.4 to 5 μm thick and possessed either a (111) or (100) crystallographic texture. Controlled stress states (compressive or tensile) were imposed upon the films with a rig designed to apply a constant gas pressure to either a PZT coated silicon wafer or a PZT coated chip bonded to a predeformed steel substrate. The remanent polarization, coercive field strength, dielectric constant, and $\tan \delta$ were measured as a function of the applied stress (sec. 3.4.4) for levels on the order of ± 100 MPa.

3.4.1. The Uniform Pressure Rig

Controlled biaxial stresses were applied to the PZT films using two separate methods. The first design is illustrated in Figure 3.1 and utilized complete 3" silicon

substrates which were clamped between two 3.5" Viton O-rings PZT side up (i.e. facing away from the housing). The PZT coated substrate, when clamped, formed a pressure seal above a small cavity behind the test sample. The subsequent evacuation (with a 1 micron roughing pump) or pressurization (with a gas bottle/regulator combination) of the pressure chamber flexed the wafer, and placed the film on the surface in a controlled state of biaxial compression or tension. The stress applied to the films was quantified via resistance strain measurements at the center of a number of PZT coated wafers as a function of applied gas pressure (± 85 kPa). Results from those tests indicated the maximum stresses to be 115 MPa and -40 MPa for the tensile and compressive configurations, respectively. The stress level of the compressive experiments was an unexpected result (discussed in detail in chapter 4) for it did not relieve the residual tension on the film (measured in the residual stress tests at about 100 MPa). That limitation forced the development of the alternative, chip-on-steel experiments (to be discussed in sec. 3.3.3.), in order to achieve the compressive stresses needed to relieve the residual stress on the films.

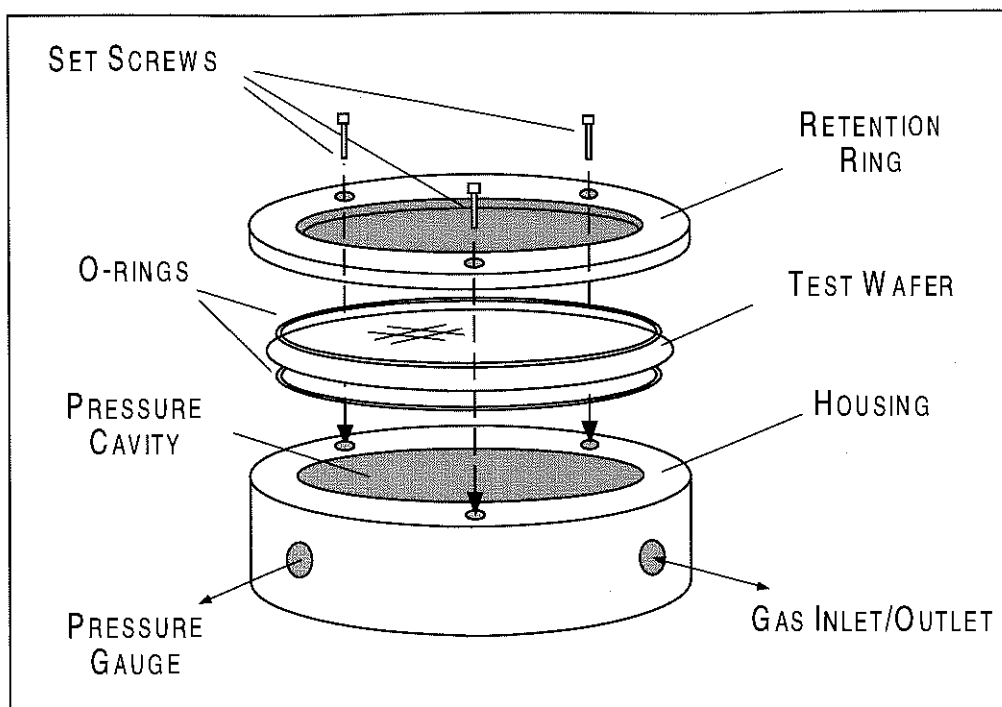


Figure 3.1. The uniform pressure rig for the controlled bending of 3" PZT coated silicon substrates.

3.4.2. Characterization of the Magnitude of Applied Stress

Resistance strain measurements were made on a number of 3" substrates to quantify the stress applied for a given air pressure during the biaxial stress experiments.¹ Subsequent compression tests were made in the chip-on-steel configuration and employed strain gauges bonded directly to the sample during the low-field experiments. The strain gauges used for all tests had a resistance of 120Ω and grid lengths of 1 to 2 mm (Omega KFG-an-120-C1-11L3M3R). Gauges were shunt calibrated prior to testing

¹ Preliminary calculations of the stress induced by the pressure changes were made using classical plate theory. However, comparisons to the measured strain response showed that the flat plate approximation

and conditioned using a Measurements Group 2100 Amplifier.

The level of stress applied to the PZT films was calculated from the strain data using a Young's modulus of 101 GPa [48] and taking the Poisson's ratio to be 0.3. The stress at the center of the wafer was calculated for the equibiaxial condition as

$$\sigma = \frac{x E}{(1 - \nu)} \quad (3.2)$$

where σ is the stress on the film (N/m^2), x is the measured strain on the film, E is Young's modulus (N/m^2), and ν is Poisson's ratio. Results from the strain experiments showed that for +85 kPa of air pressure in the cavity the biaxial stress on the PZT was about +115 MPa and for -85 kPa, of pressure the stress was -40 MPa.

3.4.3. Chip-on-Steel Design

Results from the strain gauge experiments showed that when configured for compression tests, the uniform pressure rig failed to produce stresses in films (on 3" substrates) which surpassed -100 MPa. For that reason an alternative design was developed in which PZT coated silicon chips were fitted with strain gauges and glued (Miller-Stephenson Epoxy 907) to the surface of slightly bowed steel substrates. The steel plates were 3" in diameter and 1.2 mm thick and the PZT chips were roughly 6.5 mm squares and 500 μm thick.

was incorrect for the compressive configuration and further attempts at the prediction of applied stress were abandoned in deference to the direct strain measurements.

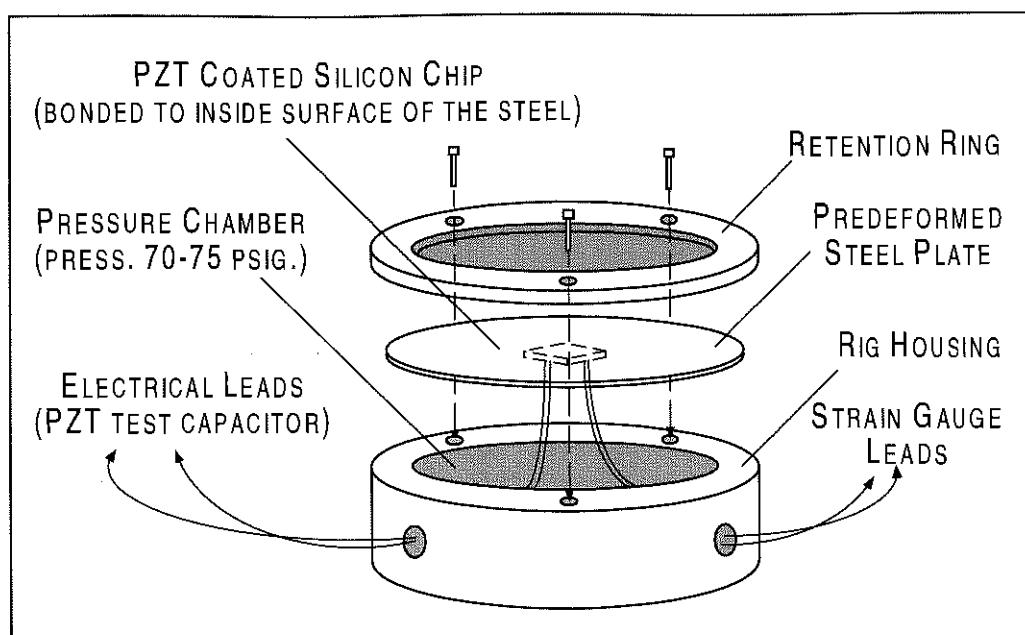


Figure 3.2. The chip on steel design for the application of large compressive stresses to PZT thin films.

Prior to bonding the test chips to the surface, the steel plates were placed in the uniform pressure rig and the rig was inflated to +85 psig. (590 kPa). The pressure in the rig caused the plates to yield and deform into shallow symmetrical domes. By gluing the chip to the convex side of the dome, i.e. to the side which was not exposed to the high pressure, and then placing the chip and plate assembly back in the rig chip side down, the chip could be forced to a highly compressive condition as the rig was inflated to 70-75 psig. (strain plateaued for pressures which exceeded that limit). The schematic in Figure 3.2 illustrates the setup. Each steel plate was used for a number of experiments however, the maximum strains of 1000×10^{-6} (140 MPa) were only achieved during the first pressure cycle. For subsequent tests, strains were lessened as a result of the plastic deformation of the plate on the first pressure cycle (the bow had been folded inside out).

Nevertheless, values achieved were found to lie between 750 and 800 μ strain (i.e. strain $\times 10^{-6}$) which produced stresses in excess of the 100 MPa target.

3.4.4. High and Low-Field Electrical Characterization

Polarization measurements were made using a Radiant Technologies RT66A ferroelectrics tester. The maximum voltages applied were varied until the polarization hysteresis loops could be saturated. Typical values ranged from 20 to 40 Volts, although some of the thicker furnace annealed samples required voltages between 100 and 200 Volts. Electric fields were dependent upon film thickness and will be reported for the specific film tested. Capacitance and $\tan \delta$ were measured using either a Hewlett Packard 4274A Multi-Frequency LCR Meter or a 4192A LF Impedance Analyzer. All low-field tests were conducted at a frequency of 10 kHz and an rms voltage of 10 mV. Experiments were conducted a minimum of two times on each sample and data reported here were taken from the second test. Capacitance and $\tan \delta$ values were recorded 1 minute after the desired test pressure was achieved. Tensile experiments were conducted on complete 3" wafers semi-clamped (i.e. a condition between clamped and simply supported) in the two O-ring configuration (see Figure 3.1) with electrical contact made via a solid point probe. Compression experiments were conducted using the chip-on-steel design (see Figure 3.2) with electrical leads hardwired (Circuit Works CW 2400 conductive epoxy) onto the platinum electrodes (top and bottom) and fed, together with the leads from the strain gauge, through a pressure seal in the housing of the pressure rig.

3.5. The Wafer Flexure Technique for the Characterization of the d_{31} Piezoelectric Coefficient

The wafer flexure technique is a simple and inexpensive method for evaluating the transverse piezoelectric coefficient (d_{31}) of piezoelectric thin films. The technique is based upon the periodic flexure of a PZT coated substrate which imparts an AC two-dimensional stress to the piezoelectric film. The surface charge generated via the mechanical loading is converted to a voltage by an active integrator. Plate theory and elastic stress analyses are used to calculate the principal stresses applied to the film. The d_{31} coefficient can then be determined from knowledge of the electric charge produced and the calculated mechanical stress.

3.5.1. Principle of Operation

The wafer flexure technique is a direct technique used to measure the transverse piezoelectric coefficient (d_{31}) of piezoelectric thin films. The equation which describes the effect is:

$$d_{31} = \frac{D_3}{(\sigma_1 + \sigma_2)} \quad (3.3)$$

where d_{31} is the transverse piezoelectric coefficient (C/N), D_3 is the dielectric displacement (C/m²), and σ_1 and σ_2 are the stresses applied in the plane of the film (N/m²). Measurements are made by subjecting clamped PZT coated wafers to small pneumatic pressures. Flexure of the substrate results in the transfer of strain from the

silicon to the PZT film and the application of a planar stress to the material. In accordance with the direct piezoelectric effect, a charge is produced which is detected electronically and used together with the stress applied to the film (as calculated from small deflection plate theory) to calculate the material's d_{31} coefficient. Figure 3.3 is an illustration of the device. The components which make up the device (i.e. the uniform pressure rig, the charge integrator, the peripheral electronics, and the mercury drop electrode) will be described in the sections which follow.

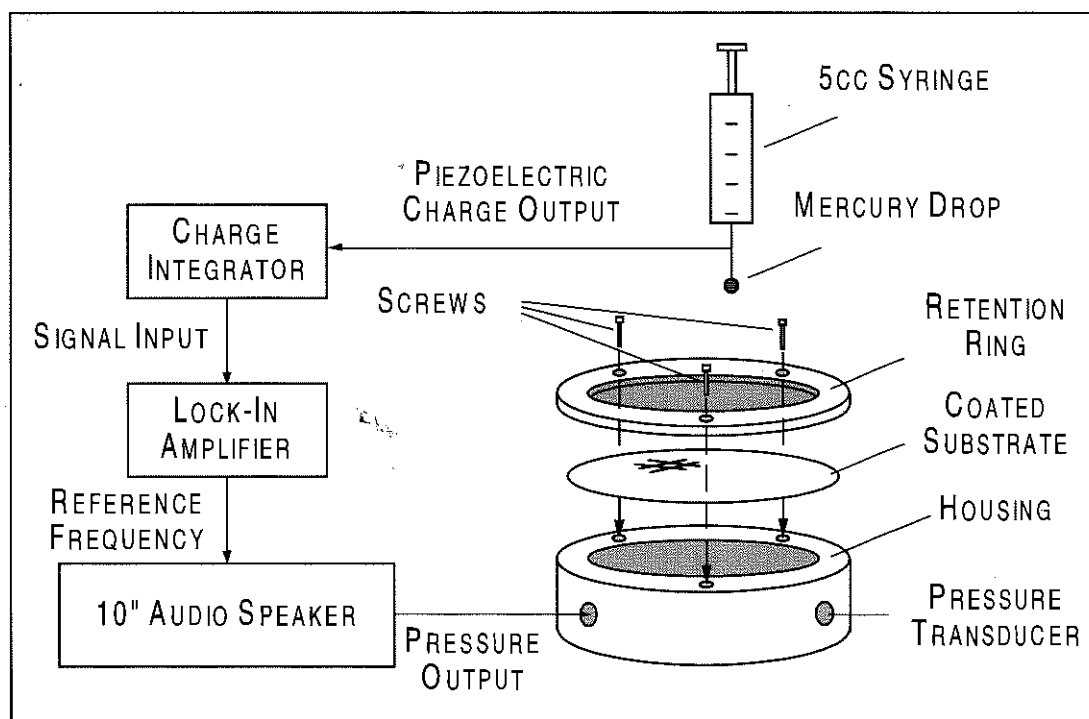


Figure 3.3. The wafer flexure d_{31} measurement setup.

3.5.1.1. Uniform Pressure Rig

The uniform pressure rig (a version of the device described in sec. 3.4) has been constructed with two separate designs. The first is illustrated in Figure 3.1 and will be referred to as the prototype rig. For piezoelectric measurements the O-rings shown in the illustration were removed and replaced with removable aluminum bushings. The inner radii of the bushings measure 1.25" (31.75 mm) and at points of contact with the sample, the aluminum has been polished to 5 μm roughness (to improve the pressure seal and to reduce the risk of substrate fracture).

The second design is shown in Figure 3.4 and will be referred to as the modified rig. The modified rig was constructed with the intent of; (1) eliminating possible errors associated with the placement of the wafer in the prototype rig and (2) expanding the capabilities of the device to allow the characterization of 100 mm (4 inch) wafers. The housing was constructed from a 5" inch aluminum round with four 1/4" pipe fittings tapped at equidistant locations around the perimeter of the device. The pressure cavity of the aluminum rig is 1" deep and sealed using one of two carbon steel base plates. The steel plates have either a 3" or 4" recess machined in their surface, which insures a consistent wafer placement from test to test. Test wafers are secured in position with a steel retention ring having an inner radius of 1.25" for the 3" measurements or 1.75" for 4" wafers. Four 8-32 screws hold the wafer in place with 2.5 in-lbs of torque.

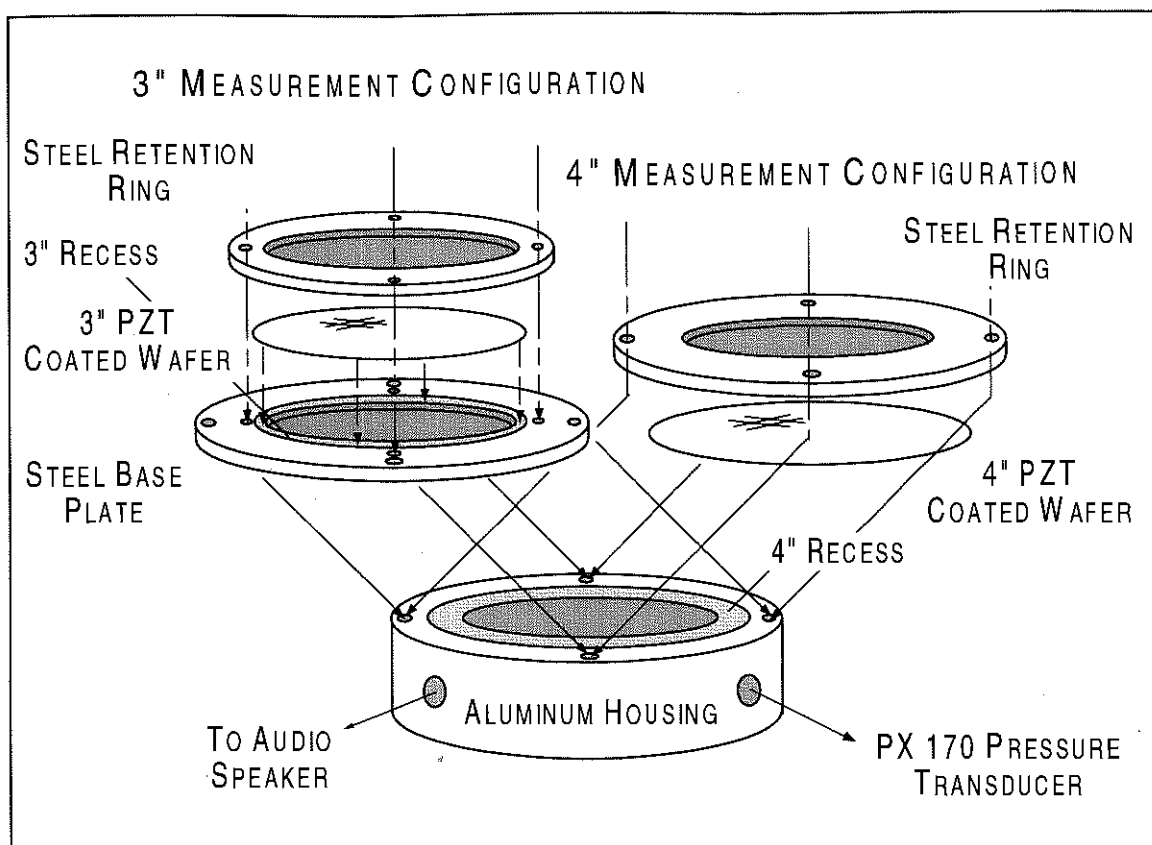


Figure 3.4. An illustration of the modified pressure rig. The rig is capable of handling either 3" or 4" PZT coated substrates.

3.5.1.2. Charge Integrator

The charge integrator used to monitor the piezoelectrically-induced charge is shown in Figure 3.5. Charge from the piezoelectric film is directed to an operational amplifier (op amp) integrator. The input to this circuit is a virtual ground so the film is held in a zero field state (to within a few millivolts). Charge is collected on a polypropylene internal reference capacitor (typically set at 10^{-8} F) which provides good temperature stability and low dielectric absorption. Since the op amp integrator circuit is

an inverting configuration, a second op amp is used to invert the output voltage from the first op amp. The output from the device is then reported as a voltage which is proportional to the amount of charge collected on the reference capacitor.

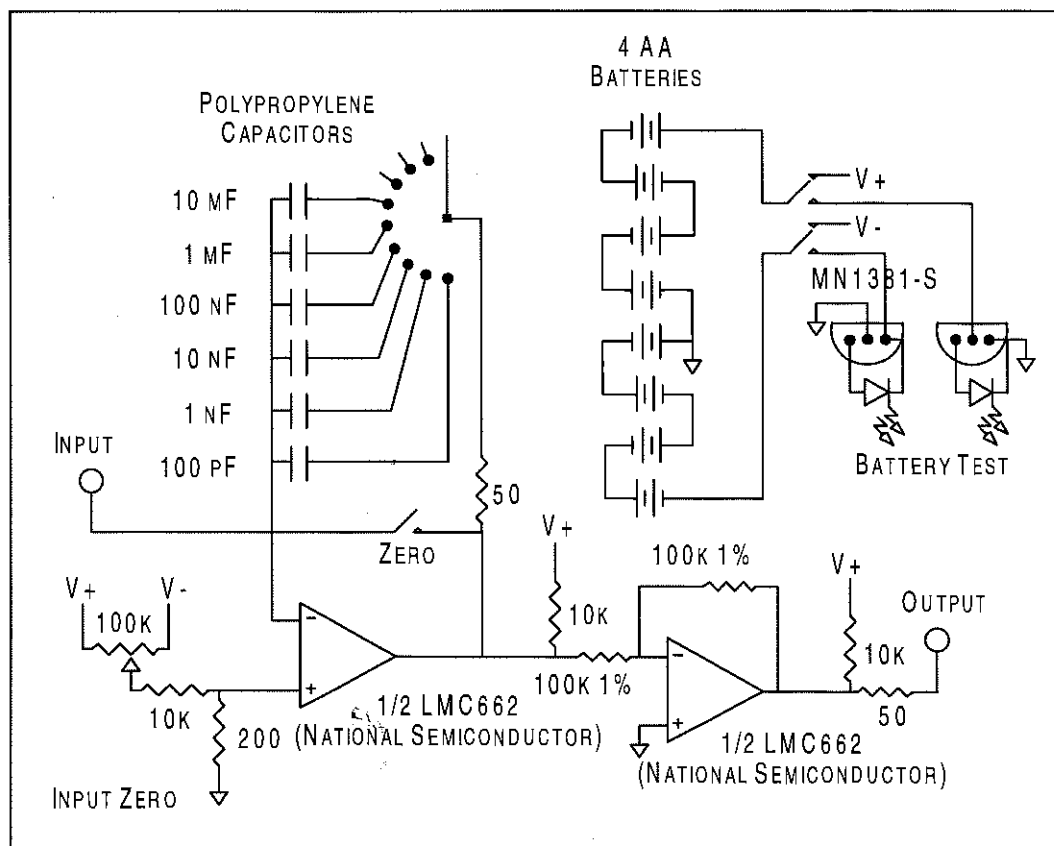


Figure 3.5. Schematic of the electric charge integrator.

3.5.1.3. Peripheral Electronics

Pressure in either rig (modified or prototype) is changed via the oscillation of a 10" audio speaker coupled to the cavity behind the clamped wafer.² The speaker is excited with the reference signal ($0.4 V_{\text{rms}}$ at 4 Hz) from an EG&G 7260 lock-in amplifier fed through a Harman/Kardon HK770 stereo amplifier. The resulting air pressure oscillation flexes the wafer, inducing a charge via the d_{31} coefficient of the film. The charge from the PZT sample is converted to an rms voltage and together with the voltage from a piezoresistive pressure transducer (Omega PX170, 0.26 psig full scale) is fed into the lock-in and measured with respect to the internal reference. From the lock-in data, output charge and applied pressure are then calculated. In general, the most reliable results were obtained with oscillation frequencies between 3 and 5 Hz.

3.5.1.4. Mercury Drop Electrode

Electrical contact is made to the top electrode of the test capacitor with the aid of custom designed mercury probe. It was found that with a solid probe the relative motion of the film surface and the probe tip (in response to the wafer's oscillation) resulted in artifacts which affected the reproducibility of the technique. A mercury probe was therefore used to eliminate extraneous charge contributions. The probe was constructed from a 5cc plastic syringe which contained one or two drops of mercury. Adjustment of the syringe's plunger allowed a single drop of mercury to be suspended from the needle's

² In the initial stages of development pressure was changed via the displacement of a 60cc syringe attached to the housing of the rig. Data collected from the earlier design will be given in chapter 5 and details of the setup can be found in reference [7].

tip. The tip was then lowered into contact with the platinum top electrode. The needle was insulated from the plastic body of the syringe and was hard wired to a BNC cable connected to the charge integrator circuit (which was in turn connected to the lock-in amp). Measurements made with the modified technique have yielded standard deviations of less than 10%, though the precision, once a sample is mounted is considerably better.

3.5.2. Stress Analysis and the Calculation of d_{31}

The determination of the film's transverse piezoelectric coefficient requires knowledge of the mechanical stress applied to the film (eq. 3.2). Small deflection plate theory was used together with the pressure applied to the wafer, the support radius, the substrate thickness, and the test capacitor location to calculate the principal stresses at a specific location on the silicon substrate. The bending stresses which result from a uniform pressure on a clamped circular plate are [42]:

$$\sigma_r = \frac{3pz}{4t^3} [(1+\nu)a^2 - (3+\nu)r^2] \quad (3.4)$$

$$\sigma_t = \frac{3pz}{4t^3} [(1+\nu)a^2 - (1+3\nu)r^2] \quad (3.5)$$

where σ_r and σ_t are the radial and tangential stresses on the plate (N/m^2), p is the pressure applied to the plate (N/m^2), z is the distance from the neutral axis (m), t is the plate thickness (m), ν is Poisson's ratio, a is the support radius (m), and r is the distance from the center of the plate (m).

Because the mechanical properties of the silicon substrate and the piezoelectric films differ, wafer stresses calculated from plate theory must be corrected to determine film stress. The assumption was made that all strain applied to the substrate was transferred to the film. Knowing the stresses applied to the substrate (eqs. 3.4 and 3.5), the strains are calculated via generalized Hooke's law as:

$$x_1^{\text{Si}} = \frac{\sigma_1^{\text{Si}}}{E_{\text{Si}}} - \nu_{\text{Si}} \frac{\sigma_2^{\text{Si}}}{E_{\text{Si}}} \quad (3.6)$$

$$x_2^{\text{Si}} = \frac{\sigma_2^{\text{Si}}}{E_{\text{Si}}} - \nu_{\text{Si}} \frac{\sigma_1^{\text{Si}}}{E_{\text{Si}}} \quad (3.7)$$

where σ_1^{Si} is applied stress in the 1 direction (1 and 2 are the principal in-plane directions corresponding to the tangential or radial orientation), x_1^{Si} is the strain in the 1 direction, ν_{Si} is the Poisson's ratio of the silicon, and E_{Si} Young's modulus of the silicon. In a similar fashion Hooke's law may be written for the PZT film:

$$x_1^{\text{PZT}} = \frac{\sigma_1^{\text{PZT}}}{E_{\text{PZT}}} - \nu_{\text{PZT}} \frac{\sigma_2^{\text{PZT}}}{E_{\text{PZT}}} \quad (3.8)$$

$$x_2^{\text{PZT}} = \frac{\sigma_2^{\text{PZT}}}{E_{\text{PZT}}} - \nu_{\text{PZT}} \frac{\sigma_1^{\text{PZT}}}{E_{\text{PZT}}} \quad (3.9)$$

Because of the conservation of strain, the equations for σ_1^{PZT} and σ_2^{PZT} can be derived explicitly by setting $x_1^{\text{PZT}} = x_1^{\text{Si}}$ and $x_2^{\text{PZT}} = x_2^{\text{Si}}$. Solving the set of two equations for the stresses on the films gives:

$$\sigma_1^{\text{PZT}} = x_1^{\text{Si}} E_{\text{PZT}} + \nu_{\text{PZT}} \sigma_2^{\text{PZT}} \quad (3.10)$$

and

$$\sigma_2^{\text{PZT}} = \frac{E_{\text{PZT}}}{(1 - \nu_{\text{PZT}}^2)} (x_2^{\text{Si}} + \nu_{\text{PZT}} x_1^{\text{Si}}) \quad (3.11)$$

The expansion of eq. 3.11 yields a more fundamental form of the equation written in terms of the elastic properties of the silicon and the elastic properties of the PZT film where:

$$\sigma_2^{\text{PZT}} = \frac{E_{\text{PZT}}}{(1 - \nu_{\text{PZT}}^2)} \left[\frac{\sigma_1^{\text{Si}}}{E_{\text{Si}}} (\nu_{\text{PZT}} - \nu_{\text{Si}}) + \frac{\sigma_2^{\text{Si}}}{E_{\text{Si}}} (1 - \nu_{\text{PZT}} \nu_{\text{Si}}) \right] \quad (3.12)$$

The expressions derived are appropriate for small deflections of a coated wafer if the ratio of the PZT film thickness to the silicon substrate thickness is small. For the case of a PZT film on a silicon substrate, the thickness ratio is much less than 1%, and deformation of the composite wafer will be governed by the elastic properties of the silicon substrate. Furthermore, because small deflection plate theory is used, the maximum deflection of the coated wafer may not exceed 20% of the thickness of the plate [42, 80]. For deflections beyond that point, membrane (i.e. stretching) stresses are no longer negligible and use of the small deflection equations would result in significant error.

3.5.3. Numerical Considerations

3.5.3.1. Elastic Modulus of the PZT Film

Equation (3.12) shows that the stress on the film is dependent upon both the elastic properties of the silicon and the PZT. Inaccuracies in those quantities will carry through the stress analysis and to the subsequent d_{31} calculation. It is important to note that although the mechanical properties of silicon are well characterized [81, 82] the properties of thin film PZT are not. That observation is important because at present all methods (converse [72] or direct [83]) for the determination of the transverse piezoelectric coefficient require explicit knowledge of the material's elastic moduli. Published values have ranged from 25 [23] to 400 GPa [22] and it should therefore be noted that the disparities among d_{31} values reported in the literature could result from the different elastic moduli used in their calculation. Values for bulk PZT are typically quoted at about 70 to 90 GPa [32, 35]. The Young's modulus used in this investigation was taken as 101 GPa [48] and was selected in order to yield a lower limit for the d_{31} coefficient (i.e. calculated stress increases and d_{31} decreases for larger Young's moduli). In addition, the value used is one of the few published reports for the elastic modulus of a PZT film. The high value relative to bulk PZT ceramics could be the result of limited non-180° domain wall motion in films, since such motion provides a deformation mechanism which decreases the material's stiffness.

3.5.3.2. Anisotropy of the Silicon Substrate

The anisotropy of the silicon substrate can, in principle, complicate the calculation of the stress applied to the piezoelectric film. However, strain gauge measurements along the $\langle 100 \rangle$ and $\langle 110 \rangle$ directions of a bare wafer showed no significant difference in the mechanical response (chapter 5). That result suggests that the elastic properties which govern deformation of the substrate can be represented with single values of Poisson's ratio and Young's modulus. A comparison of the experimental and theoretical strains (as calculated from plate theory) gave the best agreement when the average of the maximum and minimum in-plane elastic constants (the $\langle 100 \rangle$ and $\langle 110 \rangle$ directions) were used in the calculation. For that reason, the silicon was treated as an isotropic plate and the averages of both the Young's modulus and Poisson's ratio were used in the d_{31} calculations presented here. Table 3.2 summarizes the mechanical properties of both the silicon substrate and the PZT film.

TABLE 3.2. The Elastic Properties of the Silicon Substrate and PZT Thin Films

Material	Young's Modulus (GPa)	Poisson's Ratio
(100) Silicon [81]	150	0.172
PZT Thin Film [48]	101	0.3

3.6. Validation of the Wafer Flexure Technique for the Transverse Piezoelectric Characterization of Thin Films

3.6.1. Resistance Strain Gauge Measurements

An obvious concern with the development of any measurement technique is the validity of the results obtained. To begin to address that question, a number of experiments were designed in which the stress models used were validated using resistance strain gauge measurements. Strain gauges were fastened to the center of a number of 3" and 4" silicon substrates and the strains produced in response to an applied pressure in the rig were compared to those predicted by plate theory (sec. 3.5.2). Both pressure and strain measurements were made in an AC fashion with the output from the strain gauge conditioner and pressure transducer sent to the lock-in amplifier. For comparison with theory, the strain was measured as a function of air pressure by changing the drive voltage on the audio speaker between 0.2 to 0.8 Volts. The oscillation frequency was set at 4 or 5 Hz.

3.6.2. The Variation of the d_{31} Coefficient with Radial Location on a Wafer

Two experiments were conducted in which the transverse piezoelectric response was characterized as a function of position on a 3" wafer. The first test used the prototype rig with manual pressure oscillation and characterized a number of different capacitors poled with +333 kV/cm for 1 minute. It was expected that because the stress on a plate

varies as a function of radial location, the electric charge produced should also differ. However, the d_{31} coefficients were expected to be constant as a result of the homogeneity of the material. The results obtained were consistent with the objective however, it was expected that variations in the poling conditions and radius measurements led to small variations in the data. To address that deficiency, a second test was conducted using the modified setup in which the piezoelectric response of an as-deposited film was monitored over the surface of the 3" substrate. Because the sol-gel films had small as-deposited polarizations it was expected that the magnitude of the d_{31} coefficient would be constant throughout the film. For a constant oscillation pressure the charge produced from the as-deposited film could be monitored and normalized to the maximum value at the center of the wafer. When the measurement was completed it was compared to the variation of film stress as predicted from plate theory, which gave an indication of the validity of the model used.

3.7. Experiments with the Wafer Flexure Method for the Transverse Piezoelectric Characterization (d_{31}) of Thin Films

3.7.1. The Influence of Excitation Stress on the d_{31} Coefficient

The transverse piezoelectric coefficient of a 0.4 μm thick 52/48 sol-gel film was measured as a function of the amplitude of the excitation stress in the wafer flexure rig. Two experiments were conducted using the manual pressure oscillation of the prototype design. The stresses achieved ranged from 5 to 25 MPa for four different displacements

of the 60cc syringe. The film was poled at room temperature with an electric field of +150 kV/cm for less than 1 minute and data were recorded after a 10 minute aging time.

3.7.2. The Effects of Poling Time and Poling Direction on the d_{31} Coefficient

The wafer flexure technique was used to characterize the d_{31} coefficient of a number of PZT thin films. As a general rule, each PZT sample was characterized as a function of poling time and poling direction at room temperature. The magnitude of the poling field was typically two to three times the coercive voltage (as measured from the polarization hysteresis loop) and poling was done in 5 or 15 minute increments to a maximum of 1 hour. By analogy with piezoelectric ceramics [35], results from the experiments were expected to show a logarithmic increase with poling time. As such, data from the poling experiments were used to check the health of the d_{31} meter, the quality of the PZT films, and to identify/confirm the existence of internal bias fields (the d_{31} response is strongly asymmetric with respect to poling direction for films with large internal bias fields).

3.7.3. The Effects of Film Thickness on the Magnitude of the d_{31} Coefficient

Earlier work with interferometric characterization has reported that the piezoelectric coefficients of PZT films increase with film thickness [79]. To evaluate that claim, a study was designed in which the d_{31} coefficient was measured as a function of poling time and direction for four PZT films of different thickness. The films used had 52/48 compositions with (111) textures and were synthesized using the procedure

described in sec. 3.6.1. The thicknesses of the four samples tested were measured using surface profilometry and were found to be 0.6, 0.8, 1.8, and 2.5 μm (steps were chemically etched in each film using a 10 vol. % hydrofluoric acid). Platinum top electrodes with diameters of 1.5 mm were sputter deposited and rapid thermal annealed at 400°C for 10 seconds.

Prior to piezoelectric measurements, the PZT films were characterized in terms of their polarization hysteresis loops using the Radiant Technologies RT66A Ferroelectrics Tester. Test capacitors on each film showed well saturated hysteresis loops with P_r values of about 22 $\mu\text{C}/\text{cm}^2$ and E_c values between 32 (2.5 μm thick) and 55 kV/cm (0.6 μm thick). The coercive field of each film was measured and used to calculate the poling field to be applied for the subsequent d_{31} characterization. For this investigation all samples were poled at room temperature with an electric field three times their coercive field strengths. Experiments were conducted as function of poling direction and poling time and the results were correlated to film thickness.

3.7.4. The Aging Rate of the d_{31} Coefficient of PZT Thin Films

The aging of the piezoelectric response under closed circuit conditions was measured and is reported as a function of film thickness and poling direction. A number of films have been characterized including those from the thickness investigation (sec. 3.7.1) and the 4" RF sputtered samples. For each test, samples were poled with an electric field (typically two or three times their coercive field) for a time of 1 to 2 minutes. At the end of the poling period the oscillation on the measurement rig was started and the test begun. The output from the test capacitor was monitored continuously on the lock-in

display and the voltages recorded every 5 minutes for times of 1 to 60 minutes after poling. Care was taken to insure that the pressure applied to the plate was the same over the course of the experiment. To that end, the audio speaker was warmed up for 15 minutes prior to the start of any aging test.

3.8. The Characterization of the d_{31} Coefficient of Test Chips Coated with Piezoelectric Thin Films

The wafer flexure method was originally designed for characterization of the transverse piezoelectric coefficient of PZT films deposited on 3" silicon substrates. Modifications have been made however, which allow the characterization of the d_{31} coefficients of piezoelectric films deposited on small chips of substrate material. A schematic of the design is given in Figure 3.6. The basics of the setup are the same as the 3" configuration, i.e. bending the chip produces an electric charge which is measured with the charge integrator and lock-in amplifier combination. The flexure of the chip is accomplished by gluing the sample (Instant Krazy Glue) onto the surface of a bare 3" silicon substrate³ and then clamping the wafer in the test rig. As before, the pressure oscillation flexes the substrate and forces the test chip to bend. The strain applied to the film is measured either before or after the charge measurement using a resistance strain gauge fastened to the film. From the strain measurements the stress applied is calculated and used, together with the charge produced, to determine the film's d_{31} coefficient.

³ Silicon need not be the host but it was used here because of its ready availability.

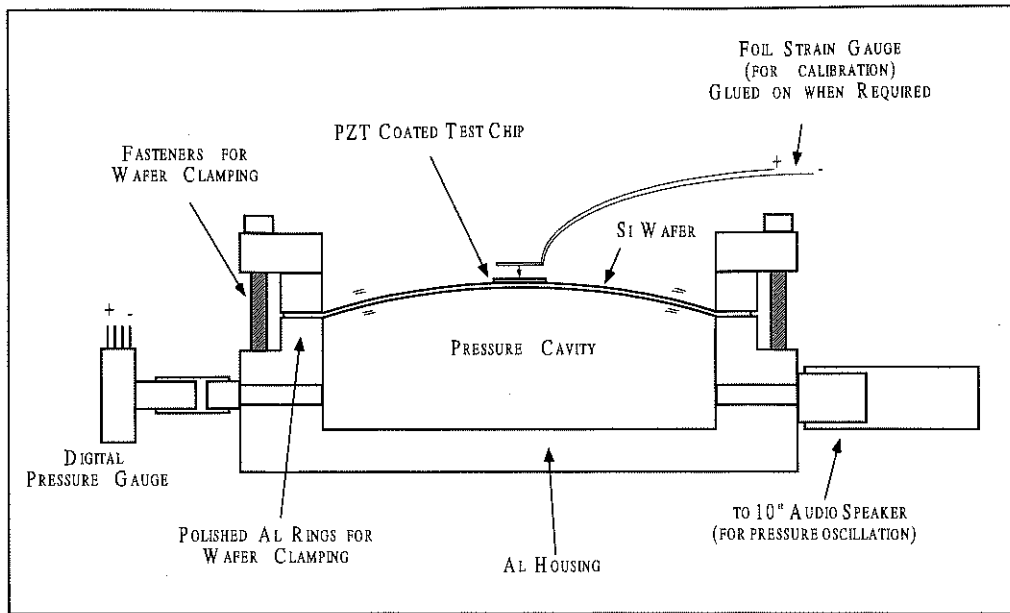


Figure 3.6. The modified wafer flexure apparatus for the characterization of millimeter sized test chips [84].

4. The Effects of Biaxial Stress on the Low and High-Field Properties of PZT Thin Films

4.1. Introduction

This chapter presents the results obtained from the investigation of the effects of biaxial stress on the low and high-field characteristics of PZT thin films. The objective of the investigation was to evaluate how applied stresses modulate the properties of PZT films particularly in light of the existing hypothesis that residual stresses limit the magnitude of their piezoelectric response. The results were also expected to contribute to an understanding of non-180° domain wall motion in the films. Experiments were conducted on samples with fixed microstructures and defect chemistries via the controlled bending of PZT coated substrates. That is important because previous work in this area relied on the differences of the thermal expansion coefficients of the film and substrate to alter the residual stress state of the film. Unfortunately, the resulting differences in film grain size, texture, and defect chemistries complicates interpretation of the results. This chapter has been constructed with the measurement of the applied strains to 3" PZT films presented as the first major section. Results from the effects of stress on the polarization hysteresis curves and the low-field dielectric properties are then given for both the wafer and O-ring and chip-on-steel configurations. The final sections of the chapter are then devoted to a discussion of the empirical results.

4.2. Residual Film Stresses in PZT Thin Films on Platinized Silicon Substrates

In order to evaluate the effect of applied stress on film properties it is desirable to be able to take the film through both tensile and compressive conditions. It is important to remember however, that for a film, the applied stress is superimposed on the residual processing stress. This residual stress must be accounted for in order to take the film through the true zero net stress state. Thus, the first step in this investigation was the characterization of the residual film stress present in the RTA'd sol-gel films studied.

The residual stress on a number of 52/48 sol-gel PZT films was measured via wafer curvature experiments. Films between 0.3 and 0.4 μm thick were deposited on platinized (100) silicon wafers with the sol-gel procedure described in sec. 3.2. The substrate's curvature was measured after the final crystallization step and again after the film was stripped from the substrate (10 vol. % HF). From the change in the wafer's curvature the stress which was required to deform the substrate was calculated. Results from the wafer curvature measurements were consistent with those of other researchers [46, 47, 85] and indicated that the residual stresses on the film's were between 70 and 100 MPa of tension.

4.3. Strain on the 3" PZT Films as a Function of Applied Pressure

In order to determine the stresses that can be applied to the films, the strain at the center of a PZT coated test wafer was measured as a function of the gas pressure in the uniform pressure rig (Figure 2.1). Figures 4.1 and 4.2 show the tensile and compressive responses, respectively. Data presented in the plots were collected from three tests in both

the tensile and compressive configurations. In Figure 4.1 it is apparent that as the pressure in the rig is increased, the tensile strain on the film increases to a maximum of 800 μ strain at a pressure of about 80 kPa (12 psig). In contrast, decreasing the pressure in the cavity (i.e. drawing a vacuum) produces a curve in which the strain saturates. The compressive strain was observed to reach a peak of about 300 μ strain (stress of about -40 MPa) at a pressure of -40 kPa (6 psig). For pressures below that threshold the magnitude of the strain decreased slightly.

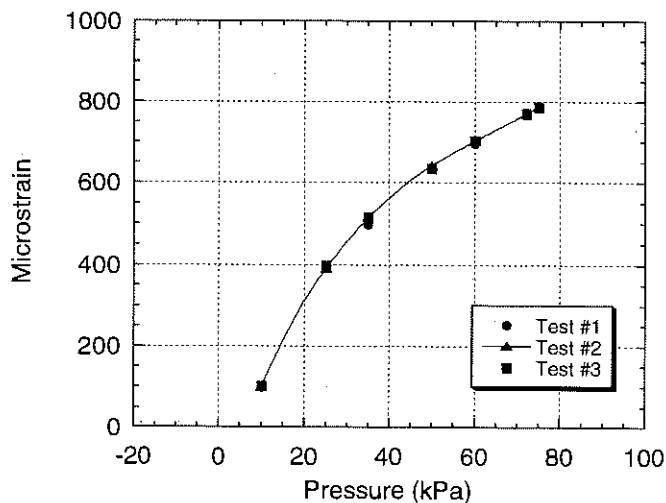


Figure 4.1. The tensile strain at the center of a PZT coated test wafer when clamped between two O-rings in the uniform pressure rig. Maximum strains achieved were about 800 μ strain, which translates to about 115 MPa of stress in the PZT.

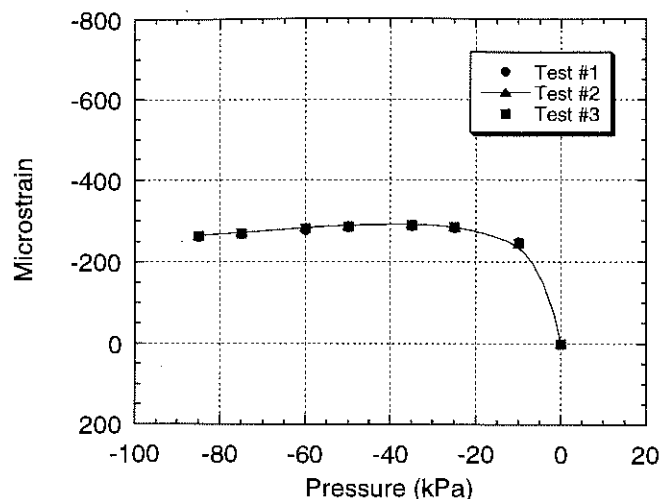


Figure 4.2. The compressive strain at the center of a PZT coated test wafer when clamped between two O-rings in the uniform pressure rig. Maximum strains achieved were about 300 μ strain, which translates to about -40 MPa of stress in the PZT.

It is clear from the strain data in Figure 4.2 that the strain achieved on the wafer surface is strongly asymmetric with the sign of the cavity pressure. Thus, the behavior of the PZT coated silicon cannot be treated with large deflection plate theory (which would predict that an increase of pressure causes an increase of strain). This asymmetric strain response is thought to relate to the initial curvature of the PZT coated silicon which is brought about from the residual stress on the film. As a result of that curvature the substrate is not subjected to pure bending, but rather behaves as a thin walled pressure vessel. As such, the bending strains applied to one side of the plate saturate and the material begins to stretch rather than bend. Consequently, the tensile data continued to increase with applied pressure and the compressive strain could not be made to exceed the limit of 300 μ strain.

4.4. Strain on PZT Chips Bonded to Predeformed Steel Substrates

As described in the previous section, and as illustrated in Figure 4.2, the compressive strain applied to a 3" PZT coated substrate was significantly less than that which was needed to relieve the residual tensile stress on the PZT films (~100 MPa). To achieve the necessary strains, square chips of PZT coated silicon (6.5 mm on a side and 500 μm thick) were epoxied onto bowed steel substrates. By placing the substrates PZT side down in the pressure rig and inflating the device to 485-520 kPa the strains applied to the PZT films approached 1000 μstrain as the dome was forced inside out on the first strain cycle. Release of the applied pressure resulted in an appreciable amount of residual compression on the chip (-275 μstrain) brought about by the plastic deformation of the steel plate. The removal (by heating the steel and chip composite to approximately 150°C on a hotplate) and subsequent rebonding of a test chip/strain gauge combination resulted in reversible strains of between -750 to -800 μstrain applied to the PZT films when gas pressures did not exceed 485-520 kPa. Pressures in excess of that value resulted in an additional deformation of the steel plate and sacrificed the reproducibility of the test. Figures 4.3 and 4.4 show the strain produced on a PZT chip from the first (i.e. as the dome was forced inside out) and second stress cycles of a bowed steel substrate.

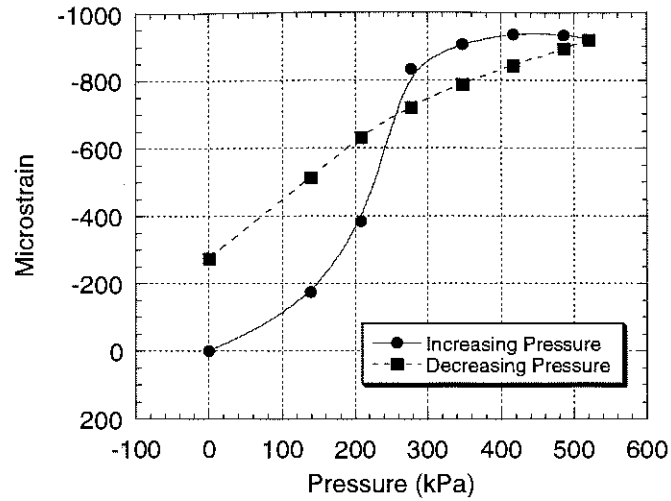


Figure 4.3. The strain applied to a 6.5 mm PZT coated test chip bonded to a predeformed steel substrate. The data were taken from the first pressure cycle, i.e. as the steel dome was folded inside out.

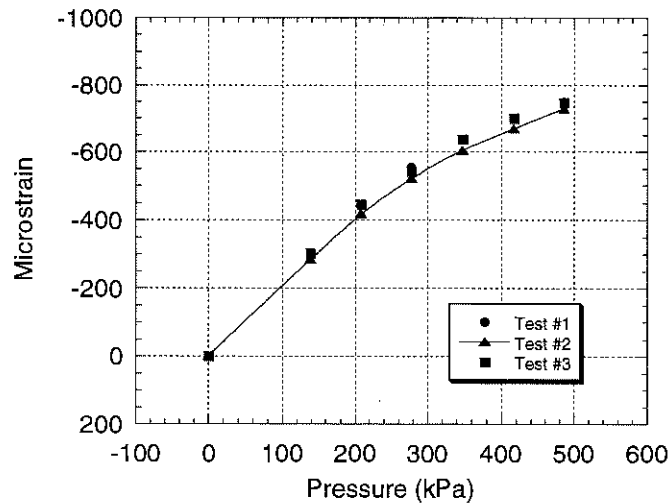


Figure 4.4. The strain applied to a 6.5 mm PZT coated test chip bonded to a steel substrate. The data shown were taken from three tests conducted on a PZT chip rebonded to the substrate after the dome had been forced inside out on the first pressure cycle.

4.5. Low-Field Characteristics of PZT Films as a Function of Applied Biaxial Stress

The application of controlled biaxial stress was accomplished in the preliminary stages of this investigation using PZT coated 3" substrates and the uniform pressure rig shown in Figure 3.1. Both tensile and compression experiments were conducted on samples with different compositions, thicknesses, and poling conditions. Data were collected for experiments conducted in the wafer and O-ring configuration as a function of the air pressure in the rig housing for both the application and release of the applied stress. From experiments with resistance strain gauges (sec. 4.3) the stresses applied to the films (as measured at the center of the wafer) were found to approach 115 MPa for +75 kPa of air pressure and -40 MPa for -85 kPa of pressure (i.e. a vacuum). The limitation on the compressive stress levels forced the design of the chip-on-steel experiments, which will be discussed in section 4.6.

4.5.1. The Low-Field Stress Response of 3" 52/48 Films in the Wafer and O-ring Configuration

The capacitance and dielectric loss of several 52/48 PZT films less than 0.5 μm thick were monitored as a function of the biaxial stress level and poling condition at an applied voltage of 10 mV (~ 0.2 kV/cm) and a frequency of 10 kHz. Figure 4.5 is an X-ray diffraction pattern for a 0.4 μm thick film which illustrates the partial (111) crystallographic texture of the films tested. Measurements were made at or near the center of the 3" wafers. The first measurements in the poled condition were taken 20

minutes after removal of the electric field, and unpoled measurements were made more than 1 month after deposition of the film.

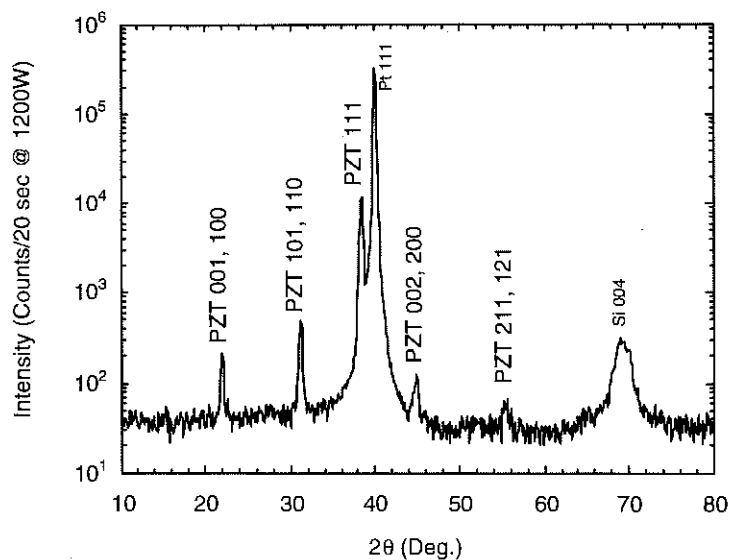


Figure 4.5. The X-ray diffraction pattern for a 0.4 μm thick 52/48 sol-gel film.

Results from the wafer and O-ring experiments for a 0.4 μm thick 52/48 film are given in Figures 4.6 and 4.7 for the film in both the poled and unpoled conditions. The dielectric constants were measured at ~ 1000 in the unpoled condition and ~ 1100 after poling with an electric field of 230 kV/cm for 10 minutes. From consideration of the tensile portion of the curves (i.e. positive pressures) it is apparent that larger changes were observed for the unpoled material, which showed a maximum change of 4% (which corresponded to the maximum principal stress of 115 MPa). In contrast, the poled sample showed a 2% decrease from the as-deposited condition. The return values upon release of the applied stress were less than those recorded at the same stress for the original application of the mechanical load. The differences between the increasing and

decreasing stress data collapsed at small loads, and on complete unloading, the capacitance values were found to be slightly larger than those of the as-deposited film.

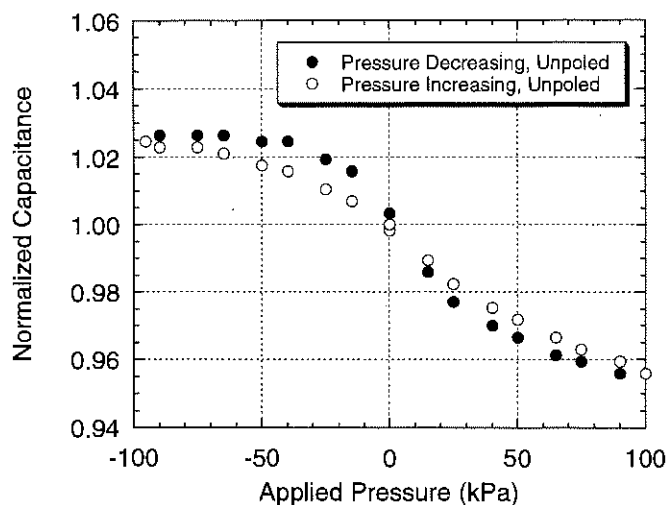


Figure 4.6. The change in capacitance of an unpoled 0.4 μm thick 52/48 sample with applied biaxial stress. The pressure range given corresponds to an applied film stress ranging from approximately -40 to 115 MPa.

The curves in Figures 4.6 and 4.7 show that when subjected to an applied compressive stress the capacitance of the sample increased between 1% for the poled sample and 3% for the unpoled. With the release of the applied stress, the capacitance dropped to values below those recorded with increasing load, mirroring the original path but at lower magnitudes. Complete removal of the applied stress returned the film's capacitance to a value just below that of the as-deposited condition for both the unpoled and poled material. Recall from Figure 4.2 that the strain applied to a PZT film did not exceed -270 μstrain and the form of the curve showed a strong similarity to the shape of the capacitance plot in Figure 4.6. The corresponding stress was therefore, no greater than

-40 MPa (which could not have relieved the +100 MPa of residual tensile stress on the film) and it is for that reason that the chip-on-steel experiments were designed.

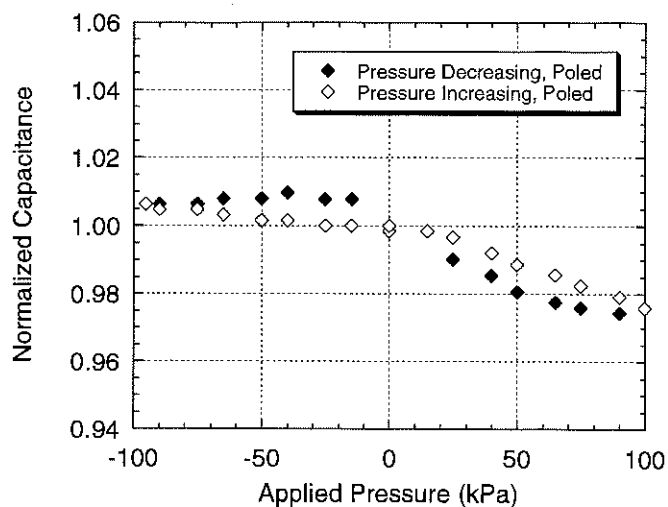


Figure 4.7. The change in capacitance of a poled 0.4 μm thick 52/48 samples with compressive stress. The pressure range given corresponds to an applied film stress ranging from approximately -40 to 115 MPa.

4.5.2. Low-Field Tensile Stress Response of 3" 40/60 and 60/40 Films

In addition to the experiments conducted on the morphotropic phase boundary films the stress response of unpoled films having both tetragonal (40/60 Zr/Ti ratio) and rhombohedral (60/40 Zr/Ti ratio) symmetries was measured using the uniform pressure technique (i.e. complete 3" substrates). Results from the studies are very similar to those shown in Figures 4.6 and 4.7 (i.e. capacitance decreased with applied tension and increased with applied compression) and are given in Figures 4.8 and 4.9. The dielectric

constants for the films in the as-deposited condition were ~ 860 for the 40/60 sample and ~ 1170 for the 60/40 film. For the experiments conducted on both films the changes produced were reversible, with their magnitudes found to be less than 5% for all tests conducted.

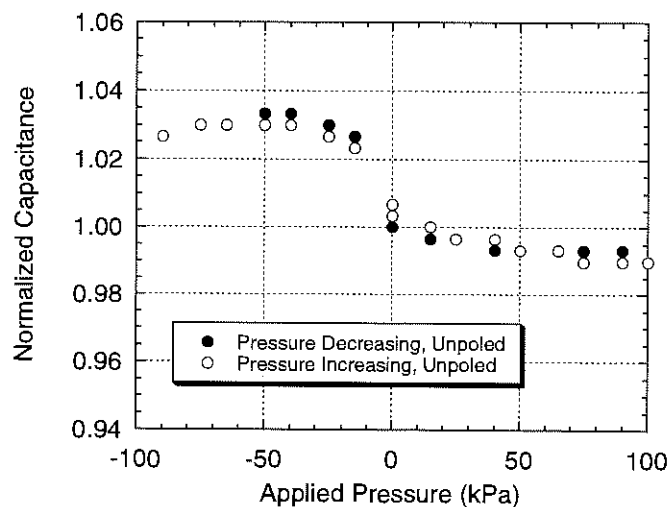


Figure 4.8. The low-field biaxial stress response of a $0.45 \mu\text{m}$ thick 40/60 film deposited on a 3" platinized silicon substrate.

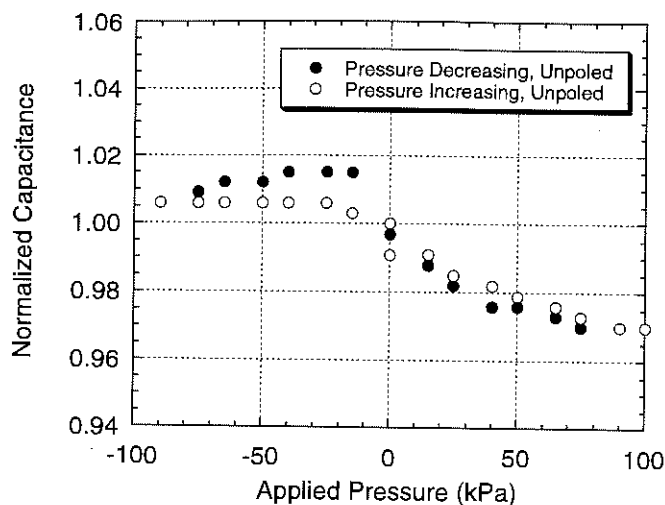


Figure 4.9. The low-field biaxial stress response of a 0.55 μm thick 60/40 film deposited on a 3" platinized silicon substrate.

4.5.3. The Effects of Film Thickness on the Low-Field Biaxial Stress Response

The biaxial stress response for a series of 3" 52/48 films was measured as a function of film thickness with the intent of identifying a critical thickness above which the behavior of the material began to approximate that of a bulk ceramic [86]. Biaxial stress experiments were conducted on a number of RTA'd and furnace annealed (FA) samples in an attempt to activate (and identify) significant extrinsic contributions to the low-field response. X-ray diffraction measurements showed the RTA'd samples had (111) orientations while the FA samples had (100) textures. The dielectric constant and $\tan \delta$ of the as-deposited films were measured prior to the outset of the stress experiments and the data are given in Table 4.1. The plot in Figure 4.10 illustrates the variation of ϵ_r with film thickness. The dielectric constant of the RTA'd films increased from 900 to

1040 for the RTA'd films, and from 1270 to 1370 for the FA samples. In general, the dielectric loss was lower for the thicker films.

TABLE 4.1. Dielectric Constant and Dielectric Loss as a Function of Film Thickness

Film Thickness (μm)	Dielectric Constant (ϵ_r)	Dielectric Loss (%)
0.6	900	4.0
0.8	960	4.0
1.8	970	2.6
2.5	1040	2.6
3.0	1270	1.6
5.0	1370	2.0

The dotted line separates data from the (111) oriented RTA'd films from that for the (100) furnace annealed samples.

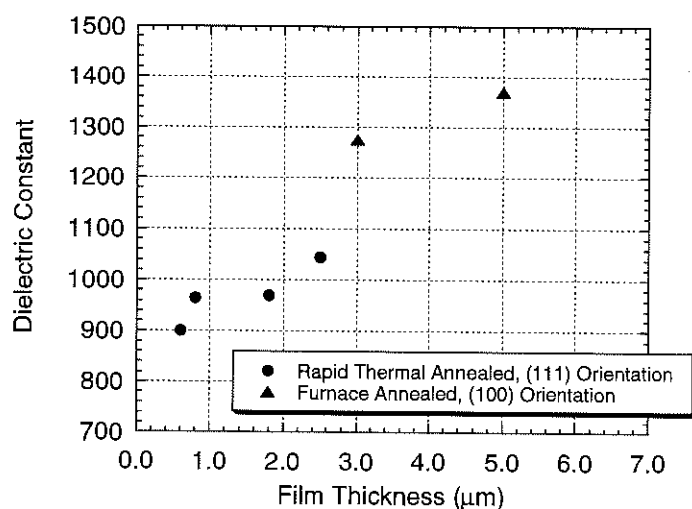


Figure 4.10. The variation of dielectric constant with film thickness. Data from both the RTA'd and furnace annealed samples are presented.

4.5.3.1. The Low-Field Biaxial Stress Response of (111) Oriented RTA'd Samples

The low-field biaxial stress response for the four (111) oriented RTA'd samples is shown in Figures 4.11 to 4.14. The data presented were taken at the center of the wafer from the second stress cycle (i.e. the second application of tensile and compressive pressures) and each point was recorded 2 minutes after the desired pressure was achieved. The data are analogous to that for films less than $0.5\ \mu\text{m}$ thick (see e.g. Figure 4.6). The films showed a modest increase of capacitance upon application of a compressive stress and a small decrease of capacitance with tensile stress. In both cases, observed changes are no more than 3% from the unstressed value and were reversible upon release of the applied loads.

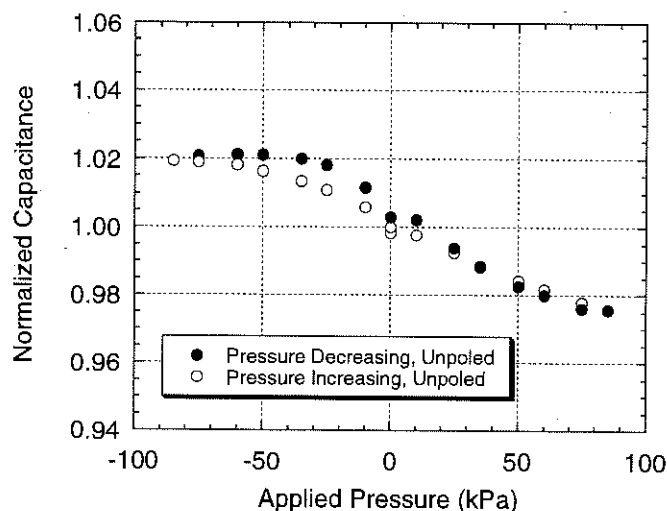


Figure 4.11. The stress response of a $0.6\ \mu\text{m}$ thick 52/48 PZT thin film. The film was prepared on a 3" platinized silicon substrate and had a (111) orientation.

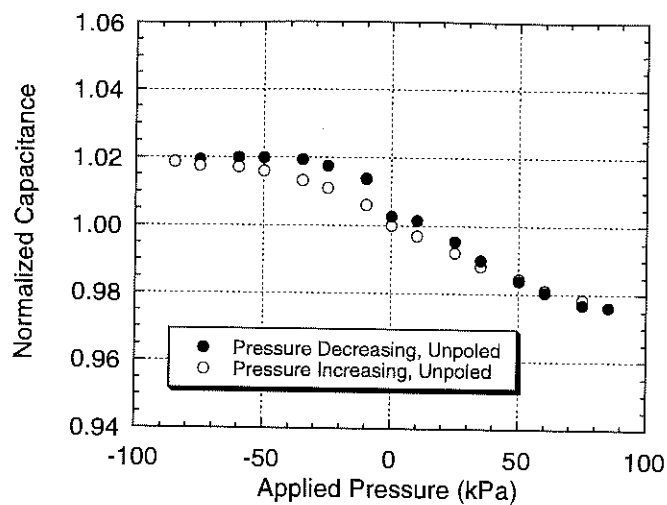


Figure 4.12. The stress response of a 0.8 μm thick 52/48 PZT thin film. The film was prepared on a 3" platinized silicon substrate and had a (111) orientation.

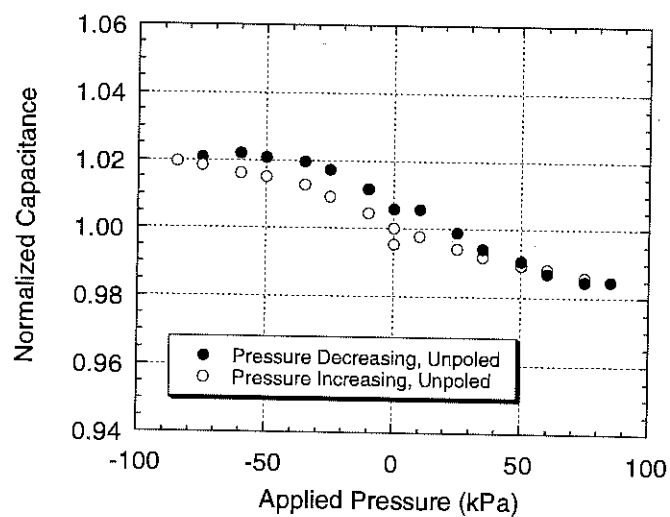


Figure 4.13. The stress response of a 1.8 μm thick 52/48 PZT thin film. The film was prepared on a 3" platinized silicon substrate and had a (111) orientation.

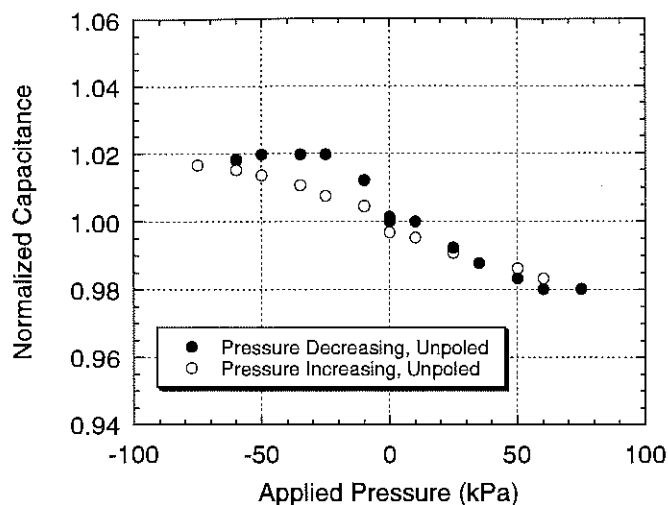


Figure 4.14. The stress response of a 2.5 μm thick 52/48 PZT thin film. The film was prepared on a 3" platinized silicon substrate and had a (111) orientation.

Two samples 3.0 and 5.0 μm thick with strong (100) textures were prepared using a conventional furnace annealing procedure. Figures 4.15 and 4.16 show the low-field data collected from the center point on both samples as a function of air pressure in the rig. The form of the compressive stress response appeared similar to the RTA'd samples i.e. applied compression increased dielectric constant. However, with increasing tension on the film the capacitance did not decrease, as did the RTA'd films, but rather increased by 2%. Measurements of the strain response as a function of applied pressure showed that these samples deform in the same way as the thinner films. Thus, this difference in the tensile response is not a consequence of an anomalous stress state imposed on the sample. Two potential sources for the variation in behavior are grain size (the thicker samples do have larger surface grain sizes of 0.5 to 0.6 μm [79] relative to 0.05 to 0.2 μm for the RTA'd films) and film orientation. This point will be addressed further in sec. 4.6.2.

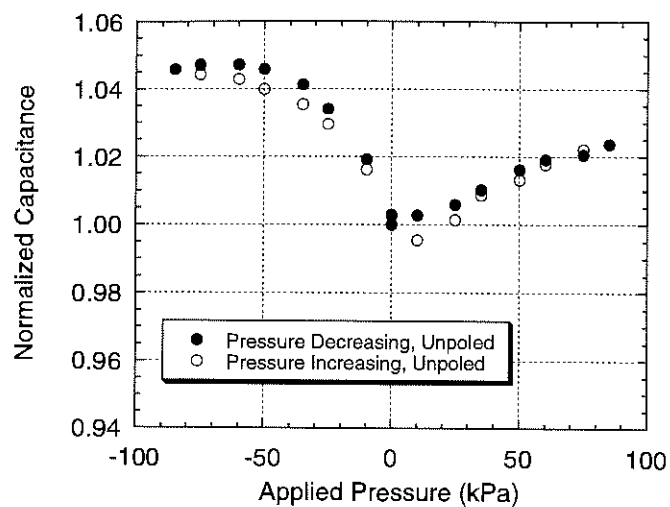


Figure 4.15. The stress response of a 3.0 μm thick furnace annealed sample. The film was prepared on a 3" platinized substrate and had a (100) orientation.

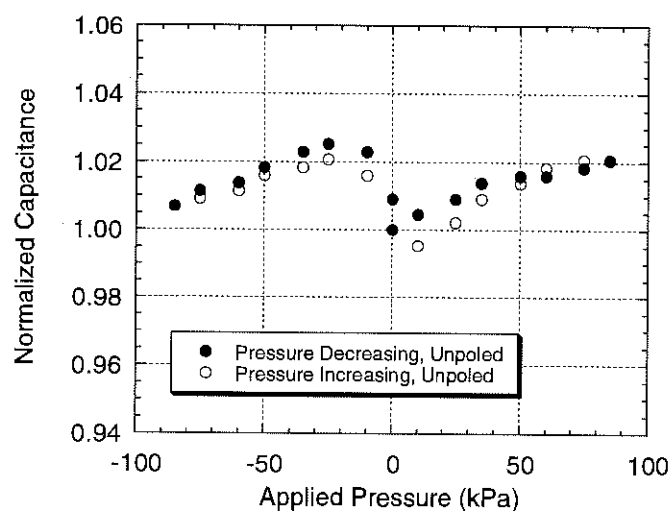


Figure 4.16. The stress response of a 5.0 μm thick furnace annealed sample. The film was prepared on a 3" platinized substrate and had a (100) orientation.

4.6. Low-Field Data Taken with the Chip-on-Steel Design

The compressive stresses achieved when using a complete 3" substrate in the uniform pressure rig did not exceed -40 MPa. Because the residual stress on the PZT films is approximately 100 MPa (sec. 4.2), an alternative mechanical design was employed (referred to as the chip-on-steel configuration) to achieve the mechanical stress needed to relieve residual tension on the film. Low-field compression experiments were conducted on PZT films having compositions of 56/44, 52/48, and 46/54. Applied strains were measured *in situ* using resistance strain gauges mounted at the center of the PZT coated chips. Test capacitors were located less than 5 mm from the measurement grids and maximum strains were found to approach -800 μ strain on all samples tested. The applied stresses were calculated assuming an equibiaxial condition and were determined to be about -115 MPa.

The low-field response of a 1 μ m thick 52/48 sol-gel film was measured in both the poled (i.e. taken through a polarization hysteresis loop) and unpoled condition and the results are given in Figure 4.17. Both samples were well aged prior to testing. Each data point was taken 1 minute after the desired rig pressure was achieved. The prestressed capacitance values corresponded to dielectric constants of ~1100 for the unpoled sample and ~1200 for the poled sample. With an increase of compressive strain, the capacitance of both the poled and unpoled samples increased to values about 3% and 6% greater than the as-deposited values. Upon release of the applied strain, the capacitance decreased and returned to values comparable with the prestressed value. It should be noted that there are data points in the plot, at zero applied pressure, that are associated with tensile strains.

The tensile strains are residual loads which are believed to have resulted from a small amount of mechanical creep in the epoxy adhesive. The residual strains are small however, and did not adversely affect the test.

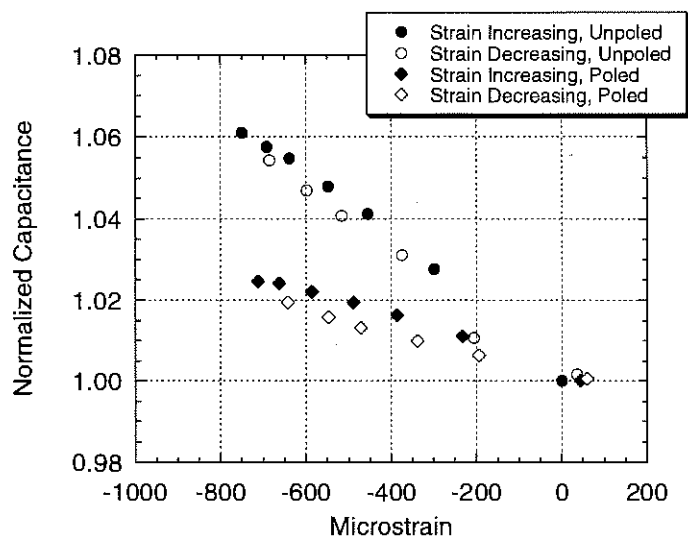


Figure 4.17. The change of capacitance for a 1 μm thick 52/48 PZT chip as a function of applied compressive strain and poling condition.

The low-field compressive stress response was also monitored for a number of compositions on either side of the morphotropic phase boundary. Figures 4.18 and 4.19 show the data collected from both the 56/44 and 48/52 compositions. The starting dielectric constants for the unpoled films were ~ 1100 for the 56/44 sample and ~ 1250 for the 48/52 chip. Trends for both compositions are similar to those observed in the experiments conducted on both the morphotropic phase boundary samples and the 60/40 and 40/60 films, i.e. with an increase of compressive strain the dielectric constant increases. The curves show a small amount of hysteresis, however the changes induced

are reversible and capacitance values return to their original magnitudes after release of the applied stress. In general, over the stress range investigated the changes observed were less than 6% and the unpoled samples displayed a greater sensitivity to compressive stress than did the poled materials.

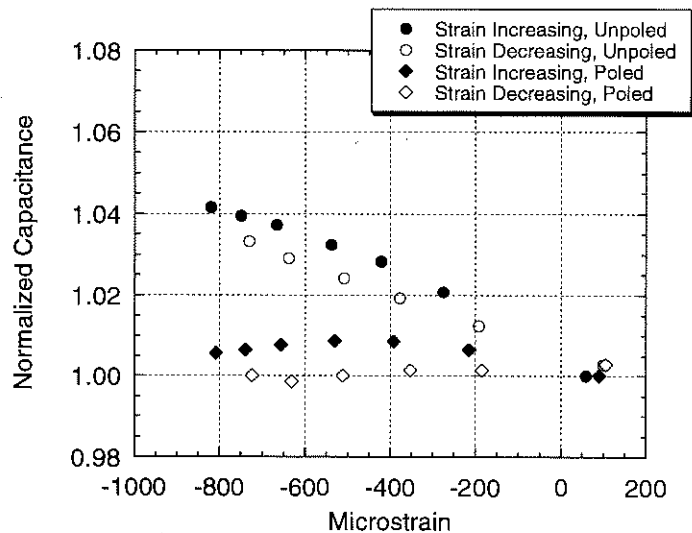


Figure 4.18. The change of capacitance for 1.2 μm (111) oriented 56/44 (rhombohedral) PZT as a function of the magnitude of the compressive strain and poling condition.

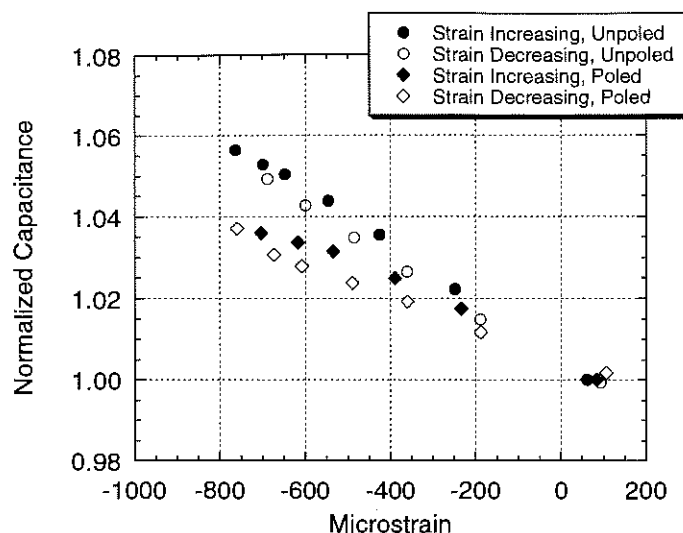


Figure 4.19. The change of capacitance for a 1.2 μm thick (111) oriented 48/52 (tetragonal) PZT as a function of the magnitude of the compressive strain and poling condition.

4.6.1. The Effects of Biaxial Stress on Dielectric Loss

The dielectric loss was monitored simultaneously (with capacitance) for all low-field experiments conducted. Results from applied tension experiments showed only a weak sensitivity of $\tan \delta$ to applied stress with the dielectric loss found to increase by less than 20% of its initial value for a stress on the order of 100 MPa. Data from the chip-on-steel tests showed that for similar applied compressive stress (-115 MPa) $\tan \delta$ increased (reproducibly) by approximately 20-25%. Changes produced were largely reversible and returned to the prestressed value after unloading. The loss data collected from the low-field experiments (chip-on-steel) shown in Figures 4.17 to 4.19 is tabulated in Table 4.2 and presented as a function of composition and poling condition. It should be noted that

the loss data was collected 1 minute after the desired cavity pressure was achieved. Fluctuations of $\pm 0.1\%$ in the loss measurements were not uncommon (e.g. $\tan \delta = 2\% \pm 0.1\%$) and in general the changes of $\tan \delta$ were about 20%.

TABLE 4.2. The Change of Dielectric Loss with Respect to the Unstressed Value for an Applied Compressive Stress of -115 MPa. The Data were Collected from Chip-on-Steel Experiments.

Sample Composition	Change of $\tan \delta$, Unpoled	Change of $\tan \delta$, Poled
52/48	+22%	+23%
56/44	+24%	+13%
48/52	+28%	+25%

4.6.2. The Effects of Crystallographic Orientation on the Low-Field Compressive Stress Response

The effect of crystallographic orientation on the biaxial compressive response was investigated using the chip-on-steel procedure, since texture was one of the factors identified as a reason for the somewhat anomalous behavior of the thick furnace annealed films under applied tension. Therefore, to evaluate the effect of texture on the compressive stress response, a 1.2 μm thick 52/48 RTA'd film was prepared with a strong (100) orientation on (100) oriented Pt coated silicon [87]. The grain size of the film was between the (111) RTA'd films (0.01 μm to 0.5 μm) and the (100) FA samples (0.5 to 0.6 μm). The compressive response is shown in Figure 4.20 and indicates that when the film is unpoled the material behaves as did the other samples tested, i.e. increasing stress increased the capacitance by about 2% and $\tan \delta$ by 23%. When the film was poled

however, the direction of the response changed and the capacitance was found to decrease by about 2% with compressive strain ($\tan \delta$ still increased 6%). The poled response is in contrast to that of the (111) textured films which showed an increase of capacitance regardless of poling condition. The discrepancy between the two behaviors suggests that the mechanisms responsible for the low-field stress response of PZT films are to some degree dependent on the orientation of the material.

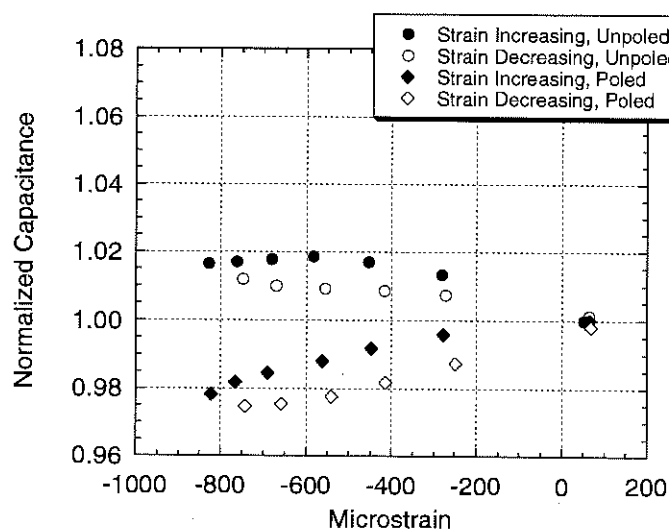


Figure 4.20. The change of capacitance for a 1.2 μm thick (100) 52/48 PZT as a function of the magnitude of the compressive strain and poling condition.

4.7. The Effects of Biaxial Stress on the High-Field Characteristics of PZT Thin Films

Changes in the polarization-electric field hysteresis loop were measured for test capacitors subjected to applied biaxial stresses with magnitudes in excess of 100 MPa. The tensile data reported were taken from complete 3" substrates while compressive data

were taken from the chip-on-steel experiments. Both tensile and compressive experiments were conducted as a function of air pressure in the uniform pressure rig and the applied stress inferred from separate strain gauge measurements (e.g. Figures 4.1 and 4.4).

4.7.1. The Effects of Applied Tension on the High-Field Characteristics of PZT Thin Films

Figure 4.21 is an example of a tensile stress response as measured for a 0.6 μm thick 52/48 sample with a (111) orientation. The film was subjected to maximum voltages of $\pm 20\text{V}$ (330 kV/cm) and the applied stresses were about 115 MPa. At the maximum tensile stress, the remanent polarization decreased 15% while the coercive field remained nearly unchanged at about 55 kV/cm. Figure 4.22 shows the tensile stress response for a 5.0 μm thick 52/48 film with a (100) orientation (sec. 3.2.2). The response shown is similar to the thinner 0.6 μm film with a change of P_r of about 23%. The coercive field of the thicker film was also insensitive to applied stress and was measured at about 25 kV/cm for both the stressed and unstressed conditions.

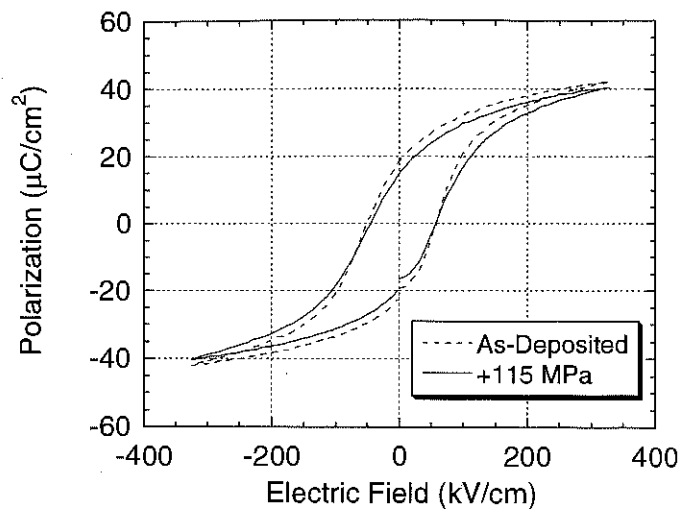


Figure 4.21. Comparison of the stressed and as-deposited polarization hysteresis loops of a 0.6 μm thick 52/48 PZT film. The average remanent polarization of the as-deposited film was 21 $\mu\text{C}/\text{cm}^2$ and the average coercive field was 55 kV/cm.

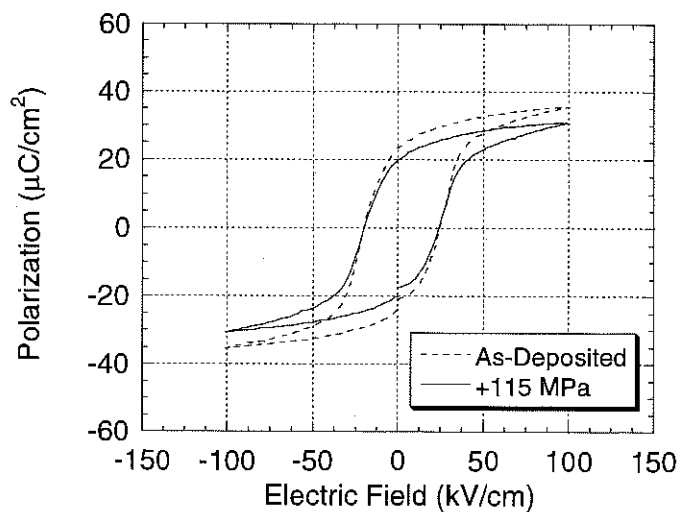


Figure 4.22. Comparison of the stressed and as-deposited polarization hysteresis loops of a 5.0 μm thick 52/48 PZT film prepared with a (100) orientation using a conventional furnace annealing procedure (sec. 3.2.2). The average remanent polarization of the as-deposited film was 23 $\mu\text{C}/\text{cm}^2$ and the average coercive field was 26 kV/cm.

4.7.2. The Effects of Applied Compression on the High-Field Characteristics of PZT Thin Films

Compressive data were taken from the chip-on-steel experiments. As described in sec. 4.4, the largest strains for the chip-on-steel studies were produced during the first pressure cycle as the steel dome was forced inside out. The plot in Figure 4.23 illustrates the effect of that stress on the polarization hysteresis loop of a 1 μm thick 52/48 test chip. The maximum stress on the chip was approximately -130 MPa. For this stress level, the polarization of the film increased reversibly by about 25%.

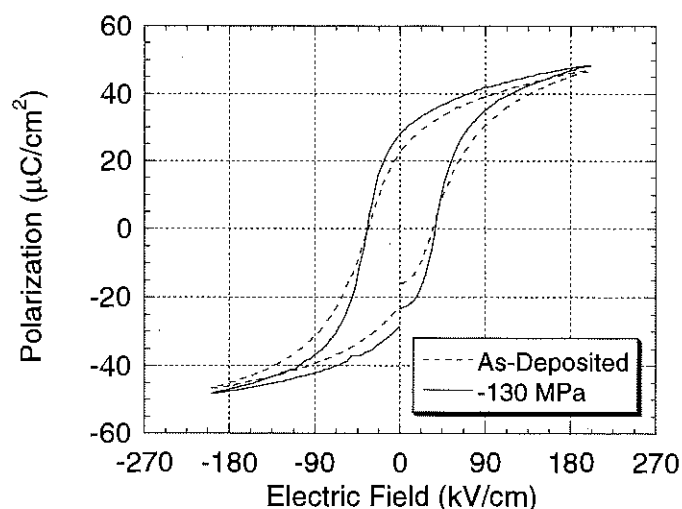


Figure 4.23. A comparison of the compressively stressed and as-deposited polarization hysteresis loops for a 1.0 μm thick (111) oriented 52/48 sol-gel PZT film. The average remanent polarization for the unstressed film was 23 $\mu\text{C}/\text{cm}^2$ and the average coercive field was 34 kV/cm .

Inspection of the plot in Figure 4.23 also indicates that the coercive field of the material increased slightly (by about 6%) with increasing compressive strain. High-field data taken from other samples with different compositions and orientations showed a similar response. This behavior is shown clearly in Figure 4.24, where the average coercive field (i.e. average of $+E_c$ and $-E_c$) and the average remanent polarization (i.e. average of $+P_r$ and $-P_r$) of the 1 μm thick 52/48 film were plotted as a function of applied gas pressure. The results bear a strong resemblance to the form of the strain curve given in Figure 4.3. As indicated, the average of both quantities increases with increasing stress up to some maximum value at pressures of about 415 kPa. For points beyond that pressure, the values decreased a small amount. The maximum increase of both the coercive field and remanent polarization were calculated to be 6% for E_c and 24% for P_r .

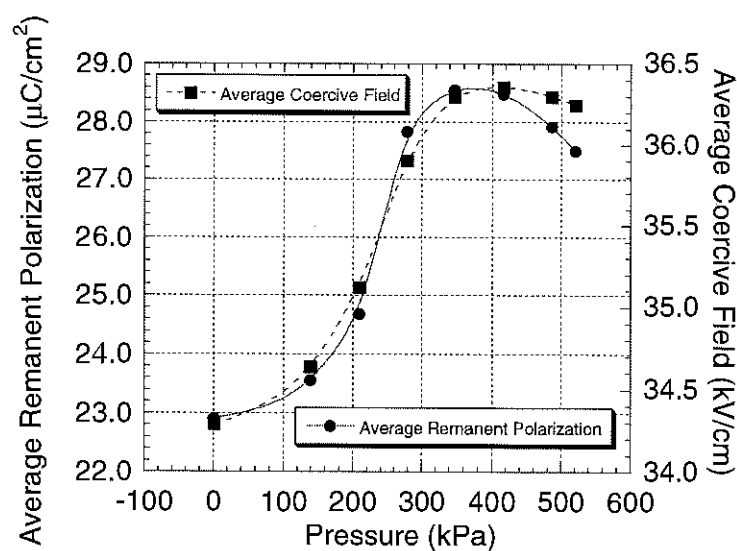


Figure 4.24. The variation of the average coercive field and average remanent polarization with the application of compressive strain. Data were taken from the first pressure cycle in the chip-on-steel experiments.

The effects of microstructural texture on the high-field compression response were investigated via the characterization of a (100) oriented 1.2 μm thick 52/48 sample. The plot in Figure 4.25 shows the change in the polarization hysteresis loop in response to an applied compressive stress of about 115 MPa. The changes produced in the P-E loop were reversible. Data in the plot show the average remanent polarization of the film increased by 23% while the coercive field was raised 9%. The magnitudes of both changes are consistent with the data taken from (111) samples of comparable thickness (Figure 4.21), which suggests that the high-field stress response is insensitive to microstructural texture.

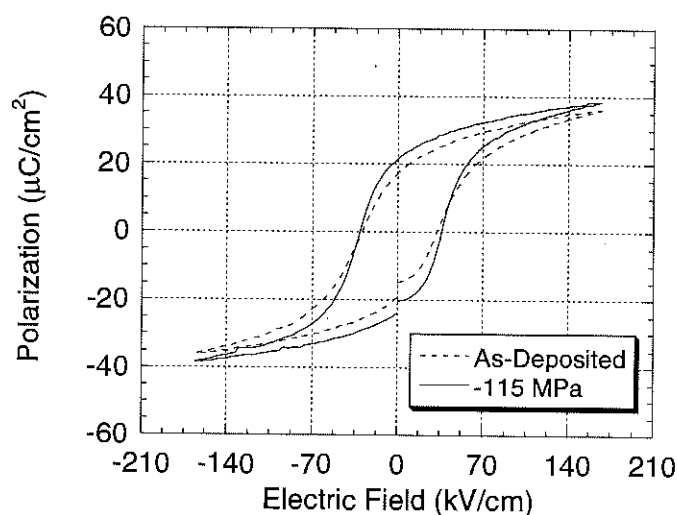


Figure 4.25. A comparison of the compressively stressed and as-deposited polarization hysteresis loops for a (100) oriented 1.2 μm thick 52/48 sol-gel PZT film. The average remanent polarization for the unstressed film was 18 $\mu\text{C}/\text{cm}^2$ and the average coercive field was 31 kV/cm.

The high-field stress response of films with 56/44 and 48/52 compositions was also measured when subjected to -115 MPa of applied compression. The results are given

in Figures 4.26 and 4.27 and illustrate behavior similar to that of the 52/48 samples, i.e. the compressive stress increased both the remanent polarization and coercive field strengths of the films. The changes of P_r were 20% for the rhombohedral film and 17% for the tetragonal film, while the changes of E_c were 4% for the rhombohedral and 8% for the tetragonal. The effects produced were reversible and with release of the applied stress the P-E loops returned to their unstressed shapes.

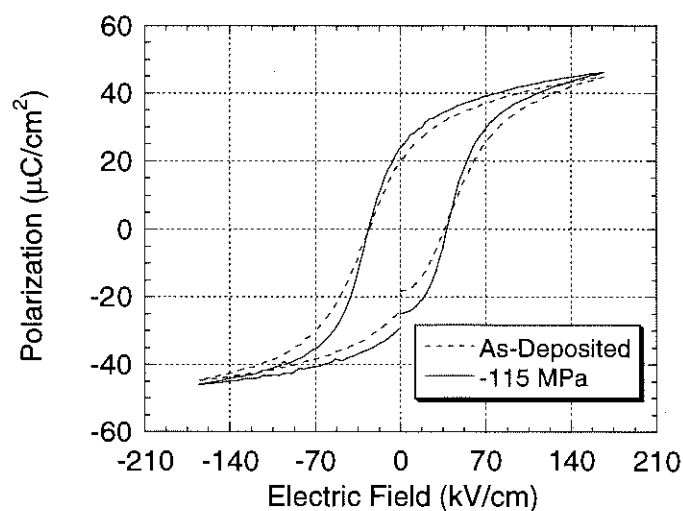


Figure 4.26. A comparison of the compressively stressed and as-deposited polarization hysteresis loops for a 1.2 μm thick 56/44 (rhombohedral) sol-gel PZT film. The average remanent polarization for the unstressed film was $23 \mu\text{C}/\text{cm}^2$ and the average coercive field was 31 kV/cm.

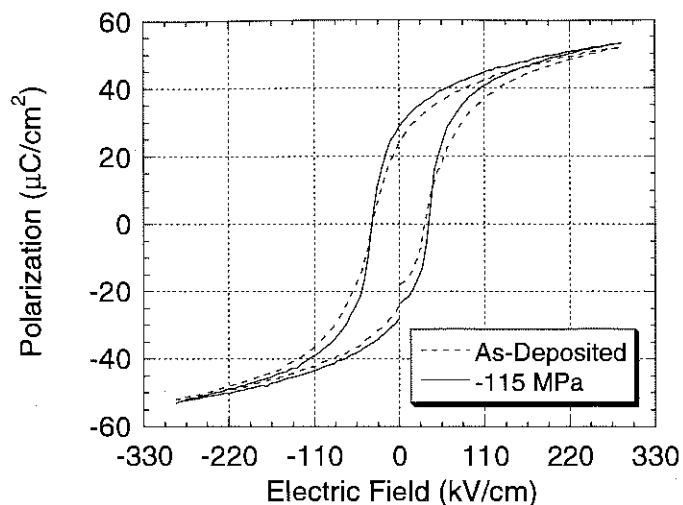


Figure 4.27. A comparison of the compressively stressed and as-deposited polarization hysteresis loops for a 1.2 μm thick 48/52 (tetragonal) sol-gel PZT film. The average remanent polarization for the unstressed film was $24 \mu\text{C}/\text{cm}^2$ and the average coercive field was $34 \text{ kV}/\text{cm}$.

4.8. Discussion of The Biaxial Stress Response of PZT Thin Films

4.8.1. Low-Field Biaxial Stress Response of PZT Thin Films

The low-field stress response of the PZT films tested contrasts strongly with the results of earlier experiments on bulk PZT ceramics [51, 57]. For bulk ceramics, two-dimensional pressures of similar magnitude to those used here, when applied perpendicular to the poling direction reduced the dielectric constant by about 20 and 40% for PZT-4 and PZT-5, respectively. The response was caused by non- 180° domain wall motion whereby the ferroelectric domains oriented nearly parallel to the applied stress

reorient so that the spontaneous polarization is directed more perpendicular to the direction of the load. The relative permittivity of the material was then decreased as a result of the anisotropy in the material's dielectric constant ($\epsilon_{11} > \epsilon_{33}$ [35]). The decrease in the dielectric constant was coupled with a 30-50% increase of the dielectric loss which was associated with the motion of domain walls. On unloading, the hard PZT-4 permittivity recovered substantially due to realignment of the polar vector by the internal field associated with defect dipoles, while the soft PZT-5 showed large irreversibility due to mechanical depoling. The small changes seen in the thin film dielectric properties, coupled with the reversible nature of the stress experiments suggest that it is difficult to reorient domains ferroelastically in the PZT films studied here. This in turn suggests non-180° domain walls will contribute little to the thin film properties over the stress range studied.

For comparison, the results of Brown on ceramic PZT [51] are illustrated in Figure 4.28 together with the results from the (111) 52/48 sol-gel films presented here. It is clear from the plot that the dielectric constant of the bulk ceramics is much more sensitive to mechanical load and that the magnitude and direction of the response of the two forms of PZT (bulk and thin film) are much different. For an applied biaxial stress of -100 MPa (i.e. sum of the principal stresses is -200 MPa) the capacitance of the unpoled 52/48 film showed an increase of about 6% while the poled sample increased by less than 3%. In contrast, the dielectric constant of both the hard and soft ceramics decreased between 20 and 40% and displayed some degree of irreversibility in both cases.

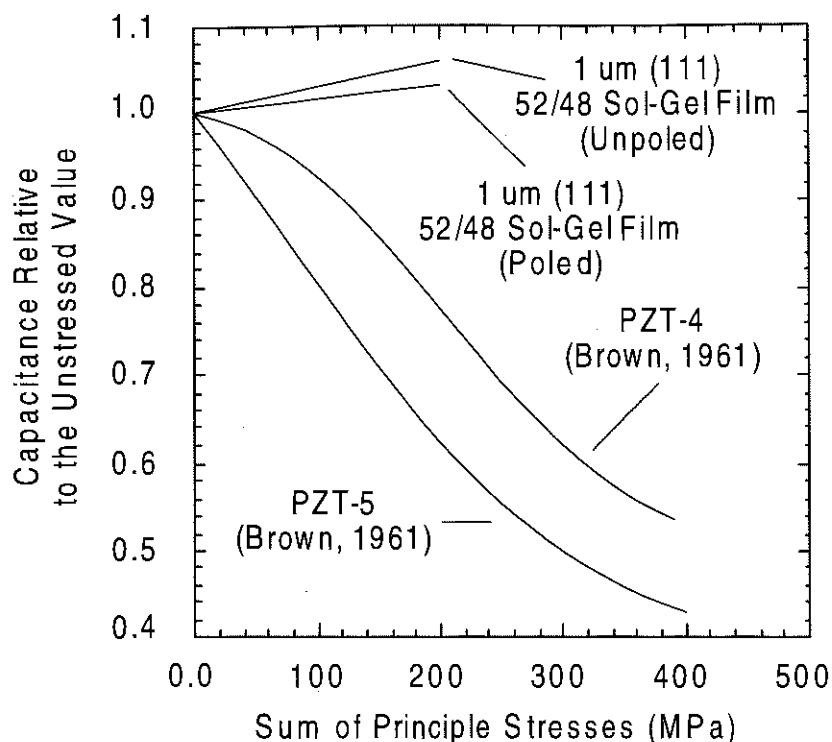


Figure 4.28. Comparison of bulk ceramic and thin film low-field stress response.

In addition to the obvious differences in the stress response of the dielectric constant (Figure 4.28), the stress dependence of the thin film dielectric loss data is inconsistent with non-180° domain wall motion. In particular, the fact that $\tan \delta$ increases with both tension and compression weighs against the activation of ferroelastic domain walls. Had domain wall motion been induced by the applied stress, tensile stress would have further clamped extrinsic contributions and reduced loss, while applied compressive stress should have increased extrinsic effects via relief of the residual tension and thus raised $\tan \delta$.

4.8.2. High-Field Biaxial Stress Response of PZT Thin Films

Results of the low-field experiments indicate that extrinsic contributions are limited in the films tested. This conclusion is supported by the high-field stress data. In particular, if ferroelastic reorientation was important, then an applied tensile biaxial stress would tend to increase the coercive field, while a compressive stress should decrease it somewhat. This was not observed in any of the thin film experiments.

It is proposed that the effects brought about in response to the applied stress were the result of the relative motion of the positions of the polarization vectors with respect to the film's surface. Domains which were oriented with positions less than 90° to the surface normal were elastically deformed in response to the applied stress. The polarization vectors were thus moved to positions closer to parallel with the substrate under applied tension, and closer to perpendicular with applied compression. The normal component of the polarization for each domain was thus either increased or reduced a small amount.

4.9. Consideration of the Mechanisms of the Thin Film Biaxial Stress Response

Because the ferroelastic response (i.e. reorientation of non- 180° domains in response to applied stress) of the films tested appears to be limited, it is interesting to consider the mechanism(s) which governs the stress-dependence of the dielectric and ferroelectric properties. Consideration of the previous work on bulk ceramics suggests that were domain reorientation the active mechanism in thin films, changes in the low-field data would be appreciably larger and in directions opposite to what is reported here

(see Figure 4.28). That however, was not the case and to explain the data a number of alternative mechanisms were considered.

It is known that the Curie point of barium titanate is sensitive to applied biaxial stress [88]. This can affect the room temperature dielectric constant since an increase of T_c would decrease ϵ_r at 25°C. The idea of a shift of the Curie point would be consistent with the capacitance data given here if the shift is brought about as a result of the increase or decrease of the volume of the PZT unit cell. Tuttle's stress transformation model [46] indicates that PZT films deposited on silicon substrates are predominately a-domain oriented (i.e. c-axis of the unit cell closer to parallel to the substrate). When compressively stressed therefore, the volume of the a-oriented domains decreases, T_c shifts downward, and the dielectric constant of the film increases. Conversely, if the films were loaded in tension, the volume of unit cells would increase, T_c would shift upwards, and the dielectric constant would decrease.

Although the majority of the low-field data are consistent with a volume induced change of T_c (for predominantly a-domain films) the prediction of the effects of the applied stress on the Curie point is a complex problem. It is therefore difficult to assign the changes of the capacitance to a shift of the Curie point and in fact, capacitance versus temperature measurements on a number of 52/48 films showed little shift in T_c [89]. In addition, the dielectric loss should decrease and the coercive field would be expected to increase with an increase of T_c (and vice versa as T_c drops). The data collected however, indicate that the dielectric loss increases regardless of the sign of the stress and the change of the coercive field is increased with compressive stress (which is inconsistent with a decrease of T_c). That observation, together the lack of a substantial observed T_c

shift, suggests that a stress-induced shift of the Curie point is not the predominant stress response mechanism in sol-gel PZT films.

The second possibility considered to explain the low-field stress response was the elastic deformation of the Pt/PZT/Pt test capacitor. As the films were stressed and the dimensions of the capacitor changed, the capacitance would rise or fall to reflect the alteration of the capacitor's geometry. However, a tensile stress would reduce the thickness of the films and increase the surface area (thereby increasing capacitance and not decreasing it) which is inconsistent with the empirical observations. Furthermore, given the similarity in the response for tetragonal, rhombohedral, and MPB films, it is clear that a residual stress induced shift in the morphotropic phase boundary is also not responsible. Therefore, the mechanism(s) responsible for changes in the dielectric characteristics are still unclear and more work is needed to identify the source of the biaxial stress response.

4.10. Possible Reasons for the Limited Extrinsic Response of PZT Thin Films

The discussion has, to this point, focused on the evidence presented which suggests that extrinsic contributions are limited in PZT thin films. There is, in addition to this investigation, substantial evidence which supports that conclusion in the form of high-field X-ray diffraction measurements [90] and piezoelectric characterization [3]. In addition, biaxial stress experiments have been conducted as a function of both film thickness and orientation (secs. 4.5.3 and 4.6.2) and the results collected are consistent from sample to sample, i.e. small reversible changes in both the low and high-field characteristics. That consistency suggests that the limited domain wall motion in PZT

films is not the result of residual stress, texture, or thickness and the lack of extrinsic contributions results from some other mechanism.

Substantial work, both experimental and theoretical [91, 92], has been conducted on grain size effects in bulk ferroelectrics. The results indicate changes in the domain structure and limitations to the extrinsic contributions as the grain size of the PZT ceramics is decreased below 1 μm . Since the grain sizes of the PZT films tested typically range from 0.01 to 0.5 μm , it is possible that the limited extrinsic contributions in films could be the result of the submicron grain sizes of the materials. The idea is supported by the work of Eatough et al. [90], who studied the ferroelectric switching behavior of PZT thin films with the aid of an X-ray micro-diffractometer. Results from that work showed, via diffraction patterns from tetragonal (40/60 and 30/70) films, that for grain sizes less than 1 μm (similar to the samples tested here) switching was considerably less than for films with grain sizes between 1 and 2 μm . There is therefore, evidence which suggests that the limited extrinsic contributions in sol-gel PZT films are related to the submicron grain structure of the material and not the global residual stress state of the film.

It should be noted, that in addition to the submicron grain sizes of the films, possible mechanisms for the reduction in non-180° domain wall motion include; (1) a limited concentration of non-180° domain walls as is commonly associated with decreasing particle size in perovskite ferroelectrics [91], (2) pinning of the existing non-180° domain walls by local rather than global stresses, e.g. the film/substrate interface, and (3) decreases in the wall mobility due to interaction with point defects such as lead and oxygen vacancies. The latter are known to form the defect dipoles which are

responsible for domain pinning in hard PZT ceramics [93] and have been linked to problems such as imprint and fatigue in PZT thin films [94].

5. The Wafer Flexure Method for the Determination of the Transverse Piezoelectric Coefficient (d_{31}) of PZT Thin Films

5.1. Introduction

The deposition and characterization of piezoelectric films has been actively pursued for over thirty years [19]. Early attempts at characterization relied not upon the specific calculation of the coefficient of interest (e.g. d_{33} or d_{31}) but rather the identification of piezoelectric activity via the generation and detection of an ultrasonic signal. Detection of the signal was considered enough to classify the film as piezoelectric. In recent years, considerable advances have been made in the area of piezoelectric film characterization. Laser beam interferometry is perhaps the most well developed method and has made a significant contribution to the characterization of both the transverse (d_{31}) and longitudinal (d_{33}) coefficients of piezoelectric thin films [3, 4]. The technique has drawbacks however, the most notable of which are its expense and complexity. In contrast, the wafer flexure technique is a simple, inexpensive method which was developed to characterize the transverse (d_{31}) coefficient of PZT thin films. The chapter which follows will present data from experiments aimed at both the basic piezoelectric characterization of PZT thin films and the validation of the wafer flexure method.

5.2. Validation of the Mechanical Plate Theory

The success of the wafer flexure technique requires that the user accurately calculate the mechanical stresses applied to the film. The models used are based upon classical plate theory to first calculate the stresses applied to the silicon substrate (sec. 3.5.2). The stress on the film is then determined by assuming conservation of strain across the film/substrate interface and writing generalized Hooke's law for both the film and substrate. The set of equations obtained are then solved for the stresses applied to the PZT and used together with the measured charge (in response to that stress) to calculate the film's d_{31} coefficient (eq. 3.3, sec. 3.5).

The electric charge produced is measured experimentally, as are the pressure and the dimensions of the test rig. The accuracy of the d_{31} measurements is then dependent upon the validity of the stress analysis used. As was shown by the strain gauge experiments in the investigation of biaxial stress effects (chapter 4), the mechanical behavior of a PZT coated wafer deviates a significant amount from that predicted by the classical theory (for large applied pressures). For that reason, the stress analysis used in the determination of the d_{31} coefficient was validated by a comparison with measured strain data for the small amplitude oscillations used in the piezoelectric characterization.

Experiments were conducted in which 120Ω resistance strain gauges were fixed to the center of PZT coated silicon wafers. The wafers were placed in the uniform pressure rig, clamped under 2.5 in-lbs of torque, and the audio speaker started. The gauges were shunt calibrated with the value of $1 \mu\text{strain}$ (i.e. $\text{strain} \times 10^{-6}$) set equal to 1 mV of output. The signal from the strain conditioner was then output to the lock-in amplifier which

displayed the rms voltage from the strain gauge as the pressure in the rig oscillated. In a similar fashion, the cavity pressure was measured from the transducer on the rig housing and used to calculate the strain on the film (from the plate theory). For the calibration experiments, the pressure oscillation was adjusted via the drive voltage on the audio speaker. The drive voltage was set using the reference signal from the lock-in amplifier to values which ranged from 0.2 to 0.8 V_{rms} at frequencies of 4 or 5 Hz.

5.2.1. Strains Measurements Made on 3" Substrates

The strain response at the center of a (100) silicon wafer is plotted together with that predicted from plate theory in Figures 5.1 and 5.2. The data were collected for both the prototype and modified uniform pressure rigs. The differences between the two, for the purposes of this discussion, are related to the clamping conditions produced by the different rigs. For the prototype design, the aluminum seats between which the wafers are clamped were removable and had been polished to a 5 μm finish.⁴ In contrast, the modified rig was not designed with removable clamps and the recesses in which the wafers were placed retained their as-fabricated finish. Theoretical strain calculations were made for a uniformly loaded clamped circular plate using the average values of Young's modulus and Poisson's ratio for (100) silicon (justification for this is given in sec. 5.2.3). Pressures in both rigs were measured at about 0.1 kPa at a drive of 0.2 V and about 0.3 kPa at a drive of 0.8 V.

⁴ The surfaces were polished originally to improve the pressure seal in the rig and to reduce the risk of sample fracture. Although an air tight chamber was not needed, the polished wafer clamps proved to be beneficial from the standpoint of meeting the criteria of the stress models.

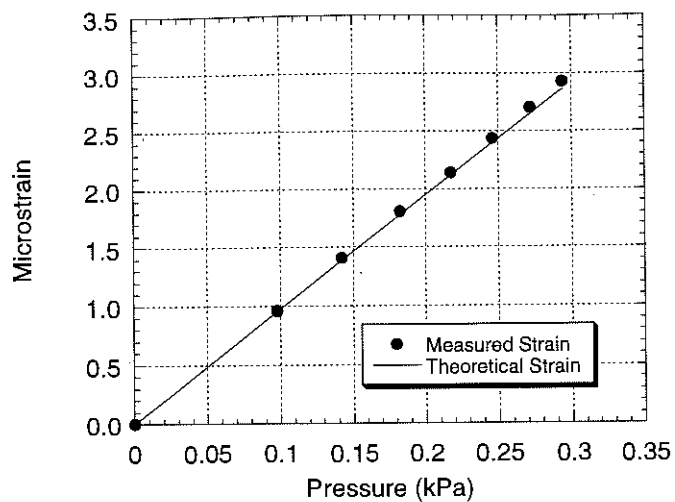


Figure 5.1. The comparison of experimental and theoretical strains at the center of a 3" silicon wafer. Data were collected from the prototype rig.

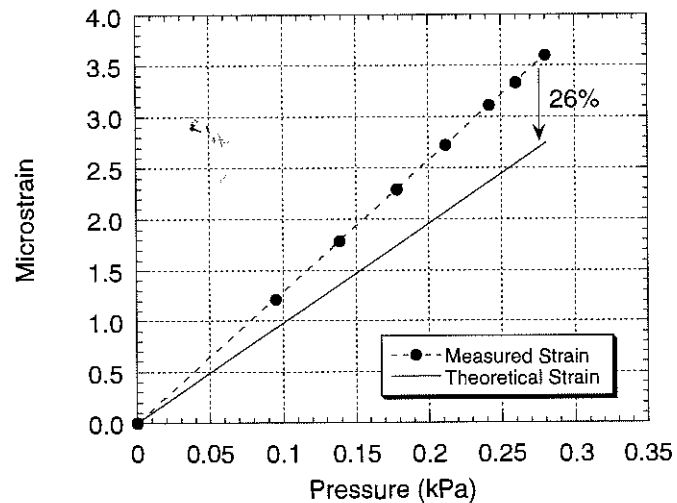


Figure 5.2. The comparison of experimental and theoretical strains at the center of a 3" silicon wafer. Data were collected from the modified rig.

The plots in Figures 5.1 and 5.2 show that data collected from the prototype rig are within 1% of theory while the data collected from the modified rig exceed the calculations for a fully clamped plate by 26%. The differences between the two configurations are probably related to the differences in the surface finish and clamping conditions of the two rigs. As stated, the surfaces of the modified rig were left as-machined. It is expected that the resulting irregularities in the surface profiles resulted in ineffective clamping of the substrate, which allows the wafer to flex in some mixed mode condition (i.e. semi-clamped). Conversely, effective clamping was produced serendipitously in the prototype design. In this case, the wafer clamps were separate from the pressure rig and retention ring. When assembled, the polished rings were forced flat against the wafer surface. Because of their detachment from the rest of the rig, the alignment of the rings was not dictated by artifacts in the rig's manufacture, but rather the flatness of the wafer. Consequently the data in Figure 5.1 suggest that the clamped condition in the prototype design more closely approximated the theoretical criteria for a uniformly loaded, clamped circular plate.

Data presented in chapter 4 indicated a significant deviation of the large deflection behavior of coated silicon substrates from that predicted by plate theory (see Figures 4.1 and 4.2). It was a concern therefore, that the manner in which the bare silicon wafers responded to the pressure oscillation (Figures 5.1 and 5.2) might differ from the way in which a PZT coated wafer would respond. Therefore, experiments were conducted in which the strain response of two 3" PZT coated silicon substrates were measured while clamped in the modified pressure rig (the prototype was not used for these tests). The experimental conditions used were the same as those for the uncoated

wafers. The strain gauges were bonded to the center of both wafers and the samples were clamped in the rig with 2.5 in-lbs of torque on the retention screws. The data collected were taken from two 52/48 sol-gel samples 0.8 and 3.0 μm thick and are given in Figures 5.3 and 5.4. Three experiments were conducted on each wafer with the substrate removed from the rig and relocated to a different position after every test. The data shown represent the average of the three experiments.

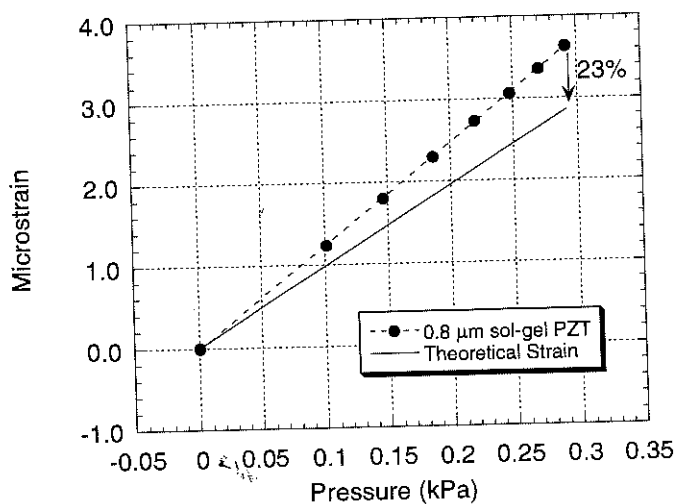


Figure 5.3. The comparison of experimental and theoretical strains (for a clamped plate) at the center of a 0.8 μm thick sol-gel PZT coated silicon wafer in the modified rig.

The strain data in Figures 5.3 and 5.4 show that the mechanical behavior of a PZT coated substrate does not differ a significant amount from that of a bare silicon wafer. In all cases tested, flexure of the substrate yielded strains approximately 25% greater than those predicted from the plate theory. Again, this is believed to be related to the seating of the wafer in the pressure rig, so that the wafer is not effectively clamped. Thus, all data

collected with the modified rig were corrected for that deviation by multiplying the calculated stresses by a factor of 1.25 prior to the calculation of a film's d_{31} coefficient.

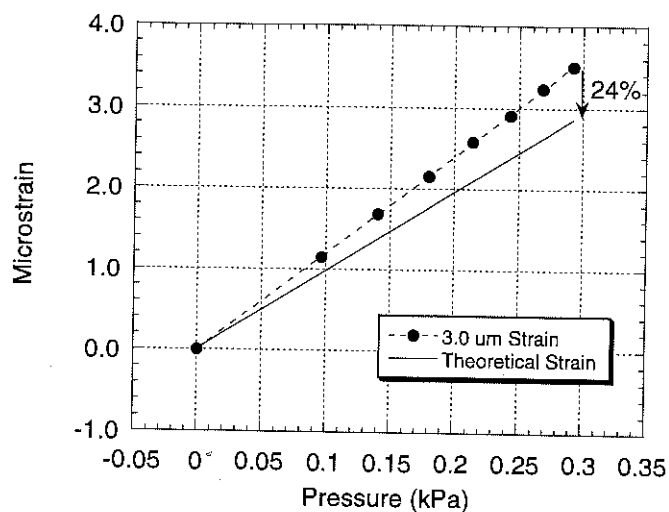


Figure 5.4. The comparison of experimental and theoretical strains (for a clamped plate) at the center of a 3.0 μm thick sol-gel PZT coated silicon wafer clamped in the modified rig.

5.2.2. Strain Measurements Made on 4" Substrates

In addition to the characterization of 3" substrates the modified wafer flexure device was designed with the capability to characterize films deposited on 4" wafers. In light of the discrepancies illustrated in Figures 5.3 and 5.4, the deviation from the classical behavior of a 4" substrate was also quantified. Based on the consistency of the 3" results it was assumed that the mechanical behavior of a PZT coated substrate could be reasonably approximated by the results obtained with a (100) silicon wafer coated with 0.2 μm of evaporated platinum. Three experiments were conducted with the

wafer remounted at a different location after every test. The results were then averaged and are plotted in Figure 5.5 together with the theoretical predictions for a uniformly loaded, clamped circular plate.

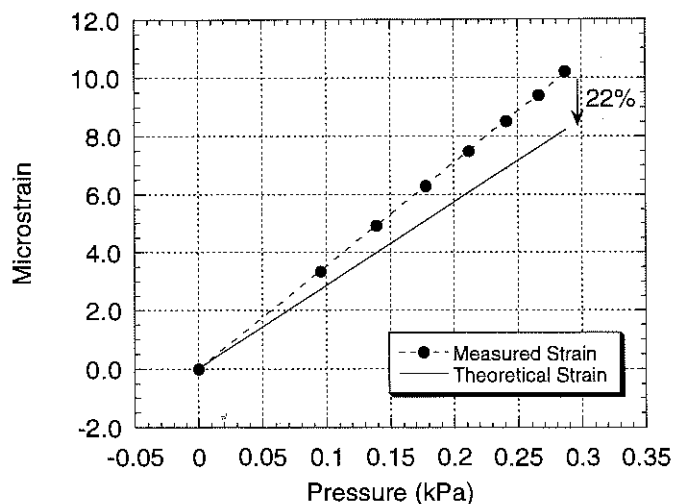


Figure 5.5. The comparison of experimental and theoretical strains (for a clamped plate) at the center of a 4" platinized silicon wafer when clamped in the modified rig.

It was found that the experimental strains are in excess of the theoretical values by 22%. The reason for the deviation is again thought to be ineffective clamping of the test wafer. Data collected with the 4" rig were corrected for that deficiency by multiplying the calculated stresses by a factor of 1.22 prior to the calculation of d_{31} .

5.2.3. Analysis of the Mechanical Anisotropy of the Silicon Wafer

The silicon wafers on which the PZT films are deposited are single crystal substrates. Thus, the anisotropy of Young's modulus and Poisson's ratio must be

accounted for in the stress analysis. One approach is to calculate bounding values of the stress (and thus two values of d_{31}) from the maximum and minimum of the in-plane elastic properties. Data calculated in that manner are reported as a range of values between which the correct d_{31} coefficient should lie. To evaluate directly the importance of the mechanical anisotropy in the calculation of d_{31} , multiple strain gauges were bonded to the same substrate along the $\langle 100 \rangle$ and $\langle 110 \rangle$ axes of a (100) silicon wafer. Any differences in the measured strains would reflect the anisotropy of the mechanical constants.

The anisotropy experiments utilized two strain gauges bonded 10 mm from the center of the wafer along the $\langle 100 \rangle$ and $\langle 110 \rangle$ crystallographic directions. The pressure in the rig housing was changed via the oscillation of the audio speaker driven with rms voltages between 0.2 and 0.8 V. Data were collected using a lock-in technique and are plotted, together with the theoretical predictions for a uniformly loaded clamped circular plate (eqs. 3.4 and 3.5) as a function of air pressure in Figure 5.6.

The plot in Figure 5.6 shows that the best fit to the empirical data for both directions is achieved when strain is calculated based on the average of the maximum and minimum in-plane elastic constants. Thus, explicit knowledge of the elastic properties at the specific location of the test capacitor need not be known, and the applied stress can be calculated using the average in-plane values of Young's modulus and Poisson's ratio.⁵

⁵ The question regarding the mechanical anisotropy of the silicon substrate could have been treated via the utilization of (111) silicon rather than (100). For wafers with that orientation the Young's modulus and Poisson's ratio are constant regardless of the test capacitor's location [81].

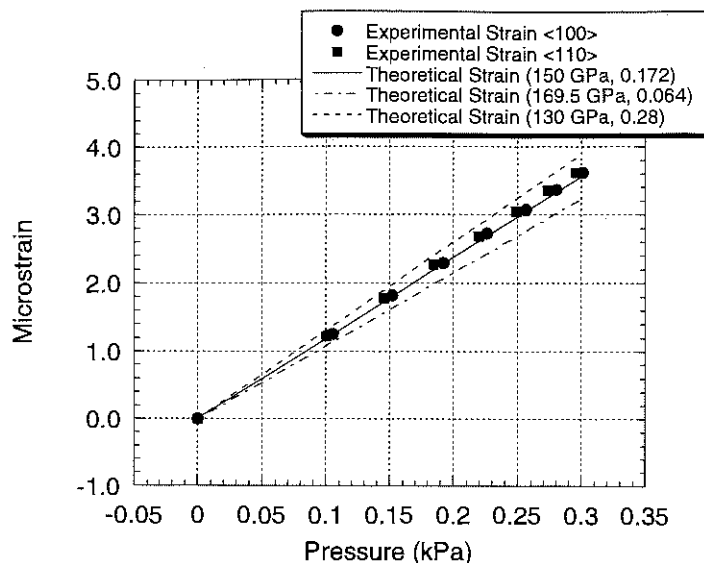


Figure 5.6. The comparison of the measured and calculated strains along the principal axes of a (100) 3" silicon wafer. Strains were measured along the <100> and <110> crystallographic axes 10 mm from the center of the substrate. The notation used in the legend corresponds to the values of Young's modulus and Poisson's ratio used in the calculations.

5.3. Transverse Piezoelectric Characterization with the Prototype Configuration

The prototype wafer flexure apparatus was designed to operate in a semi-AC fashion. That meant that the pressure oscillation in the rig was made by hand (with a 60cc syringe) and the charge produced was derived from the trace recorded on an oscilloscope. This configuration was used to validate the measurement technique, and the results were incorporated into an improved design that used mechanized pressure oscillation and a lock-in charge measurement.

5.3.1. Variation of d_{31} over the Surface of a 3" Wafer

The d_{31} coefficient of a 0.3 μm thick 52/48 sol-gel film was monitored as a function of position over the surface of a 3" wafer. It was expected that the transverse coefficient of a homogenous film would be independent of radial position (on the wafer) and the characterization of a number of different spots would therefore provide an indirect validation of the stress analysis (since the stress does depend on radial position). Seven different test capacitors on the surface of a 3" wafer were poled with +330 kV/cm for 10 minutes (top electrode positive). The d_{31} coefficient was measured after a 10 minute age and the data collected were correlated to the average remanent polarization of the sample (calculated from $+P_r$ and $-P_r$). Results were consistent from spot to spot and are tabulated together with the sample position and remanent polarization in Table 5.1.

TABLE 5.1. The d_{31} Coefficients of a 0.3 μm Thick 52/48 Sol-Gel Film Measured as a Function of Radial Location on a 3" Substrate

Radius (mm)	Magnitude of d_{31} (pC/N)	P_r (avg.), $\mu\text{C}/\text{cm}^2$
2.4	-43	24
11.3	-40	21
11.3	-40	20
14.0	-44	20
16.4	-40	23
17.6	-46	21
19.5	-36	22

5.3.2. d_{31} Measured as a Function of the Excitation Stress in the Uniform Pressure Rig

The transverse piezoelectric coefficient of a $0.3\ \mu\text{m}$ thick 52/48 sol-gel film was measured as a function of the excitation stress in the prototype rig over a range of 5 to 25 MPa (as measured with resistance strain gauges). The film was poled with an electric field of $+150\ \text{kV/cm}$ for less than 1 minute and data were collected for four different displacements of the syringe. The results from two experiments conducted on different test capacitors are given in Figure 5.7 as a function of the applied air pressure in the rig.

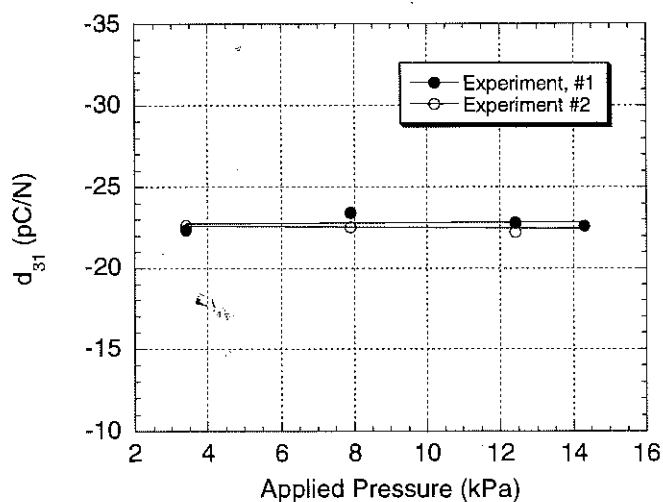


Figure 5.7. The change of the d_{31} coefficient as a function of excitation pressure for a $0.3\ \mu\text{m}$ thick 52/48 sol-gel film. The endpoint stresses applied to the film have been calculated (from resistance strain gauge measurements) to be approximately 5 and 25 MPa.

Damjanovic et al. have shown that application of 5-7 MPa of uniaxial AC stress leads to an increase in the piezoelectric activity (as measured by the direct longitudinal effect) of barium titanate and PZT ceramics by about 40% [38, 39]. The enhanced

piezoelectric coefficient was attributed to the activation of non-180° domain wall motion in the ceramic samples. In contrast, results presented here (chapter 4) and elsewhere [90] have shown that the amount of ferroelastic domain reorientation is modest in PZT films. As a result of the limited extrinsic effects, the piezoelectric coefficients, when measured as a function of the applied excitation stress (i.e. in a manner similar to Damjanovic et al.) should remain constant. That was in fact the case, and the results in Figure 5.7 serve to further illustrate the limited twin wall motion in sol-gel films.

5.3.3. Resolution of the Wafer Flexure Technique

The resolution of the wafer flexure method was demonstrated with a series of low-field poling experiments in which a film was mounted and then exposed to an applied field of +33 kV/cm ($E_c = 45$ kV/cm). The as-deposited sample was first poled for 150 min with the top electrode the anode, over which time the d_{31} value increased from -2 to -9 pC/N. After an overnight age, the sample was poled with the same field but with the top electrode the cathode. In the negative bias tests (i.e. the top electrode negative) d_{31} decreased with poling time from an initial value of -5 pC/N (the value measured after the overnight age) down to almost zero after poling for 200 minutes. At points beyond the zero mark the magnitude of the film's transverse coefficient increased to a maximum value of about -3 pC/N after poling for 21 hours.

The data are plotted in Figure 5.8 with negative values of d_{31} listed both above and below the x-axis (i.e. the sign reversal in the net polarization has been accounted for). When plotted this way, a logarithmic relation can be fitted to the data which better illustrates the resolution of the technique. Five points were noted with magnitudes of less

than 1 pC/N and their adhesion to the log relation was taken as evidence of their validity (the curve fit had a residual of better than 0.99).

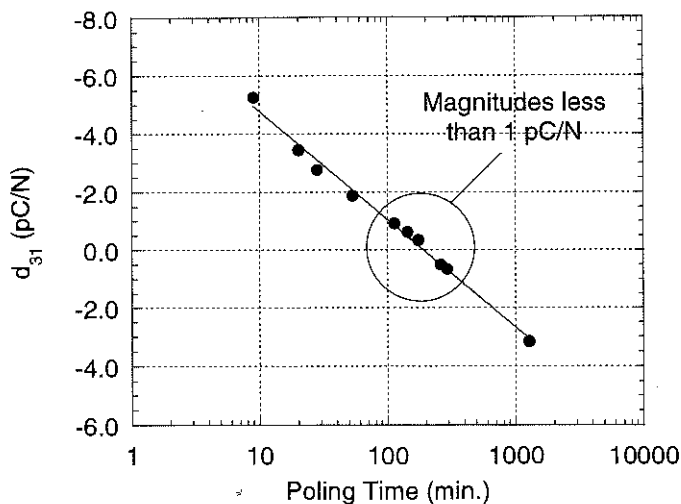


Figure 5.8. The change of the d_{31} coefficient with poling time for a 0.3 μm thick 52/48 sol-gel film. The sample was poled with 33 kV/cm with the top electrode negative.

5.4. Measurements Made with the Modified Wafer Flexure Technique

The prototype wafer flexure apparatus was modified to operate as an AC technique with the addition of mechanized pressure oscillation and lock-in charge detection (chapter 3, sec. 3.5.1). Air pressure within the rig housing is changed periodically via the displacement of a 10" audio speaker. The charge produced in response to the applied pressure is probed with a mercury drop electrode (sec. 3.5.1.4) and the output is sent to the charge integrator. The voltage across the integrator's reference capacitor is measured with the lock-in amplifier from a comparison with the

internal reference (which is used to drive the speaker). As described in sec. 5.4.1 changes made to the device improve the reproducibility of the technique and increase the speed with which films are characterized.

5.4.1. Statistical Evaluation of the Modified Wafer Flexure Rig

The confidence with which the d_{31} coefficients could be reported was characterized with a number of tests designed to quantify the variability of the results. Experiments were made on test capacitors on both 3" and 4" diameter substrates. Measurements were made in the modified wafer flexure rig as a function of the relative position of the test wafers with respect to the retention ring and the rig housing. Four positions were tested in both the 3" and 4" configurations at 12, 3, 6 and 9 o'clock around the perimeter of the circular recess. The 3" sample was a 3 μm thick 52/48 sol-gel film. The 4" sample was a RF magnetron sputtered, 50/50 film and was 3.3 μm thick. Experiments with the sol-gel film were conducted on four separate capacitors, three of which were poled with +67 kV/cm (i.e. top electrode was positive) for 5 minutes, with the fourth poled under similar conditions a number of months prior to the test. The three freshly poled samples were aged at ambient conditions for 1 hour before the test. The sputtered film displayed large as-deposited polarizations and therefore significant d_{31} values in the as-received state (to be discussed in sec. 5.4.4). For that reason the two capacitors tested were not poled prior to the outset of the reproducibility experiments.

The data collected from the 3" and 4" samples are tabulated in Tables 5.2 and 5.3. The four locations at which the wafers were placed are denoted as numbers 1, 2, 3, and 4. For both experiments there was an overlap in the testing with the wafers relocated at the

first position after the fourth measurement. Included in the tables are the averages of the five measurements together with the standard deviation of the sample population.

Measurements on the sol-gel films showed average d_{31} values to be about -52 pC/N for the recently poled samples with the well aged sample having a d_{31} coefficient of -27 pC/N. The standard deviations of the four sets of measurements ranged from 6 to 8% of the average. Characterization of the sputtered film in the 4" rig configuration showed the average d_{31} values of both capacitors to be about -70 pC/N. The standard deviations were slightly better than the 3" measurements, with values calculated to be about 5% of the average.

The reproducibility data given in Tables 5.2 and 5.3 indicate that the wafer flexure method is a reliable method for the transverse piezoelectric characterization of PZT thin films. The data have standard deviations under 10%, with slightly better results obtained from the 4" configuration. The residual uncertainty is thought to be related to variations in the placement of the wafer, which lead to inconsistencies in the test to test capacitor position and changed the manner in which the substrate bent (sec. 5.2).

TABLE 5.2. The Variation of the d_{31} Coefficient for a 3 μm Thick 52/48 Sol-Gel Film in the Modified 3" Configuration

Location Number	Capacitor #1 d_{31} (pC/N)	Capacitor #2 d_{31} (pC/N)	Capacitor #3 d_{31} (pC/N)	Capacitor #4 d_{31} (pC/N)
1	-53	-57	-53	-26
2	-50	-47	-50	-26
3	-51	-49	-54	-30
4	-58	-53	-57	-29
1	-53	-51	-48	-26
Average	-53	-52	-52	-27
Standard Deviation	6%	8%	7%	7%

TABLE 5.3. The Variation of the d_{31} Coefficient for a 3.3 μm Thick 50/50 RF Sputtered Film in the Modified 4" Configuration

Location Number	Capacitor #1 d_{31} (pC/N)	Capacitor #2 d_{31} (pC/N)
1	-68	-66
2	-76	-65
3	-75	-62
4	-76	-67
1	-70	-68
Average	-73	-66
Standard Deviation	5%	4%

5.4.2. The Variation of the Transverse Piezoelectric Response as a Function of Radial Location

The d_{31} coefficient of an as-deposited film was measured across the surface of a 3" wafer. A shadow mask was used to place 1.5 mm diameter electrodes at 3.6 mm intervals along the $\langle 100 \rangle$ and $\langle 110 \rangle$ axes of the substrate. The piezoelectric charge produced in response to a constant pressure oscillation was then measured at known locations across the face of the substrate. Assuming that the d_{31} coefficient is constant

over the surface of the wafer then a relation between the variation of the applied theoretical stress and the piezoelectric charge can be derived which gives an indication of the validity of the stress analysis. If d_{31} at the centerpoint (c) of the wafer is expressed in terms of the dielectric displacement D_3 and the sum of the applied stresses σ_1 and σ_2 as:

$$d_{31}^c = \left(\frac{D_3}{\sigma_1 + \sigma_2} \right)^c \quad (5.1)$$

and the d_{31} coefficient at a position (r) removed from the center is described as:

$$d_{31}^r = \left(\frac{D_3}{\sigma_1 + \sigma_2} \right)^r \quad (5.2)$$

then eqs. 5.1 and 5.2 can be set equal, which yields:

$$\frac{D_3^r}{D_3^c} = \frac{(\sigma_1 + \sigma_2)^r}{(\sigma_1 + \sigma_2)^c} \quad (5.3)$$

From eq. 5.3 it is clear the ratio of the electric charge produced is simply the ratio of the sum of the principal stresses (if d_{31} is constant). The measured normalized charge data should then scale with radius in the same manner as the sum of the theoretical plate stresses.

The plot shown in Figure 5.9. illustrates the variation of the piezoelectric charge as a function of radial location. The sample measured was an *unpoled* sol-gel film 3 μm thick with a 52/48 composition. Because the as-deposited films have small spontaneous polarizations (d_{31} coefficients as-deposited are typically -3 to -5 pC/N) measurements made in the unpoled condition eliminated errors associated with variations of poling

conditions or differences in aging behavior. Data in the plot has been normalized to the charge produced at the center electrode (i.e. the maximum charge) and is compared to variation in the theoretical stress predicted for a uniformly loaded clamped circular plate. The agreement is quite good near the center of the plate, with some deviation noted towards the edges of the wafer.

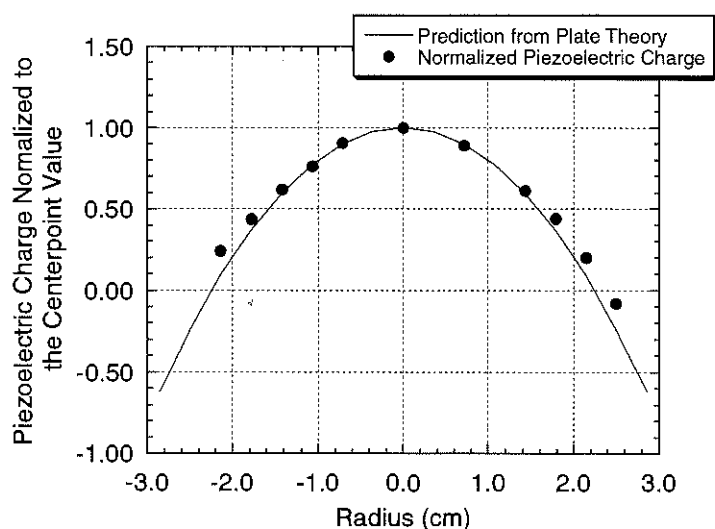


Figure 5.9. The variation of theoretical plate stress and empirical charge normalized to their respective values at the center of the 3" substrate.

5.4.3. The Influence of Film Thickness on the Magnitude of the d_{31} Coefficient of 52/48 Sol-Gel PZT Thin Films

Four RTA'd sol-gel films with thicknesses of 0.6 to 2.5 μm were characterized in terms of their d_{31} coefficients as a function of both poling direction and poling time. The poling fields used for the experiments were taken to be three times the coercive field of

the capacitor tested (where E_c was calculated from the average of the $\pm E_c$'s reported during the P-E measurements). The sample to be measured was then poled for increasing lengths of time, up to 31 minutes, at this field level. For each experiment a virgin electrode was used. The results from the experiments with the top electrode made positive are given in Figure 5.10 and with the top electrode made negative are given in Figure 5.11.

The data in Figures 5.10 and 5.11 show that the piezoelectric coefficient of all films tested increases in a logarithmic fashion with poling time. For all samples measured the piezoelectric coefficients were largely saturated after poling for 16 minutes. The data from each sample were thus taken for that poling time and the results plotted in Figure 5.12 to indicate the change of d_{31} with film thickness.

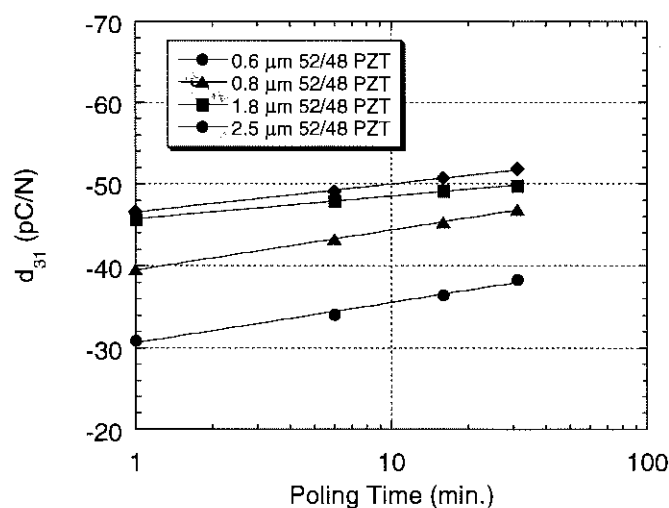


Figure 5.10. The variation of d_{31} as a function of film thickness and poling time with the top electrode positive. Films tested had 52/48 compositions and were poled with fields equal to three times the coercive field of the film.

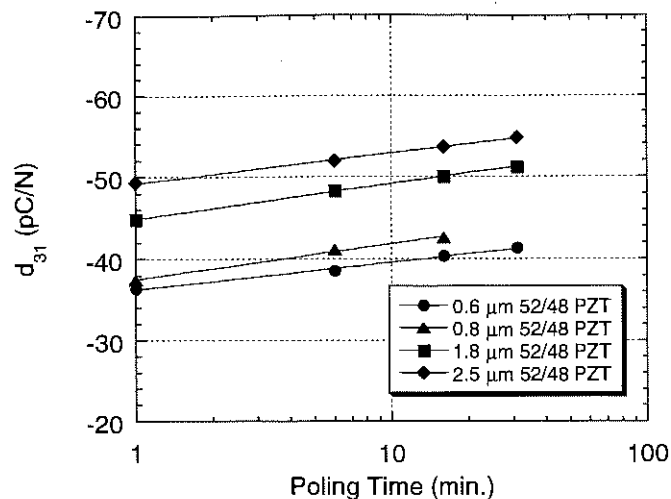


Figure 5.11. The variation of d_{31} as a function of film thickness and poling time with the top electrode negative. Films tested had 52/48 compositions and were poled with fields equal to three times the coercive field of the film.

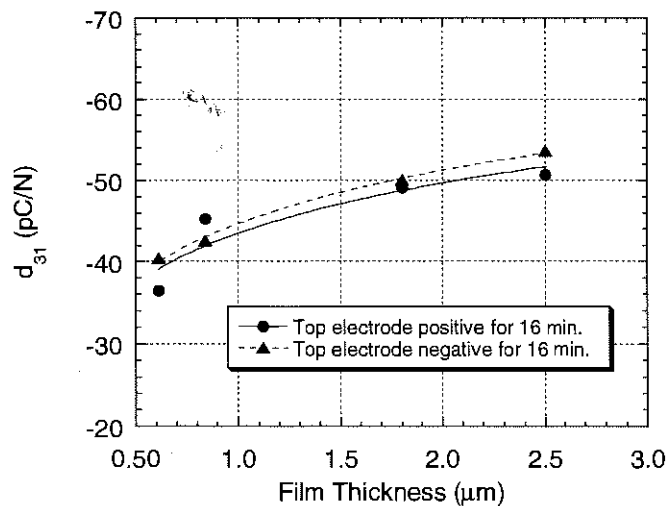


Figure 5.12. The variation of the d_{31} coefficient with an increase of film thickness. Measurements were made after poling the films, with the top electrode either positive or negative, for 16 minutes at three times their coercive field.

The data from Figure 5.12 indicates that with an increase of film thickness from 0.6 to 2.5 μm the d_{31} coefficient was increased from -40 to -50 pC/N. Because extrinsic contributions are limited in the films tested (chapter 4) and their remanent polarizations are comparable as shown in Figure 5.13, the source of the 25% increase is believed to be due to an increase in the dielectric constant with thickness.

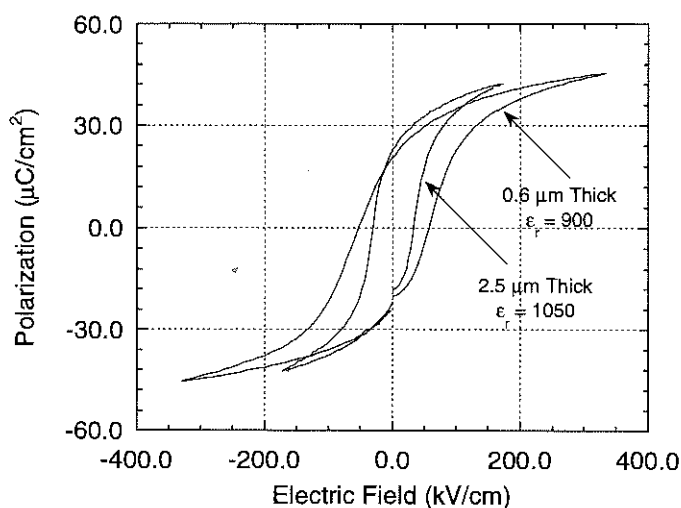


Figure 5.13. A comparison of the polarization hysteresis loops produced by 0.6 μm and 2.5 μm thick 52/48 sol-gel films.

It was found that the dielectric constants of the films increased from 900 (0.6 μm film) to 1050 (2.5 μm film). If the twin wall motion in the films is restricted to the point where the piezoelectric behavior can be approximated on the basis of phenomenological theory, then the d_{31} coefficient can be written as [37, 95]:

$$d_{31} = 2\epsilon_{33}\epsilon_0 Q_{12}P_r \quad (5.4)$$

where Q_{12} is the electrostriction coefficient, ϵ_{33} is the relative dielectric constant, ϵ_0 is the permittivity of free space, and P_r is the net polarization on the film. Consideration of eq. 5.4 shows that the ratio of the d_{31} coefficients is, because all other terms are constant, just the ratio of the values of ϵ_{33} . Thus the d_{31} coefficient of the 2.5 μm film should be about 17% greater than the 0.6 μm film. The remaining 8% difference could be related to a combination of effects. Work in a later section (sec. 5.5) shows that the thinner films age faster than the thicker films, which would lead to a smaller measured d_{31} coefficient (for the 0.6 μm film) after the one minute age. In addition, the electrical characteristics of a specific film will change from spot to spot, and the measurement technique itself has a small amount of variability (sec. 5.4.1).

5.4.4. Characterization of the d_{31} Coefficients of 50/50 RF Magnetron Sputtered PZT Thin Films

Initial measurements of the sputtered films were presented in sec. 5.4.1, where the strong as-deposited polarization of the films was demonstrated. The as-deposited films had d_{31} coefficients of about -70 pC/N. Results presented here are given as a function of poling time and direction. The d_{31} coefficients were calculated from data collected after poling the film with ± 60 kV/cm for times of 1 to 61 minutes. The magnitude of the poling field was selected based on experiments which showed that larger fields began to delaminate the top electrode. The data are presented as a function of poling time in Figure 5.14 with both the top and bottom halves of the y-axis made negative for clarity. The change in the d_{31} coefficient shows the expected logarithmic relation for both poling directions but the magnitude of the slopes show a strong contrast.

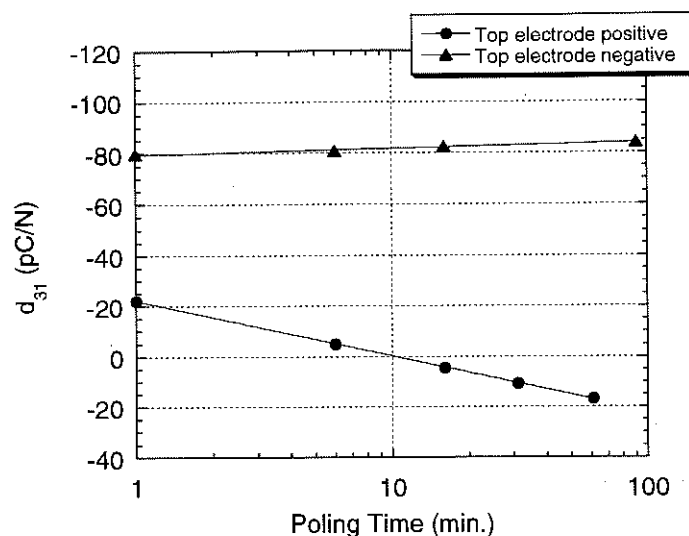


Figure 5.14. The change of the d_{31} coefficient of a $3.3 \mu\text{m}$ thick 50/50 sputtered film with poling time. The data show a strong sensitivity to poling direction. As-deposited values of d_{31} were measured at about -70 pC/N .

The data collected from the sputtered film illustrate a number of striking results. The first is the large value of the d_{31} coefficient in the as-deposited films. d_{31} values were on the order of -70 pC/N which were increased with poling to values which approached -85 pC/N . Those numbers are themselves encouraging because they represent some of the largest d_{31} values reported for polycrystalline PZT films (see Table 2.3 in sec. 2.9.3). Furthermore, there is significant asymmetry in the d_{31} coefficient as a function of the poling direction. When poled with the top electrode negative, the d_{31} increased by about 20% for poling times of 60 minutes. In contrast, poling the sample in the opposite direction changed the d_{31} coefficient by a factor of two.

The reason for the large as-deposited d_{31} and the strong asymmetry in the poling behavior is probably related to an internal electric field in the film. The existence of

internal bias fields have been well documented for PZT ceramics [96] and thin films [97] and their presence is usually manifested as a shift in the polarization hysteresis loop or an asymmetry in the current voltage (I-V) curve. The P-E loop for the 50/50 film is given in Figure 5.15. Inspection of the positive and negative coercive fields indicates that the shift of the P-E loop is 15 kV/cm, which is assumed to be equal to the film's internal field. It is expected that the bias field poles the material as it cools from its deposition temperature (600°C) which leads to a large as-deposited polarization and an appreciable piezoelectric effect. The subsequent application of a poling field in excess of, and in a direction parallel to, the internal bias yields only minimal gains in the d_{31} coefficient. The application of a field in a direction antiparallel to the internal field however, results in appreciable changes of the as-deposited polarization and therefore, the film's d_{31} coefficient. There is also the possibility that the preferred polarization direction is the result of a strain gradient in the film, though given the distance between the film and the neutral axis of the film/substrate system, a large strain gradient seems unlikely. For simplicity therefore, the mechanism responsible for the shift in the hysteresis loop will be described as an internal field.

The effect of the preferred polarization direction is illustrated most clearly in Figure 5.16, which plots the response of both a 3 μm 52/48 sol-gel film and the 50/50 sputtered film as a function of poling time. The data in the plot illustrate the strong contrast between the poling behavior of the two materials which is believed to result from the relative magnitude of the film's internal bias fields.

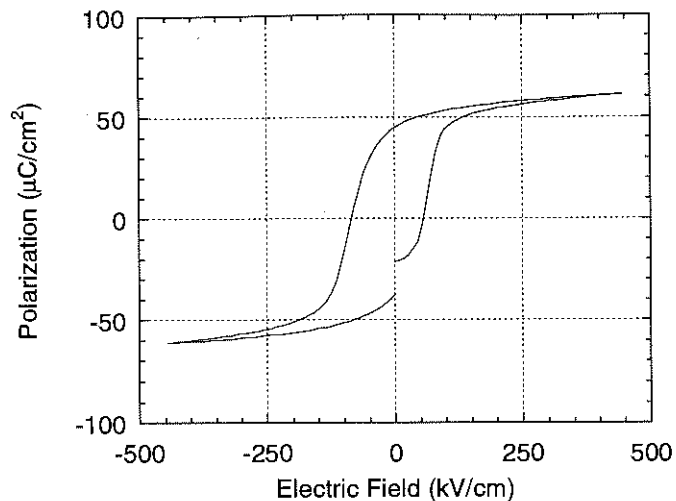


Figure 5.15. The polarization hysteresis loop for a $-3 \mu\text{m}$ thick 50/50 RF sputtered PZT film. The plot shows the average remanent polarization of the film is $41 \mu\text{C}/\text{cm}^2$ and the average coercive field is $70 \text{ kV}/\text{cm}$. The internal bias field is calculated from the offset on the field axis to be $15 \text{ kV}/\text{cm}$.

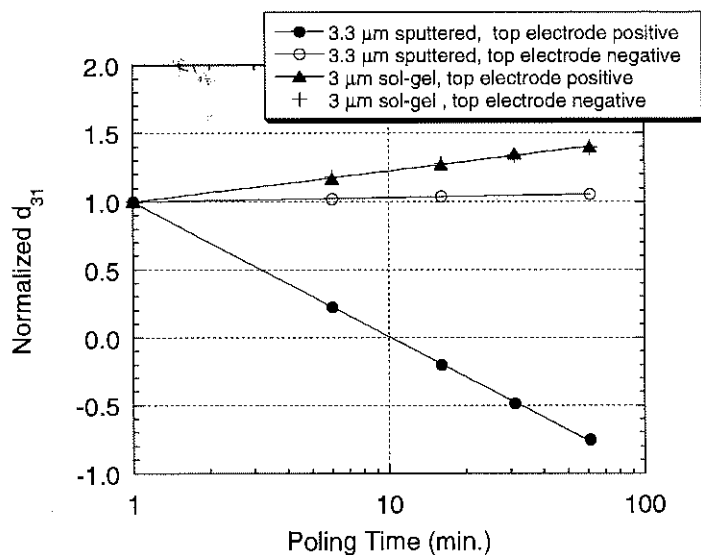


Figure 5.16. The normalized d_{31} coefficients as a function of poling time. Data for both a $3 \mu\text{m}$ sol-gel film and a $3.3 \mu\text{m}$ sputtered film.

The internal bias of the sputtered film was calculated to be about 15 kV/cm, which is an order of magnitude larger than the ~1 to 2 kV/cm bias on the sol-gel films. The large internal field in the sputtered films poles the material almost completely as the material is cooled through T_c . The sputtered films therefore, display only small gains when poled in a direction parallel to the internal bias and show large changes when poled in a direction antiparallel. In contrast, the internal fields of the sol-gel films are much lower (than the sputtered films). The net polarization produced in either direction is therefore comparable and the response produced is symmetric.

5.5. Aging Behavior of the Transverse (d_{31}) Piezoelectric Coefficient

The aging rates of the transverse piezoelectric coefficients for both sol-gel and sputtered PZT films were measured using the wafer flexure technique. The d_{31} coefficients were monitored at regular intervals after poling and their decay plotted versus the logarithm of time. The aging rate of the material was then calculated from a logarithmic relation fit to the empirical data.

5.5.1. Aging Work with the Prototype Wafer Flexure Rig

Initial studies on the aging behavior of the d_{31} coefficient were carried out using the prototype rig with manual pressure oscillation. Results were collected from a number of 52/48 sol-gel films with submicron thicknesses. Data indicate that the aging rates were in considerable excess of the 1 to 3% per decade which has been reported for PZT ceramics [98]. The plot in Figure 5.17 shows the data from a 0.3 μm thick sample poled

with a field of +330 kV/cm for times of 1 and 60 minutes. The initial d_{31} coefficients were measured at between -42 and -51 pC/N which decayed to about -30 and -38 pC/N after aging times of about 7 days. The data from Figure 5.17 are normalized to their starting values and replotted in Figure 5.18. The curves produced are identical and indicate that the aging rate of this particular film is independent of poling time at 10% per decade.

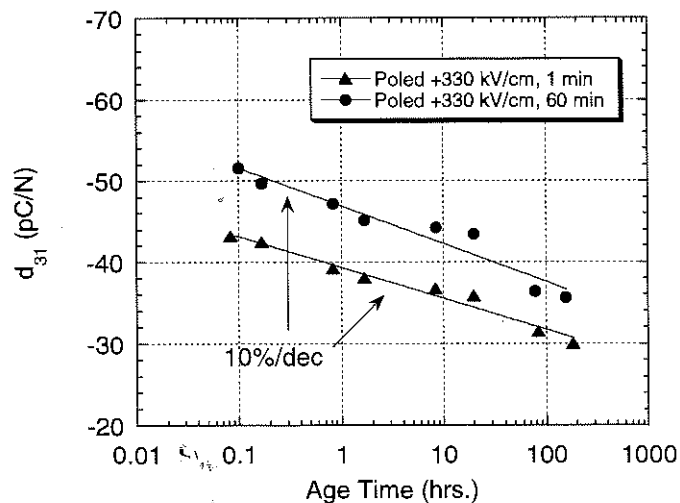


Figure 5.17. The aging behavior of the d_{31} coefficient for a 0.3 μm thick sol-gel 52/48 PZT thin film.

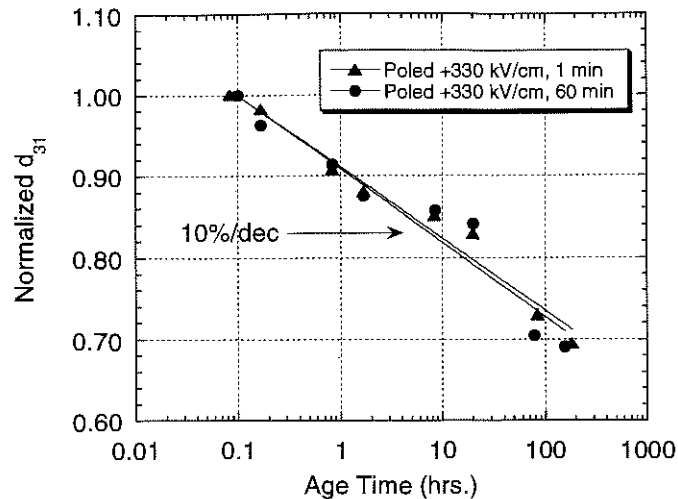


Figure 5.18. The normalized aging behavior of the data shown in Figure 5.17.

5.5.2. Aging Work with the Modified Wafer Flexure Rig

The effect of film thickness on the aging rates of the d_{31} coefficients was measured in the modified wafer flexure rig. Data were collected at times of 1 to 60 minutes after the poling field was removed. Experiments were conducted with sol-gel films poled in either direction at room temperature with fields equal to three times their coercive field strength. Poling times for the experiments conducted were either 1 or 2 minutes. Figures 5.19 and 5.20 give the aging data from the experiments conducted with the top electrode made either positive or negative. The rates for all experiments are tabulated from the slopes of the fitted logarithmic curves and are given in Table 5.4.

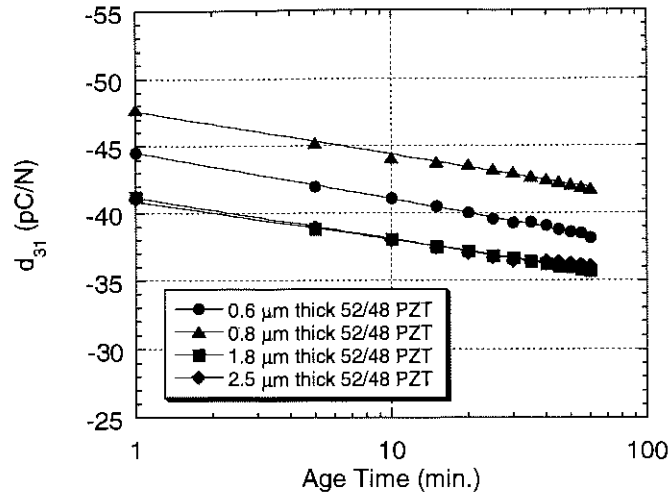


Figure 5.19. The aging of the d_{31} coefficient for four sol-gel films ranging in thickness from 0.6 to 2.5 μm . Samples were all poled with three times the coercive field for 1 minute with the top electrode positive.

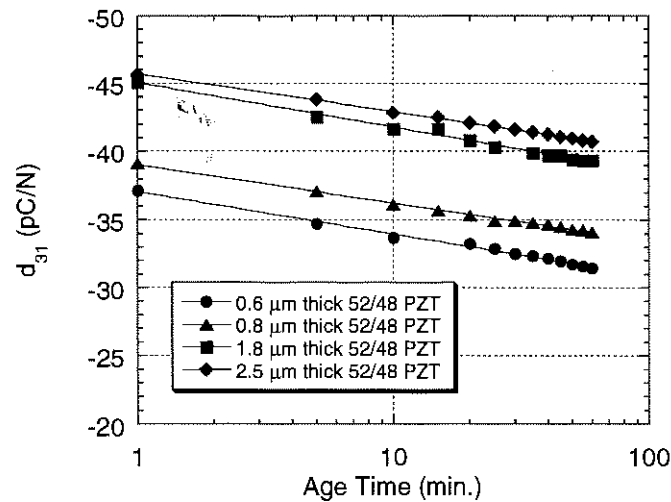


Figure 5.20. The aging of the d_{31} coefficient for four sol-gel films ranging in thickness from 0.6 to 2.5 μm . Samples were all poled with three times the coercive field for 1 minute with the top electrode negative.

TABLE 5.4. Aging Rates (percent per decade) of the d_{31} Coefficient of 52/48 Sol-Gel PZT Thin Films

Film Thickness (μm)	Poling time: 1 min. Top electrode: "+"	Poling time: 1 min. Top electrode: "-"	Poling time: 2 min. Top electrode: "+"
0.6	8%	8%	7%
0.8	7%	7%	5%
1.8	7%	7%	5%
2.5	6%	7%	4%

Similar experiments were conducted on a 4" RF sputtered 50/50 PZT film. The film investigated was 3.0 μm thick with an as-deposited d_{31} coefficient of about -45 pC/N. Test capacitors were poled with an electric field of 150 kV/cm, which was approximately equal to two times the coercive field strength. The aging rate was evaluated as a function of poling time and direction with the data taken from different test capacitors on the same film.

Figure 5.21 is a plot of the decay of the transverse piezoelectric coefficient for the sputtered film poled with a field of ± 150 kV/cm for 1 minute at room temperature. The plot shows a strong asymmetry in the film's aging rate, with the sample poled at -150 kV/cm (top electrode negative) measured at 2% per decade while the sample poled in the opposite direction decayed at 26% per decade. Figure 5.22 is a similar illustration taken from the samples poled for 15 minutes. The data in the plot show an aging rate of 4% per decade when poled with the top electrode negative and an aging rate of 20% per decade when poled with the top electrode positive.

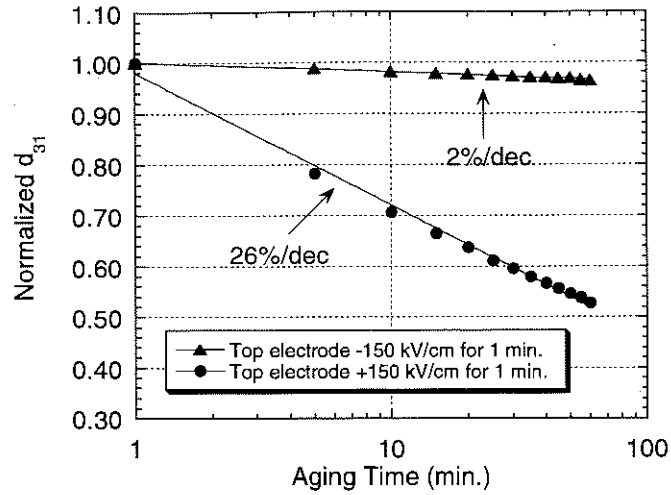


Figure 5.21. The aging rate of the d_{31} coefficient of a $3.0 \mu\text{m}$ thick 50/50 RF sputtered PZT film. The film had been poled for 1 minute with a field of $\pm 150 \text{ kV/cm}$.

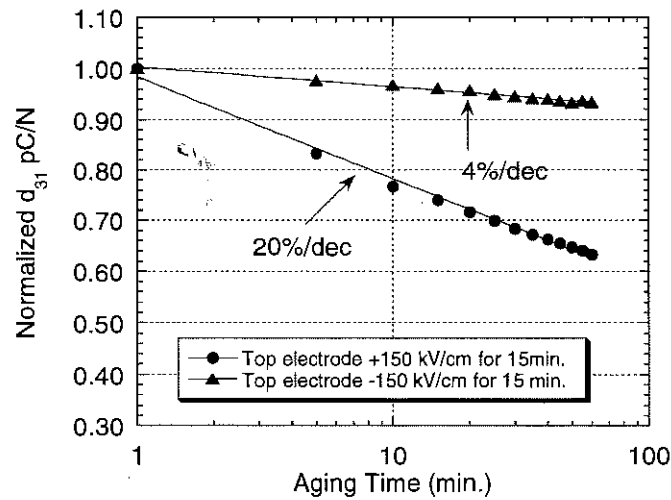


Figure 5.22. The aging rate of the d_{31} coefficient of a $3.0 \mu\text{m}$ thick 50/50 RF sputtered PZT film. The film had been poled for 15 minutes with a field of $\pm 150 \text{ kV/cm}$.

The aging data collected from both the sol-gel and RF sputtered films make an interesting contrast to data reported for bulk ceramics. In bulk materials, the decay of the dielectric and piezoelectric constants and the evolution of the constricted P-E loops are attributed to ferroelastic stress relief and domain stabilization [99]. Because extrinsic contributions to the dielectric and piezoelectric characteristics are limited in films (chapter 4) and the decay of the dielectric constant proceeds at only a few percent per decade [100, 101], the mechanism(s) responsible for the decay of the electromechanical constants has been attributed to the reduction of the film's remanent polarization [100].

In this work, the aging data collected show a correlation with the presence of an internal bias field as is indicated by the asymmetric aging rates of the RF sputtered films ($E_{\text{bias}} = 15$ to 20 kV/cm). When poled in a direction parallel to the internal bias, the sputtered films showed modest aging rates of 2-4% per decade, while the application of an antiparallel field produced aging rates of 20-26% per decade. The accelerated aging effect results from the misalignment of the polarization vectors with the internal field. Removal of the poling field results in the rapid reorientation of switched domains (i.e. the film begins to switch back to the original orientation) and a rapid decrease of the film's d_{31} coefficient. In contrast to the RF sputtered films, the net internal fields of the sol-gel films ($E_{\text{bias}} = 1$ to 2 kV/cm) are smaller and as a result their response is independent of poling direction (Figures 5.19 and 5.20).

The symmetric aging response of the sol-gel films suggests that depolarization does not result from a net internal electric field. Earlier work on PZT ceramics has shown that large mechanical stresses can result in significant amounts of depolarization [51, 52] however, data presented in chapter 4 show that the effects of mechanical stress are less

pronounced in PZT films. In addition, the limited extrinsic contributions in PZT films suggest that depolarization results from the backswitching of aligned domains and not non-180° reorientation or domain wall pinning. Because 180° switching is not a stress relief mechanism, mechanical depolarization cannot be responsible for the aging behavior of thin films. Rather, it is expected that the origins of the accelerated aging rates are related to interfacial or defect-related effects comparable to those responsible for the polarization degradation of FRAM devices [94].

Extensive work has been conducted on degradation mechanisms in films, with both lead and oxygen vacancies identified as potential sources of the problem(s) [94]. It is expected that the high volatility of lead oxide at the elevated crystallization temperatures (typically 600 to 700°C) results in large concentrations of charged defects in a shallow layer at the film's surface [77]. There are several possible consequences of this. First, the defective material could form a discrete semiconducting layer at the film surface. Earlier work has suggested that a low- ϵ_r region at one of the film's surfaces results in the reduced dielectric constant of thin (sub-micron thickness) PZT films [102]. A similar region may be responsible for the spontaneous depolarization of the material. In particular, it is suggested that when subjected to *large* poling fields, charge is injected through this layer and domain reversal is possible. After the voltage is removed however, a depolarization field is created which cannot be compensated effectively by the defective layer. In the absence of an external voltage, the limited conductivity of the lead deficient layer prevents additional charge from being transported to compensate the depolarization field. As a result the material depoles, which leads to the accelerated decay of the film's piezoelectric coefficient.

A second possibility is that $V_{Pb}''-V_O''$ defect dipoles in the near surface regime align with respect to the ferroelectric dipoles on cooling through the transition. Since the domain structure is initially random, there is little net internal bias. If the field associated with these dipoles is not too high, then the material could be poled. However, at room temperature it is unlikely that all of the defects would be reoriented (especially for short poling times). Thus, after poling they would act to drive the film back to its original random domain configuration, which would result in accelerated piezoelectric aging.

There are data presented both here and elsewhere [100] which suggest that the aging rates of the piezoelectric coefficients can be decreased with increased poling times (Table 5.4). The beneficial effects of poling time can be explained within the framework of imprint phenomena which attributes the voltage offset of the P-E loop (i.e. the imprint) to the alignment of defect dipoles with the film's polarization vector [103]. With increased poling times the defects (predominantly oxygen vacancies) which are responsible for imprint have time to migrate through the film. The migration and reorientation of defect dipoles stabilize the film's domain structure, which prevents depolarization and reduces the aging rate.

The asymmetric aging rates of the d_{31} coefficient of the RF sputtered films are comparable to behavior which has been reported by Maria [84]. In that work, the aging rates of the d_{31} coefficient of thin PMN-PT epitaxial films were measured using a modification of the wafer flexure technique. Results from the experiments showed that the films had large asymmetries in the aging rates with maximum and minimum values reported to be about 30% and less than 1% per decade, respectively. The source of the aging behavior in Maria's films was attributed to the presence of a large internal bias

which shifted the P-E loops to one side of the origin, i.e. both coercive fields had the same sign.

The explanation given for the large offset was focused on the effects of energetic bombardment. Maria reasoned that defect dipoles could not be responsible for the internal bias because his films could not be thermally imprinted. In addition, the effects of lattice mismatch as proposed by Abe et al. [104] were dismissed because different epitaxial films did not show a comparable shift of the P-E loop under similar interfacial strains. It was speculated therefore, that energetic bombardment, either through implantation or ion peening, was responsible for a displacement of the oxygen sublattice. The shift of the oxygen atoms led to a preferred polarization direction and thus produced the large internal field (and the asymmetry in the aging rates) in the as-deposited films. A similar mechanism could explain why the sputtered films in this work showed asymmetric aging rates while the sol-gel films (which never see bombardment) did not.

6. Conclusions and Recommendations for Future Work

6.1. The Effects of Biaxial Stress on the Low and High-Field Characteristics of PZT Thin Films

The effects of residual film stress on the dielectric and piezoelectric characteristics of PZT thin films were investigated. Experiments were conducted on a number of different films with compositions across the morphotropic phase boundary, of different crystallographic orientations, and with thicknesses ranging from 0.3 to 5.0 μm . For both the wafer and O-ring and chip-on-steel configurations the stresses applied to the films were quantified with resistance strain gauges and were found to be about ± 115 MPa.

Results from the low-field experiments showed that regardless of composition the changes of the dielectric constant were less than 10% in response to the applied stress. In general, tensile stresses decreased the capacitance, compressive stress increased the capacitance, and in both cases the changes produced were reversible. The dielectric loss was found to increase about 20% regardless of the sign of the stress. Exceptions in the low-field response were noted for the 3.0 and 5.0 μm thick (100) oriented films where the tensile data showed a 2% increase of the dielectric constant.

Results from the high-field tests showed that for all films the remanent polarization decreased with applied tension and increased with applied compression. In

both cases, the changes produced were reversible and the magnitudes were on the order of 20%. Tensile data showed the coercive field to be insensitive to applied stress. Compressive experiments showed that regardless of composition or thickness, the coercive field increased in proportion to the applied stress. The changes produced were reversible and less than 10% of the as-deposited value for all samples tested.

Comparison of both the low and high-field stress data with earlier studies on bulk ceramics indicates that ferroelastic domain reorientation is limited in sol-gel PZT films. Experiments conducted here showed that the changes produced in all parameters were small (for ± 115 MPa) and in all cases were largely reversible. The effects observed were found to be independent of composition and thickness. Based on the similarity of the empirical results therefore, the limited extrinsic contributions in PZT thin films cannot be attributed to compositional effects, submicron film thicknesses, and are not the result of residual film stress. It is possible that local stresses, small grain sizes, or high defect concentrations are responsible for the reduction in non-180° domain wall mobility. The reduction in the extrinsic contributions limits the magnitude of the dielectric and piezoelectric properties of these PZT films to values comparable with hard PZT ceramics.

6.2. The Wafer Flexure Technique for the Characterization of the Transverse (d_{31}) Piezoelectric Coefficient of Thin Films

The wafer flexure technique was developed to characterize the transverse piezoelectric coefficient of piezoelectric thin films. PZT coated silicon wafers are clamped in a uniform pressure device and the air in the chamber behind the sample oscillated via the change in displacement of a 10" diameter audio speaker. The pressure

change in the cavity results in the controlled bending of the substrate, which applies a biaxial stress to the film. The applied stress results in the production of an electric charge in accordance with the direct piezoelectric effect. The charge created is monitored electronically with an electric charge integrator and a lock-in amplifier together with the pressure change in the chamber. The stresses applied to the film are then calculated using classical plate theory and an elastic stress analysis. The technique can be used to measure the d_{31} coefficient at any point on a 3" or 4" diameter substrate and has been modified to measure the transverse coefficient of millimeter sized test chips.

The data collected with the wafer flexure technique compare well with other d_{31} data reported in the literature. The d_{31} coefficients were found to increase with both poling time and film thickness, with maximum values for 52/48 sol-gel PZT films measured at about -50 to -60 pC/N. Substantial work was conducted to characterize the validity of the technique. Empirical results showed that the d_{31} values were independent of radial location and strain gauge experiments were made which validated the stress analysis used. Results from both sets of experiments indicated that the wafer flexure method is an accurate technique for the characterization of the d_{31} coefficient of thin films.

The wafer flexure method was used to monitor the aging rates of the d_{31} coefficient for a number of 52/48 sol-gel and 50/50 RF sputtered PZT films. The results showed that the d_{31} coefficient decreased in a linear fashion with the logarithm of time. The aging rates measured for the sol-gel films were found to be between 4 and 10% per decade with the thickest films tested (2.5 μm) displaying the smallest rates. Similar experiments were conducted on RF sputtered PZT films. The films tested had large as-

deposited d_{31} coefficients of about -45 pC/N for a $3 \mu\text{m}$ thick film. In contrast to the aging behavior of the sol-gel films, the aging rates of the sputtered samples showed a strong anisotropy of the decay rate. Rates were measured at as much as 26% per decade when the sample was poled against the as-deposited polarization and as little as 2% per decade when poled in the preferential direction.

The aging rates of PZT films are large when compared to the few percent per decade reported for bulk ceramics. The mechanism responsible for the piezoelectric aging of the PZT films is believed to be depolarization of the material. The RF magnetron sputtered films display large asymmetries in their aging response which is probably the result of a large internal field present in the film. When poled in a direction parallel to the internal bias, the film's polarization is stable and the aging rates are modest. If however, the films are poled antiparallel to the internal field, the remanent polarization is unstable and the aging rates are accelerated. In contrast to the sputtered films, the aging rates of the sol-gel samples were independent of poling direction. The symmetry of aging rate indicated that the net internal fields in the sol-gel films, which were about an order of magnitude less than those in the RF sputtered films, were not the predominant depolarization mechanism in the material. The origin of the aging response in the sol-gel samples was attributed to charged defects or a defective layer which resulted in the backswitching of domains.

The wafer flexure technique developed in this investigation is rapid, and the device has been constructed from simple hardware. The technique is robust with small fluctuations in sample placement or other experimental variations producing only minor effects on the reproducibility. No sample preparation is required with the rig constructed

capable of measuring 3" or 4" diameter substrates, or millimeter sized test chips. As a result the wafer flexure technique is viable tool for the routine characterization of the d_{31} coefficient of piezoelectric thin films.

6.3. Recommendations for Future Work

6.3.1. Experiments with Sub-Micron Ceramic Samples

The investigation of the effects of biaxial stress on the dielectric characteristics of sol-gel PZT films indicated that extrinsic effects are limited in the materials tested. It has been suggested that one mechanism which could be responsible for the limited extrinsic response is the submicron grain sizes of the films. Experimental confirmation of that hypothesis cannot be readily achieved with sol-gel films (grain sizes cannot be varied over a wide range on platinized silicon substrates) however, fine grained PZT ceramics can be polished to thicknesses less than 10 μm [105], characterized in the chip-on-steel rig, and the data used for the direct evaluation of grain size effects. In addition, because the materials are prepared using bulk ceramic processing techniques hard, soft and undoped compositions can be tested. The experiments conducted will provide additional information on the effects of grain size, substrate clamping, and composition on the biaxial stress response of PZT thin films.

In addition to the evaluation of biaxial stress effects, the thinned bulk samples can be used to calibrate the wafer flexure technique. As was discussed in sec. 3.8, the wafer flexure method has been modified to characterize the d_{31} coefficient of test chips coated

with piezoelectric films. The utilization of thinned ceramic specimens allows the material to be characterized with an established technique (e.g. a resonance method). After the conventional measurement, the sample can be bonded to a silicon wafer, and characterized with the techniques outlined in chapters 2 and 5.

6.3.2. Investigations into the Mechanisms Responsible for the Accelerated Aging Rates of the Transverse Piezoelectric Coefficients of PZT Thin Films

The discussion presented in sec. 5.5 attributed the accelerated aging rates of the sol-gel films to spontaneous depolarization. There has been extensive work in the past which suggests that the presence of large concentrations of charged defects (predominantly oxygen vacancies) can result in a number of different degradation phenomena such as polarization fatigue and imprint [103]. In addition, charged defects have been connected to retention failure (i.e. the loss of switched polarization) which could in fact be the source of the piezoelectric decay of PZT films. The utilization of lead oxide overlayers, metallic oxide electrodes, and various doping strategies are expected to produce a modification of the defect concentration and experiments designed to investigate their effects will lead to an enhanced understanding of piezoelectric aging effects in sol-gel films.

6.3.3. The Investigation of the Influence of Stress at the Curie Point on the Microstructural Texture of PZT Thin Films

Previous investigations by Tuttle et al. [46] have indicated that PZT thin films adopt different microstructural textures depending upon the substrate material used. The cause of the different texture was correlated to the sign of the film stress at the Curie point (T_c) and the sign of the stress was dictated by the thermal expansion mismatch between the film and the substrate. Films subjected to a tensile stress (e.g. those on silicon substrates) produce a (100) texture as the c -axes of the unit cells release strain by orienting parallel to the film surface. Conversely, films subjected to a compressive stress (e.g. on magnesium oxide substrates) have (001) textures as the c -axes of the material are forced into configurations perpendicular to the surface.

The (001) texture of PZT films deposited on magnesium oxide results in larger remanent polarization values (P_r). The increase of P_r would be expected to enhance the piezoelectric coefficients (relative to PZT on silicon) which makes the (001) films attractive for MEMS applications. Because however, MEMS devices are typically fabricated on silicon substrates, the utilization of magnesium oxide to produce the desired microstructure is not practical. As was shown in this thesis, different levels of stress can be applied to PZT films via the mechanical manipulation of a coated substrate. If an alternative stress rig can be designed to operate at high temperatures (e.g. a piston on ring design), the film stress at T_c can be changed and the microstructure of the films will reflect that condition. If the transformation stress model is valid, high temperature stress

experiments could lead to the enhancement of the piezoelectric characteristics of PZT films.

References

- [1] T. Tamagawa, D. L. Polla, and C. C. Hsueh, "Lead Zirconate Titanate (PZT) Thin Films in Surface-Micromachined Sensor Structures," Proc. IEDM, pp. 26.2.1-26.2.4, 1990.
- [2] P. Muralt, M. Kohli, T. Maeder, A. Kholkin, K. Brooks, N. Setter, and R. Luthier, "Fabrication and Characterization of PZT Thin-Film Vibrators for Micromotors," *Sen. and Act.*, vol. A48, pp. 157-165, 1995.
- [3] A. L. Kholkin, C. Wutchrich, D. V. Taylor, and N. Setter, "Interferometric Measurements of Electric Field-Induced Displacements in Piezoelectric Thin Films," *Rev. Sci. Instrum.*, vol. 67, pp. 1935-1941, 1996.
- [4] P. Luginbuhl, G.-A. Racine, P. Lerch, B. Romanowicz, K. G. Brooks, N. F. de Rooij, P. Renaud, and N. Setter, "Piezoelectric Cantilever Beams Actuated by PZT Sol-Gel Thin Film," *Sen. and Act.*, vol. A54, pp. 530-535, 1996.
- [5] J. L. Deschanvres, P. Rey, G. Delabouglise, M. Labeau, J. C. Joubert, and J. C. Peuzin, "Characterization of Piezoelectric Properties of Zinc Oxide Thin Films Deposited on Silicon for Sensors Applications," *Sen. and Act.*, vol. A33, pp. 43-45, 1992.
- [6] M. Toyama, R. Kubo, E. Takata, K. Tanaka, and K. Ohwada, "Characterization of Piezoelectric Properties of PZT Thin Films Deposited on Si by ECR Sputtering," *Sen. and Act.*, vol. A45, pp. 125-129, 1994.
- [7] J. F. Shepard Jr., P. J. Moses, and S. Trolrier-McKinstry, "A Technique for the Measurement of d_{31} Coefficient of Piezoelectric Thin Films," *Materials for Smart Systems II*, vol. 459, pp. 225-230, 1996.
- [8] S. M. Sze, *Semiconductor Sensors*. New York: John Wiley & Sons, Inc., 1994.
- [9] B. Folkmer, P. Steiner, and W. Lang, "A Pressure Sensor Based on a Nitride Membrane Using Single-Crystalline Piezoresistors," *Sen. and Act.*, vol. A54, pp. 488-492, 1996.

- [10] G. M. Sessler, "Acoustic Sensors," *Sen. and Act.*, vol. A25-A27, pp. 323-330, 1991.
- [11] P. R. Scheeper, A. G. H. van der Donk, W. Olthuis, and P. Bergveld, "A Review of Silicon Microphones," *Sen. and Act.*, vol. A44, pp. 1-11, 1994.
- [12] T. Sasayama, S. Suzuki, S. Tsuchitani, A. Koide, M. Suzuki, T. Nakazawa, and N. Ichikawa, "Highly Reliable Silicon Micromachined Physical Sensors in Mass Production," *Sen. and Act.*, vol. A54, pp. 714-717, 1996.
- [13] A. H. Epstein, S. D. Senturia, G. Anathasuresh, A. Ayon, K. Breuer, and K. S. Chen, "Power MEMS and Microengines," *Proc. Transducers 97*, pp. 753-756, 1997.
- [14] R. Allen, "Silicon MEMS Technology is Coming of Age Commercially," *Electronic Design*, vol. January 20, pp. 75-88, 1997.
- [15] J. Bryzek, "MEMS: A Closer Look," *Sensors*, vol. July, pp. 4-38, 1996.
- [16] J. Markoff, "New Wave in High-Tech: Deus Ex Tiny Machina," in *The New York Times*. New York, 1997.
- [17] Sandia National Laboratories, Intelligent Micromachine Initiative, <http://www.mdl.sandia.gov/Micromachine/images8.html>, 1998.
- [18] M. H. Kiang, O. Solgaard, R. S. Muller, and K. Y. Lau, "Micromachined Polysilicon Microscanners for Barcode Readers," *IEEE Photonics and Technology Letters*, vol. 8, 1996.
- [19] N. F. Foster, "Piezoelectricity in Thin Film Materials," *J. Acoust. Soc. Am.*, vol. 70, pp. 1609-1614, 1981.
- [20] S. S. Lee, R. P. Ried, and R. M. White, "Piezoelectric Cantilever Microphone and Microspeaker," *J. Microelectromech. Syst.*, vol. 5, pp. 238-342, 1996.
- [21] *Landolt Bornstein Tables*, vol. II. Berlin: Springer-Verlag, 1979.
- [22] D. L. Polla and L. F. Francis, "Ferroelectric Thin Films in Microelectromechanical Applications," *MRS Bulletin*, July, pp. 59-65, 1996.

- [23] K. R. Udayakumar, J. Chen, A. M. Flynn, S. F. Bart, L. S. Tavrow, D. J. Ehrlich, L. E. Cross, and R. A. Brooks, "Ferroelectric Thin Films for Piezoelectric Micromotors," *Ferroelectrics*, vol. 160, pp. 347-356, 1994.
- [24] P. Muralt, A. Kholkin, M. Kohli, T. Maeder, and N. Setter, "Characterization of PZT Thin Films for Micromotors," *Microelectronic Engineering*, vol. 29, pp. 67-70, 1995.
- [25] Y. Nemirovsky, A. Nemirovsky, P. Muralt, and N. Setter, "Design of a Novel Thin-Film Piezoelectric Accelerometer," *Sen. and Act.*, vol. A56, pp. 239-249, 1996.
- [26] T. Itoh, J. Chu, I. Misumi, K. Kataoka, and T. Suga, "New Dynamic Scanning Force Microscopes Using Piezoelectric PZT Microcantilevers," *Proc. Transducers 97*, pp. 459-462, 1997.
- [27] J. J. Bernstein, S. L. Finberg, K. Houston, L. C. Niles, H. D. Chen, L. E. Cross, K. K. Li, and K. Udayakumar, "Micromachined High Frequency Ferroelectric Sonar Transducers," *IEEE Transactions on Ultrasonics, Ferroelectrics, and Frequency Control*, vol. 44, pp. 960-969, 1997.
- [28] L. E. Cross and K. H. Hardtl, *Encyclopedia of Chemical Technology*, vol. 10, 3rd ed: John Wiley and Sons Inc., 1980.
- [29] M. E. Lines and A. M. Glass, *Principles and Applications of Ferroelectrics and Related Materials*. London: Oxford University Press, 1977.
- [30] J. M. Herbert, *Ferroelectric Transducers and Sensors*, vol. 3. New York: Gordon and Breach, 1982.
- [31] W. D. Kingery, H. K. Bowen, and D. R. Uhlmann, *Introduction to Ceramics*, 2nd ed. New York: John Wiley and Sons, 1976.
- [32] A. J. Moulson and J. M. Herbert, *Electroceramics: Materials, Properties, Applications*. London: Chapman and Hall, 1990.
- [33] A. Ballato, "Piezoelectricity: Old Effect, New Thrusts," *IEEE Transactions on Ultrasonics, Ferroelectrics, and Frequency Control*, vol. 42, pp. 916-926, 1995.

- [34] G. W. Taylor, J. J. Gagnepain, T. R. Meeker, T. Nakamura, and L. A. Shuvalov, "Piezoelectricity," in *Ferroelectricity and Related Phenomena*, vol. 4, G. W. Taylor, Ed. New York: Gordon and Breach, 1985.
- [35] B. Jaffe, J. W. R. Cook, and H. Jaffe, *Piezoelectric Ceramics*. India: R. A. N., 1971.
- [36] X. L. Zhang, Z. X. Chen, L. E. Cross, and W. A. Schulze, "Dielectric and Piezoelectric Properties of Modified Lead Titanate Zirconate Ceramics from 4.2 to 300 K," *J. Mat. Sci.*, vol. 18, pp. 968-972, 1983.
- [37] Q. M. Zhang, H. Wang, N. Kim, and L. E. Cross, "Direct Evaluation of Domain-Wall and Intrinsic Contributions to the Dielectric and Piezoelectric Response and Their Temperature Dependence on Lead Zirconate-Titanate Ceramics," *J. Appl. Phys.*, vol. 75, pp. 454-459, 1994.
- [38] D. Damjanovic and M. Demartin, "Contribution of the Irreversible Displacement of Domain Walls to the Piezoelectric Effect in Barium Titanate and Lead Zirconate Titanate Ceramics," *J. Phys.: Condens. Matter*, vol. 9, pp. 4943-4953, 1997.
- [39] M. Demartin and D. Damjanovic, "Dependence of the Direct Piezoelectric Effect in Coarse and Fine Grain Barium Titanate Ceramics on Dynamic and Static Pressure," *Appl. Phys. Lett.*, vol. 68, pp. 3046-3048, 1996.
- [40] D. Damjanovic, "Stress and Frequency Dependence of the Direct Piezoelectric Effect in Ferroelectric Ceramics," *J. Appl. Phys.*, vol. 82, pp. 1788-1797, 1997.
- [41] S. Timoshenko and S. Woinowsky-Krieger, *Theory of Plates and Shells*, 2nd ed. New York: McGraw-Hill, 1959.
- [42] A. Ugural, *Stresses in Plates and Shells*. New York: McGraw-Hill, 1981.
- [43] S. P. Murarka, *Metallization: Theory and Practice for VLSI and ULSI*. Boston: Butterworth-Heinemann, 1993.
- [44] J. A. Thornton and D. W. Hoffman, "Stress-Related Effects in Thin Films," *Thin Solid Films*, vol. 171, pp. 5-31, 1989.
- [45] D. L. Smith, *Thin Film Deposition*. New York: McGraw-Hill, 1995.

- [46] B. A. Tuttle, J. A. Voigt, T. J. Garino, D. C. Goodnow, R. W. Schwartz, D. L. Lamppa, T. J. Headly, and M. O. Eatough, "Chemically Prepared Pb(Zr,Ti)O₃ Thin Films: The Effects of Orientation and Stress," Proc. The 8th International Symposium on Applications of Ferroelectrics, pp. 344-348, 1992.
- [47] G. A. C. M. Spierings, G. J. M. Dormans, W. G. J. Moors, M. J. E. Ulenaers, and P. K. Larsen, "Stresses in Pt/Pb(Zr,Ti)O₃/Pt Thin Film Stacks for Integrated Ferroelectric Capacitors," *J. Appl. Phys.*, vol. 78, pp. 1926-1933, 1995.
- [48] T. Tuchiya, T. Itoh, G. Sasaki, and T. Suga, "Preparation and Properties of Piezoelectric Lead Zirconate Titanate Thin Films for Microsensors and Microactuators by Sol-Gel Processing," *J. Ceram. Soc. Japan*, vol. 104, pp. 159-163, 1996.
- [49] I. Kanno, S. Fujii, T. Kamada, and R. Takayama, "Piezoelectric Properties of c-Axis Oriented Pb(Zr,Ti)O₃ Thin Films," *Appl. Phys. Lett.*, vol. 70, pp. 1378-1380, 1997.
- [50] B. A. Tuttle, T. J. Garino, J. A. Voigt, T. J. Headley, D. Dimos, and M. O. Eatough, "Relationships Between Ferroelectric 90° Domain Formation and Electrical Properties of Chemically Prepared Pb(Zr,Ti)O₃ Thin Films," in *Science and Technology of Electroceramic Thin Films*, O. Auciello and R. Waser, Eds.: Kluwer Academic Publishers, 1995, pp. 117-132.
- [51] R. F. Brown, "Effect of Two-Dimensional Mechanical Stress on the Dielectric Properties of Poled Ceramic Barium Titanate and Lead Zirconate Titanate," *Can. J. Phys.*, vol. 39, pp. 741-753, 1961.
- [52] H. H. A. Krueger, "Stress Sensitivity of Piezoelectric Ceramics: Part 1. Sensitivity to Compressive Stress Parallel to the Polar Axis," *J. Acoust. Soc. Am.*, vol. 42, pp. 636-645, 1967.
- [53] H. H. A. Krueger, "Stress Sensitivity of Piezoelectric Ceramics: Part 2. Heat Treatment," *J. Acoust. Soc. Am.*, vol. 43, pp. 576-582, 1967.

- [54] H. H. A. Krueger, "Stress Sensitivity of Piezoelectric Ceramics: Part 3. Sensitivity to Compressive Stress Perpendicular to the Polar Axis," *J. Acoust. Soc. Am.*, vol. 43, pp. 583-591, 1967.
- [55] R. Y. Nishi, "Effects of One-Dimensional Pressure on the Properties of Several Transducer Ceramics," *The Journal of the Acoustical Society of America*, vol. 40, pp. 486-495, 1966.
- [56] Q. M. Zhang, J. Zhao, K. Uchino, and J. Zheng, "Change of the Weak-Field Properties of $\text{Pb}(\text{Zr,Ti})\text{O}_3$ Piezoceramics with Compressive Uniaxial Stress and its Links to the effect of Dopants on the Stability of the Polarizations in the Materials," *J. Mater. Res.*, vol. 12, pp. 226-234, 1997.
- [57] R. F. Brown and G. W. McMahon, "Material Constants of Ferroelectric Ceramics at High Pressure," *Can. J. of Phys.*, vol. 40, pp. 672-674, 1962.
- [58] N. A. Roi, "The Dependence of the Coercive Force and The Permittivity of Ceramic Barium Titanate Upon Mechanical Stresses," *Soviet Phys.-Acoustics*, vol. 1, pp. 366-269, 1955.
- [59] B. A. Rotenberg, "The Effect of Pressure on the Piezoelectric Properties of Barium Titanate," *Soviet Physics Solid State*, vol. 1, pp. 1627-1630, 1960.
- [60] S. Watanabe, T. Fujiu, and T. Fujii, "Effect of Poling on Piezoelectric Properties of Lead Zirconate Titanate Thin Films Formed by Sputtering," *Appl. Phys. Lett.*, vol. 66, pp. 1481-1483, 1995.
- [61] F. J. von Preissig, H. Zeng, and E. S. Kim, "Measurement of Piezoelectric Strength of ZnO Thin Films for MEMS Applications," *Smart Materials and Structures*, accepted, 1998.
- [62] D. L. Allensworth, "Interferometer for the Determination of Strains Due to Domain Switching in Ferroelectrics," *Rev. Sci. Instrum.*, vol. 51, pp. 1330-1334, 1980.
- [63] Q. Zhang, W. Y. Pan, and L. E. Cross, "Laser Interferometer for the Study of Piezoelectric and Electrostrictive Strains," *J. Appl. Phys.*, vol. 63, pp. 2492-2496, 1988.

- [64] W. Y. Pan and L. E. Cross, "A Sensitive Double Beam Laser Interferometer for Studying High-Frequency Piezoelectric and Electrostrictive Strains," *Rev. Sci. Instr.*, vol. 60, pp. 2701-2704, 1989.
- [65] J. F. Li, P. Moses, and D. Viehland, "Simple, High-Resolution Interferometer for the Measurement of Frequency-Dependent Complex Piezoelectric Responses in Ferroelectric Ceramics," *Rev. Sci. Instr.*, vol. 66, pp. 215-221, 1995.
- [66] G. L. Dybwad, "c-Axis Orientation of Sputtered ZnO Films," *J. Appl. Phys.*, vol. 42, pp. 5192-5194, 1971.
- [67] V. N. Zima, "Device for Registration of Piezoelectric Effect in Films," *Instruments and Experimental Techniques*, vol. 32, pp. 504-506, 1989.
- [68] Z. Surowiak and D. Czekaj, "The Structure and the Piezoelectric Properties of Thin $\text{Pb}(\text{Zr}_{0.53}\text{Ti}_{0.045}\text{W}_{0.01}\text{Cd}_{0.01})\text{O}_3$," *Thin Solid Films*, vol. 214, pp. 78-83, 1992.
- [69] K. Lefki and G. J. M. Dormans, "Measurement of Piezoelectric Coefficients of Ferroelectric Thin Films," *J. Appl. Phys.*, vol. 76, pp. 1764-1767, 1994.
- [70] W. Ren, H. Zhou, X. Wu, L. Zhang, X. Yao, "Measurement of Piezoelectric Coefficients of Lead Zirconate Titanate Thin Films by the Normal Load Method Using a Composite Tip," *Materials Letters*, vol. 31, pp. 185-188, 1997.
- [71] F. Xu, C. Fan, J. F. Shepard Jr, and S. Trolier-McKinstry, "Measurement of the Effective Longitudinal Piezoelectric Coefficient of PZT Thin Films by the Direct Piezoelectric Effect," in *Ferroelectric Thin Films VI*, vol. 493: Materials Research Society, 1997, pp. 427-432.
- [72] P. Muralt, A. Kholkin, M. Kohli, and T. Maeder, "Piezoelectric Actuation of PZT Thin-Film Diaphragms at Static and Resonant Conditions," *Sens. and Act.*, vol. A53, pp. 398-404, 1996.
- [73] M. R. Steel, F. Harrison, and P. G. Harper, "The Piezoelectric Bimorph: An Experimental and Theoretical Study of its Quasistatic Response," *J. Phys. D: Appl. Phys.*, vol. 11, pp. 979-989, 1978.

- [74] M. Sakata, S. Wakabayashi, H. Goto, H. Totani, M. Takeuchi, and T. Yada, "Sputtered High d_{31} Coefficient PZT Thin Film for Micro Actuators," Proc. The Ninth Annual International Workshop on Micro Electro Mechanical Systems, pp. 263-266, 1996.
- [75] K. D. Budd, S. K. Dey, and D. A. Payne, "Sol-Gel Processing of $PbTiO_3$, $PbZrO_3$, PZT, and PLZT Thin Films," *Brit. Ceram. Proc.*, vol. 36, pp. 107-121, 1985.
- [76] M. Hendrickson, T. Su, S. Trolier-McKinstry, and R. Zeto, "Processing of PZT Piezoelectric Thin Films for Microelectromechanical Systems," *10th Int. Symp. Appl. Ferroelectrics*, vol. II, pp. 683-686, 1996.
- [77] T. Tani and D. A. Payne, "Lead Oxide Coatings on Sol-Gel Derived Lead Lanthanum Zirconium Titanate Thin Layers for Enhanced Crystallization into the Perovskite Structure," *J. Am. Ceram. Soc.*, vol. 77, pp. 1242-1248, 1994.
- [78] F. Chu, T. Su, and S. Trolier-McKinstry, "Effect of Thickness and Texture on the Ferroelectric Properties of Lead Zirconate Titanate Thin Films by Sol-Gel Processing," Proc. The 8th US-Japan Seminar on Dielectric and Piezoelectric Ceramics, pp. 120-123, 1997.
- [79] H. D. Chen, K. R. Udayakumar, C. J. Gaskey, and L. E. Cross, "Fabrication and Electrical Properties of Lead Zirconate Titanate Thick Films," *J. Am. Ceram. Soc.*, vol. 79, pp. 2189-2192, 1996.
- [80] R. J. Roark and W. C. Young, *Formulas for Stress and Strain*, 6th ed. New York: McGraw-Hill, 1989.
- [81] W. A. Brantley, "Calculated Elastic Constants for Stress Problems Associated with Semiconductor Devices," *J. Appl. Phys.*, vol. 44, pp. 534-535, 1973.
- [82] J.-A. Schweitz, "Mechanical Characterization of Thin Films by Micromechanical Techniques," *MRS Bulletin*, July, pp. 34-45, 1992.
- [83] J. F. Shepard Jr., P. J. Moses, and S. Trolier-McKinstry, "The Wafer Flexure Technique for the Determination of the Transverse Piezoelectric Coefficient (d_{31}) of PZT Thin Films," *Sen. and Act.*, Accepted, 1998.

- [84] J. P. Maria, "Epitaxial $\text{Pb}(\text{Mg}_{1/3}\text{Nb}_{2/3})\text{O}_3\text{-PbTiO}_3$," Ph. D. Thesis, The Pennsylvania State University, 1998.
- [85] T. J. Garino and M. Harrington, "Residual Stress in PZT Thin Films and its Effect on Ferroelectric Properties," *Mat. Res. Soc. Symp. Proc.*, vol. 243, pp. 341-347, 1992.
- [86] J. F. Shepard Jr., C. Fan, and S. Trolier-McKinstry, "The Effects of Film Thickness on the High and Low-Field Stress Response of Lead Zirconate Titanate Thin Films," in *Ferroelectric Thin Films VI*, vol. 493, Materials Research Society, pp. 81-86, 1997.
- [87] F. Chu and S. Trolier-McKinstry, "Thickness Dependence of the Electrical Properties of Sol-Gel Derived Lead Zirconate Titanate Thin Films with (111) and (100) Texture," in *Ferroelectric Thin Films VI*, vol. 493, Materials Research Society, 1997, pp. 409-414.
- [88] H. Jaffe, D. Belincourt, and J. M. McKee, "Effect of Pressure on the Curie Temperature of Polycrystalline Ceramic Barium Titanate," *Physical Review*, vol. 105, pp. 57-58, 1957.
- [89] F. Xu, "personal communication," 1998.
- [90] M. O. Eatough, D. Dimos, B. A. Tuttle, and W. L. Warren, "A Study of Switching Behavior in $\text{Pb}(\text{Zr,Ti})\text{O}_3$ Thin Films Using X-Ray Diffraction," *Mat. Res. Soc. Symp. Proc.*, vol. 361, pp. 111-116, 1995.
- [91] W. Cao and C. A. Randall, "Grain Size and Domain Size Relations in Bulk Ceramic Ferroelectric Materials," *J. Phys. Chem Solids*, vol. 57, pp. 1499-1505, 1996.
- [92] G. Arlt, "Twinning in Ferroelectric and Ferroelastic Ceramics: Stress Relief," *J. Mat. Sc.*, vol. 25, pp. 2655-2666, 1990.
- [93] U. Robels and G. Arlt, "Domain Wall Clamping in Ferroelectrics by Orientation of Defects," *J. Appl. Phys.*, vol. 73, pp. 3454-3460, 1993.
- [94] W. L. Warren, D. Dimos, and R. Waser, "Degredation Mechanisms in Ferroelectric and High-Permittivity Perovskites," *MRS Bulletin*, vol. 21, pp. 40-45, 1996.

- [95] M. J. Haun, "Thermodynamic Theory of the Lead Zirconate-Titanate Solid Solution System," Ph. D. Thesis, The Pennsylvania State University, 1988.
- [96] S. Takahashi, "Effects of Impurity Doping in Lead Zirconate-Titanate Ceramics," *Ferroelectrics*, vol. 41, pp. 143-156, 1982.
- [97] W. L. Warren, D. Dimos, G. E. Pike, B. A. Tuttle, and M. V. Raymond, "Voltage Shifts and Imprint in Ferroelectric Capacitors," *Appl. Phys. Lett.*, vol. 67, pp. 866-868, 1995.
- [98] Piezo Kinetics Inc., "Piezo Kinetics Product Specifications," Bellefonte, PA.
- [99] W. A. Shulze and K. Ogino, "Review of the Literature on Aging of Dielectrics," *Ferroelectrics*, vol. 87, pp. 361-377, 1988.
- [100] A. Kholkin, E. Colla, K. Brooks, P. Muralt, M. Kohli, T. Maeder, D. Taylor, and N. Setter, "Interferometric Study of Piezoelectric Degredation in Ferroelectric Thin Films," *Micro. Eng.*, vol. 29, pp. 261-264, 1995.
- [101] J. F. Shepard Jr. and S. Trolier-McKinstry, "unpublished results," 1997.
- [102] K. R. Udayakumar, P. J. Schuele, J. Chen, S. B. Krupanidhi, and L. E. Cross, "Thickness-Dependent Electrical Characteristics of Lead Zirconate Titanate Thin Films," *J. Appl. Phys.*, vol. 77, pp. 3981-3986, 1995.
- [103] G. E. Pike, W. L. Warren, D. Dimos, B. A. Tuttle, R. Ramesh, J. Lee, V. G. Keramidis, and J. T. Evans, "Voltage Offsets in (Pb,La)(Zr,Ti)O₃ Thin Films," *Appl. Phys. Lett.*, vol. 66, pp. 484-486, 1995.
- [104] K. Abe, S. Komatsu, N. Yanase, K. Sano, and T. Kawakubo, "Asymmetric Ferroelectricity and Anomalous Current Conduction in Heteroepitaxial BaTiO₃ Thin Films," *Jpn. J. Appl. Phys.*, vol. 36, pp. 5846-5853, 1997.
- [105] TRS Ceramics, "Product Specifications," 1998.

Vita

Joseph F. Shepard Jr. was born in Mt. Kisco, New York on March 16th, 1970. He received his Bachelor of Science degree in Mechanical Engineering in 1992 from Syracuse University in Syracuse, New York. He attended graduate school at The Pennsylvania State University and earned his Masters of Science degree in 1995 from the Combustion Laboratory in the Fuel Science program. Mr. Shepard then moved to the Materials Research Laboratory (MRL) where he conducted research on ferroelectric thin films and learned that, “to be a good scientist, you must:

(1) have a good heart,

(2) you must sing,

and (3) you must drink.”

Okazaki - 1995

With that in mind, Mr. Shepard received his Ph.D. in August of 1998 and accepted a position with International Business Machines in East Fishkill, New York.